AUTOMATED DETERMINATION OF ARTERIAL INPUT FUNCTION AREAS IN PERFUSION ANALYSIS

A Thesis

by

QUN LIU

Submitted to the Office of Graduate Studies of
Texas A&M University
in partial fulfillment of the requirements for the degree of

MASTER OF SCIENCE

Approved by:

Chair of Committee,	Mark Lenox
Co-Chair of Committee,	Kenith Meissner
Committee Member,	Jim Ji
Head of Department,	Gerard L Cote

May 2013

Major Subject: Biomedical Engineering

ABSTRACT

Perfusion in biological system refers to capillary-level blood flow in tissues, and is a critical parameter used for detecting physiological changes. Medical imaging provides an effective way to measure tissue perfusion. Quantitative analysis of perfusion studies requires the accurate determination of the arterial input function (AIF), which describes the delivery of intravascular tracers to tissues. Automating the process of finding the AIF can save operating time, remove the inter-operator variability, and correct the errors in the presence of the dispersion of the arterial system. Even though several methods are currently developed for automatically extracting an AIF, they are specific to a single modality and particular to a certain tissue.

In this thesis, we developed an algorithm to automatically determine an AIF by classifying the characteristic parameters of image pixels' dynamic evaluation curves between blood feeding areas and tissues. This automated AIF determination can be used to facilitate the generation of parametric maps for perfusion studies based on various imaging modalities and covering a variety of tissues. Automatic AIF determination was accomplished by extracting characteristic parameters such as maximum slope, maximum enhancement, time to peak, time to wash-out, and wash-out slope. Multi-dimensional data containing the characteristic parameters were converted and reduced into two-dimensional (2-D) representations, which were presented as a plurality of 2-D plots. Then physiological phases were localized within the simplified representations.

Automated segmentation of non-AIF tissues and determination of AIF areas were accomplished by automatically finding peaks and valleys of each physiological phase on the plurality of 2-D plots. The algorithm was tested in CT myocardial perfusion studies, in which a pig was used as a model of myocardial ischemia and perfusion. PET gastrointestinal (GI) perfusion studies were performed using this algorithm, in which GI perfusion was evaluated when cardiac outputs were controlled with four modes. This automated AIF determination study was compared with manual selection of AIF in PET imaging and microsphere studies to assess the effectiveness of this algorithm. In the CT myocardial perfusion study, the perfusion of infarcted myocardium was significantly lower than that of non-infarcted areas and lower than that when it was normal. In the PET abdominal perfusion study, PET imaging data gives lower value of standard deviation relative to the mean than that in microsphere results. In the manual AIF selection study, a slight change in selecting the AIF region caused a big influence on the result. On the contrary, the automated AIF selection remains consistent in the entire study and reduces inter-operator variation.

A conclusion was made that this technique is applicable to several imaging modalities, such as PET, CT and MRI, and is effective on many tissues. In addition, this algorithm is straightforward and provides consistent results. More importantly, this automated AIF determination technique replaces the conventional spatial classification method with the functional classification method, taking more physiological considerations and explanations involved.

DEDICATION

This thesis is dedicated to my mom, Mrs. Shuhua Li and my dad, Mr. Dianchen Liu, for their support and deep love throughout my life. Without them, I could not be who I am today.

Also, it is dedicated to Dr. Mark Lenox for help step me into the fascinating world of medical imaging.

ACKNOWLEDGEMENTS

I would like to thank many people who have helped me on the path towards obtaining my Master's degree. In any case, I am indebted to them for providing me with an unforgettable experience and contributing their valuable assistance in the completion of this study.

First and foremost, it is with immense gratitude that I acknowledge the support and guidance of my academic advisor, Dr. Mark Lenox. You introduced me into the fascinating world of medical imaging and, for that, I am truly grateful. In addition, you guided me to the right path towards the life I wanted to have. You are the best example of being a hardworking scientist, a brilliant engineer and a dedicated leader. These past two years have been an invaluable period in my life since I have learned a great amount from you on how to become successful. You have always been patient and encouraging in times of new ideas and difficulties; and you have always listened to my ideas and led me further to key insights. Your deep insight and prompt direction always turns on a light in the dark, and your encouragement makes me believe in what I am doing. You helped me step on the stages to get awards in competitions, and I know that I would not be there if it were not for you.

Additionally, I would like to share the credit of my work with Dr. Egemen Tuzun and Dr. Matt Miller, who helped me with animal studies. I am very grateful to you for

the assistance on physiology knowledge and immense guidance on my work. I would also like to thank my committee co-chair, Dr. Kenith Meissner and committee member, Dr. Jim Ji, for your insightful comments and continuous help throughout my study and research.

I consider it an honor to work with the entire imaging lab at Texas A&M Institute for Preclinical Studies. Dr. Lee-jae Guo, thank you for your sincere help with the physiological analysis, and for dedicating your time during our late night study sessions. Robin Terry, thank you, my sister, for your support and, without you, I would have not survived from our hardest semester and my hard times. I give great thanks to Rachel Johnson, for teaching me about MRI knowledge and your willfulness to teach me new things. Thank you, Dr. L.A. King, for your support and unwavering encouragement.

Furthermore, I want to thank Shuo Feng from the Department of Electrical Engineering, for your help on MATLAB programming. Also, thank you, Peer Shafeeq Shajudeen, for strong assistance on medical image processing. I would especially thank Dr. Steve Wright, Dr. Mary McDougall, Dr. Jim Ji and Dr. Raffaella Righetti for helping me get my foot in MRI engineering and medical image processing.

In addition, I cannot find words to express my gratitude to Dr. John Criscione, who supported me with my PolyFim project and provided valuable funding, space and mentorship on this project. It was great working with you.

I have been very privileged to have Dr. Christie Sayes and Dr. Ivan Ivanov as my advisors during my first year of graduate school. You offered an opportunity for me to come to the United States and opened a door for my bright future. I would especially like to thank Dr. Ivan Ivanov for your mathematical knowledge and mentorship throughout my life. You will always be one of my best friends forever.

It gives me great pleasure in acknowledging all the faculty and staff at Texas A&M Institute for Preclinical Studies and the Department of Biomedical Engineering at Texas A&M University.

I also would thank Mr. Christopher Schwartze and Ms. Sarah J. Knight for your prompt action on my patent provisional application. I owe my deep gratitude to College of Veterinary Medicine for the funding for my patent application.

My sincere thanks also go to my MedImKin and PolyFilm teams: Peer Shafeeq Shajudeen, Lu Gao, Esteban Carbajal, and Matthew Holliday from MedImKin, and Amir Karimloo, Dawei Zhang, Josh Silveus and Daniel Callahan from PolyFilm. Thank you for helping with building the teams and giving me opportunities to work on our awesome products. Especially thanks to Shafeeq Shajudeen and Lu Gao for working with me during 3Day Startup event and helping develop our products within 72 hours.

I also would like to thank Mr. James Lancaster, Dr. Richard Lester, Mr. Ping Zhou, Mrs. Shelly Brenckman, Mr. Blake Petty, Dr. Peter Walsh and Dr. Don Luis, for teaching and helping me to become an entrepreneur. Thank you, Startup Aggieland, for offering a free office and valuable resources for my business.

Thank you, my friends, Yun Li, Xiayun Huang, Yuan Yang, Yanjun Wang, Ming Han, Shuna Cheng, Shu Wang, Lin Liu, Kate Grawl (and her family) and the Supercinski' family, for your supportive and continuous love. I appreciate you staying by my side no matter what.

Last but not least, I would like to give my deepest gratitude to my family. I thank my parents for their endless love and for helping me become who I am today. You are the ones who walk in when the rest of the world walks out. You continuously support me no matter where I am, and I am so proud to have you to be my parents. Thank you, Simba, for bringing so much joy to my parents. I want thank my cousin/brother, Shuai Zhang, for supporting me both financially and spiritually. I look up to you so much for you have been such a good influence in my life. I am also indebted to my other relatives who consistently support me towards my goals and dreams.

I love you, all.

Qun (Maxine) Liu

NOMENCLATURE

AIF	Arterial Input Function
2-D	Two-Dimensional
CT	Computed Tomography
PET	Positron Emission Tomography
MRI	Magnetic Resonance Imaging
ROI	Region of Interest
SPECT	Single Photon Emission Computed Tomography
RF	Radiofrequency
DSC-MRI	Dynamic Susceptibility Contrast-Magnetic Resonance Imaging
GE-EPI	Gradient-Echo Echoplanar Imaging
SE-EPI	Spin-Echo Echoplanar Imaging
HU	Hounsfield Units
DEC	Dynamic Evaluation Curve
PET-TAC	PET-Time Activity Curve
CT-TAC	CT-Time Attenuation Curve
TIC	Time Intensity Curve
TBF	Tissue Blood Flow
TBV	Tissue Blood Volume
MTT	Mean Transit Time
3-D	Three-Dimensional

S vs. T	Maximum Slope vs. Time to Peak
E vs. T	Maximum Enhancement vs. Time to Peak
W vs. T	Wash-Out Slope vs. Time to Wash-Out
CAD	Coronary Artery Disease
MI	Myocardial Infarction
IACUC	Institutional Animal Use and Use Committee
LAD	Left Anterior Descending
MDCT	Multi-Row Detector CT
MBF	Myocardial Blood Flow
GI	Gastrointestinal
^{62}Cu-PTSM	^{62}Cu-labeled pyruvaldehyde bis (N-4-methylthiosemicarbazone) copper (II)
LVAD	Left Ventricle Assist Device
TOF	Time-of-Flight
FOV	Field of View
HFS	Head First-Supine
DICOM	Digital Imaging and Communications in Medicine
SNR	Signal-to-Noise Ratio
NEMA	National Electrical Manufacturers Association

TABLE OF CONTENTS

Page

LIST OF FIGURES

Page

LIST OF TABLES

Page

CHAPTER I

INTRODUCTION AND LITERATURE REVIEW

1.1 Perfusion

Perfusion describes the amount of blood that passes through the capillary beds of a volume of tissue per unit time; whereas the blood pool traveling straight through the blood feeding areas, such as arteries and veins, should not be considered as perfusion (*1*). **Figure 1** demonstrates a perfusion process in a general tissue. In the perfusion process, the blood is assumed to be neither metabolized nor absorbed by the tissue through which it traverses. Tissue perfusion is a measure of the capability of the central cardiovascular mechanisms to deliver oxygen to the peripheral tissue for meeting metabolic needs (*2*). Since it is closely related to oxygen and nutrient transfer, it becomes an essential parameter used for diagnosis of physiological changes in some cases, such as ischemic stroke, tumor, cardiac infarction and inflammation.

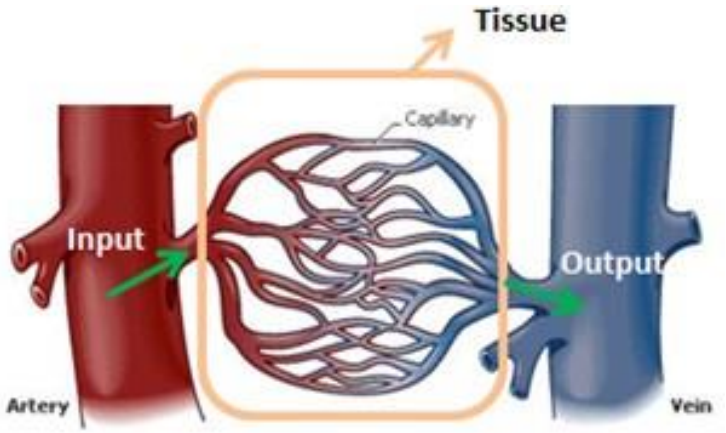

Figure 1. Perfusion process should only be considered at the capillary beds in tissues.

1.2 Tracer Kinetics

In perfusion studies, tracers are always used to label blood so that the information about the blood flow can be detected and monitored. The biodistribution and kinetics of the tracer are key components to study tissue perfusion. Based on different physical and biological properties of tracers, their kinetics are modeled in different ways to define the relationship between the measured data and physiological parameters, represented by the uptake and metabolism of tracers. The quantitative and semi quantitative assessment of tissue perfusion requires the application of tracer kinetic modeling techniques. The tracer kinetic models in quantitative assessment are used for building a mathematical framework for calculating the concentration of input and output to help understand the rate of biological processes. In perfusion studies, the tracer kinetic model is used to estimate biological parameters through fitting a mathematical model to the dynamic evaluation curve of a pixel or a region of interest (ROI) based on the change of pixel intensities over the dynamic time evaluation. Generally, the tracer kinetic modeling technique is divided into model-driven and data-driven methods (*3*). The difference between the two is that the model-driven method is based on a particular compartmental structure to estimate and describe the behavior of the tracer and further the parameters of the biological system (*4*). On the other hand, the data-driven method is mostly based on graphical analysis—Patlak plot (*5, 6*) and Logan plot (*7, 8*)—and derives the parameters from a graphic description of the kinetic processes. However, both the model-driven and data-driven methods are based on the knowledge of compartment structures (**Figure 2**).

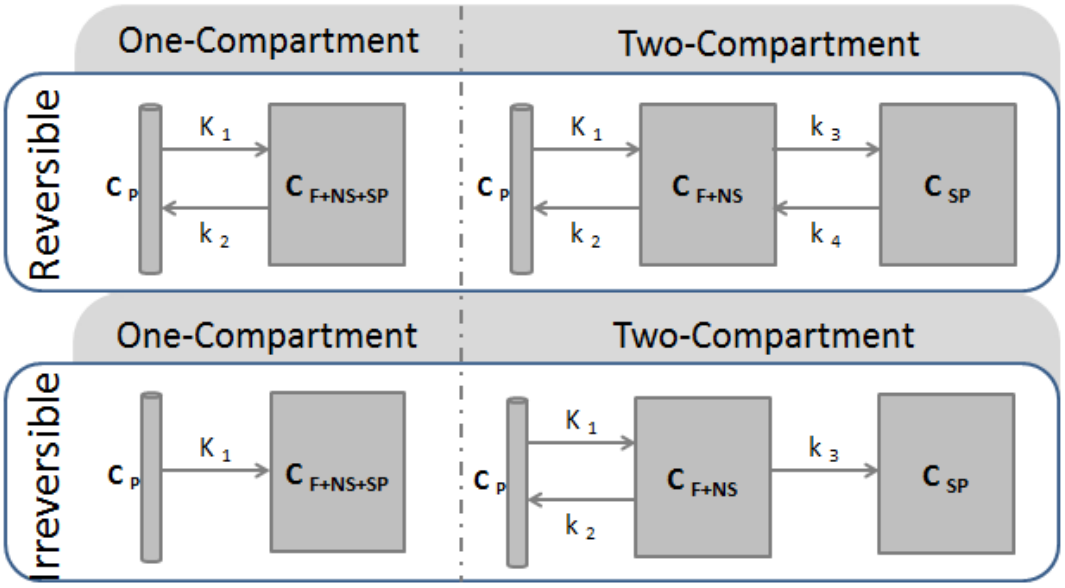

Figure 2. Compartmental models with first-order transfer rate constants (K_1, k_2, k_3 and k_4) describing the flux of tracer between compartments. C_p denotes the concentration of tracer in arterial plasma, C_{F+NS} the concentration of free and nonspecifically bound tracer in the target tissue, C_{SP} the concentration of specifically bound tracer in the target tissue.

In order to interpret the tracer behaviors inside the body, we assume that the subjects who interact with tracers are physiologically separated into several pools of tracer substance, termed as "compartments". The common models are one irreversible/reversible compartment and two irreversible/reversible compartments (**Figure 2**). Compartmental models with first-order transfer rate constants (K_1, k_2, k_3, k_4) describe the flux of tracers between compartments. The tracers are infused into the arterial blood (plasma), and then pass into the first compartment. If the tracers are completely trapped by this compartment, we say that it is a one-compartment model. The categories of irreversible models and reversible models are dependent on whether the tracers inside the first compartment exchange with the plasma or not. If the first

compartment is a nonspecific-binding compartment that exchanges with the plasma, and then there is another compartment called specific binding region, we call this model as two-compartment model. The categories of irreversible and reversible models are determined by the exchanging status of the second compartment.

1.3 Perfusion "Gold Standard" Study—Microsphere Study

The most widely used techniques to measure regional tissue perfusions are deposition techniques. The basic principle of these kinds of techniques is that the deposition of tracers injected is proportional to the blood flow in per unit volume/mass of tissues. In other words, the amount of the cardiac output travelling to a certain region is determined by the deposition of a tracer within that region (*9*). The ideal deposited tracers are able to provide a measure of blood flow at the level of the capillaries within a certain volume of the tissue. In addition, the tracers are not metabolized by the organ since the blood fraction of a tissue is not equal to the metabolism fraction of the organ.

The current "Gold Standard" technique to measure blood flow is to employ non-diffusible labeled tracers—microspheres. Microspheres are small spherical or irregularly shaped particles that are larger than capillaries (usually with the diameter larger than 12 micons (*9*)). After the microspheres are injected through the left atrium or ventricle, they embolize the first capillary bed they encounter and remain within the capillary beds for a sufficiently long time until the particles break down and are excreted out of the body. Since microspheres are injected into the left atrium or ventricle, they are delivered to

individual organs with the proportion to the blood flow to the organ. The requirement of injection of the microspheres into the left atrium or ventricle is to avoid extraction of particles by the lungs.

However, one of the disadvantages of microsphere measurement is that the process is usually invasive, because tissue biopsies are harvested for the microsphere analysis. In addition, this technology might lead to microembolizaton of the capillaries due to blood flow blocked by the accumulation of the particles. Therefore, only a small amount of microspheres can be injected. Lastly, microsphere measure is very subject to the technique itself, which means that slight changes can have a large effect on the sample if operators are not careful.

1.4 Medical Imaging Modalities for Perfusion Study

1.4.1 Single Photon Emission Computed Tomography (SPECT) Imaging

Nuclear medicine techniques use pharmaceuticals labeled with radionuclides, called radiopharmaceuticals, as tracers for the diagnosis and treatment of disease. Essentially, gamma radiation, which is non-particulate and penetrating, is emitted from the body through radiopharmaceuticals decay and measured by external radiation detectors. The radioactive tracer, combined with physiological process, can functionally assess the tissue activity, rather than anatomic or structural detail (*10*). The two commonly used nuclear medicine techniques in perfusion studies are single photon emission computed tomography (SPECT) and positron emission tomography (PET).

In SPECT, the collimated gamma camera moves in a circular or elliptical orbit around the patient and acquires projection images at multiple angles. Since the 1980s, SPECT has become the clinical gold standard in tissue perfusion studies. By measuring the uptake and distribution of the radionuclide tracer—usually either technetium or thallium—in the tissue in different states or stages, SPECT allows a three-dimensional assessment of the tissue perfusion and viability (*11*). SPECT tracers are designed so their distribution is nearly proportional to tissue perfusion, with the ideal condition of a relatively high first-pass extraction fraction and retention in the tissue through high chemical affinity (*12*). The technique has a relatively high accuracy in diagnosis. In myocardial perfusion studies, for example, the specificity is around 87-94% and the sensitivity 85-90% (*11, 13, 14*). However, SPECT requires a tracer dependent radiation dose that is normally really high and a long examination time. Furthermore, variable soft tissue attenuation leads to apparent defects, shown as lack of perfusion, interfering with quantitative analysis and diagnosis (*10*). The limitations in spatial and temporal resolution of SPECT might also hamper the assessment of the slight difference of perfusion, resulting in some mistakes in diagnosis. In clinical use, the cost for this technique is moderately high, approximately $1,000.

1.4.2 Positron Emission Tomography (PET) Imaging

1.4.2.1 PET Physics

Similar to SPECT, PET is a tomographic technique that is used for measuring physiology, as well as function, instead of anatomy and structure. Principally, a

radioactive tracer labeled with a positron emitting isotope is introduced into the body, usually through intravenous injection. It is then distributed in tissues in a manner of physiological properties of the different tissues. The isotope decays by emitting a positively charged electron—positron—which undergoes annihilation with an electron within the body, followed by a pair of gamma photons of 511 KeV energy emitted in almost opposite directions. The high-energy photons have a good probability to escape from the body. The pair of gamma photons is simultaneously detected by two series of detectors axially surrounding the patient. The detectors convert the photons into electronic signals for the later on electronics transference. Approximately 10^6 to 10^9 decays (events) are required per frame to achieve a necessarily statistical signal to noise, as stated in mCT (PET-CT) performance published by Jakoby (*15*). More counts usually give better signal-to-noise ratio (SNR), but not absolutely. According to Jakoby, for a 70 cm long NEMA (National Electrical Manufacturers Association) scatter phantom, the optimal SNR can be achieved with the count rate to be 800,000 trues/sec. However, after the optimal count rate, the SNR slightly drops down. Noise is dominated by the counting statistics of the coincidence events detected. Therefore, more events detected means better counting statistics of estimated true value. The poor counting statistics can be compensated by longer acquisition time in individual frame. These events are corrected by several factors, such as dose calibration factor, scatter fraction factor and decay factor, and then are reconstructed into a tomographic image. The resulting signal intensity in a voxel/pixel of the image is proportional to the amount of the radionuclide in the corresponding pixel. Since unlike SPECT, PET can be accurately corrected for

attenuation, a true quantified distribution can be computed. Accordingly, using PET imaging data, the spatial distribution of tracers can be mapped so that quantitative analysis is able to be performed (*16*).

1.4.2.2 PET Perfusion Studies

In perfusion studies, 15-Oxygen-water can be considered the most ideal tracer due to its property of being non-metabolized by the tissue. However, the use of 15-Oxygen-water remains limited in the clinical application since it requires an on-site cyclotron to generate. Other common tracers, such as 82-Rubidium and 13-N-Ammonia permit dynamic and static acquisition with a short scan time, as well as low radiation exposure (*17*). The advantages of 13-N-Ammonia and 82-Rubidium are their relatively high first-pass tissue extraction—65-70% for 13-N-Ammonia (*18*) and 60-65% for 82-Rubidium (*19*). For tracers used for perfusion studies, the higher first-pass tissue extraction, the better tracer distribution around the tissue we can estimate. Another benefit for using 13-N-Ammonia as a tracer is its long life times—9.96 min, which allows longer image acquisition time and better count statistics. However, like 15-Oxygen-water, 13-N-Ammonia requires on-site cyclotron to generate. 82-Rubidium can be obtained by a generator, while its short life time—76 second—limits its use in the perfusion studies, which are high tracer concentrated studies.

In perfusion studies, imaging begins with the infusion of radioactive tracers. The scan continues for anywhere from seven to forty minutes, with multiframe or dynamic

image sequence. The entire scan time depends on the properties of the tracer. Usually for the tissue-trapped tracers, the scan should not stop until the tracer is cleared from the artery-system and trapped completely by the tissue.

The kinetics of the tracer when the PET imaging is performed represents the first pass of it travelling through the tissues. Since the signal intensities represent the amount of the tracers in the corresponding pixels, the changes in pixel intensities reflect the blood flow and distribution in that area. The radioactivity changing around a tissue over time generates the tracer enhancement curves for the tissue.

One of the PET perfusion's unique properties is to measure the tracer concentration in regional tissue in absolute units, allowing for the homogenous spatial resolution throughout the field of view. Practically, the spatial resolution of modern PET system is approximately 0.54 mm to 10.5mm (*20*), which is tracer and system dependent. Resolution in positron imaging is limited by mean free path of the positron. The more emission energy of the isotope has, the longer path the emitted positron takes to annihilate with an electron. The location of the annihilation spot is measured to estimate the actual location of the positron or the isotope. Therefore, the longer mean free path, the more blurred image. In addition, the resolution is also limited by colinearity/deviation angle. The more energy the isotope has means the bigger momentum it takes. The two gamma photons emitted then carry the momentum in the original direction. Accordingly, if the energy is too large, the colinearity is bad, and the

resolution is low. The high contrast resolution allows a sensitive and accurate detection of a slight change in perfusion with an average sensitivity of 90% and specificity of 89% in myocardial perfusion, for example (*21*). Compared to SPECT, PET has higher temporal resolution, which contributes to the ability of the measurement of rapid changes in radioactive tracer concentration in tissues. The cost of PET is relatively high, around $1, 850, but this method is able to provide better and more reliable results with a reduced radiation dose than SPECT does.

1.4.3 Magnetic Resonance Imaging (MRI)

1.4.3.1 MRI Physics

The MRI signal derives from protons in the body, mostly existing in water, but also in the lipid. The proton, a polarized spin with angular momentum, behaves as a small magnet when the patient inside a static magnetic field. The spin precesses around the direction of the static magnetic field. The application of a radiofrequency (RF) pulse, a circularly polarized wave that contains a rotating magnetic field, interferes with the spins' equilibrium and excites the protons. The relaxation after the excitation can be encoded with rapidly changed magnetic fields and magnetic field fluctuations caused by molecular motion, and can produce signals that present spatially localized information (*22*, *23*).

1.4.3.2 MRI Perfusion Studies

The method commonly used in MRI perfusion studies is dynamic susceptibility contrast MRI (DSC-MRI), or dynamic contrast enhanced MRI (DCE-MRI). DSC-MRI is based on the technology of bolus tracking. Essentially, gadolinium is a paramagnetic substrate that serves as contrast agent, because it profoundly affects the signal (up to 50%) on a gradient echo scan (*24*) and remains inside intravascular structures inside the tissue. As the contrast agent passes through the blood vessels, a big change in the magnetic field is produced by the gadolinium-doped blood, and the different magnetic fields cause the MRI signal to dephase, resulting in a progressive signal loss (characterized by T2*, gradient-echo echoplanar imaging (GE-EPI)). Recently, researchers have started to use T2-weighted spin-echo scan (spin-echo echoplanar imaging (SE-EPI)), as well, to study the tissue perfusion. In this scan, the signal loss mostly arises from the passage or the diffusion of gadolinium—causing static field inhomogeneity effects—through the capillaries instead of through the larger blood vessels.

The pixel intensities from the MRI present signal intensities themselves. The abnormal part of the tissue will show less signal loss compared to the surrounding tissues. The kinetic model used for DSC-MRI in perfusion studies is, similar to PET perfusion studies, also based on the principle of tracer kinetic modeling techniques. The perfusion tracer is neither metabolized nor absorbed by the tissue through which it traverses. In addition, in order to make the later calculation work, the tracer should be

non-diffusible, so that it could be accumulated inside tissue. In order to simplify the computation, one compartment irreversible model is used: the contrast flows from the artery (input) into the capillary bed of the tissues, accumulates inside the tissue, and flows out through the vein (output) without flowing back.

MRI perfusion studies show high spatial and temporal resolution and no radiation exposure, which makes MRI a safe and clinically-used modality to assess both anatomy and functionality of tissues. More importantly, MRI allows semi-quantitatively measurements of the tissue perfusion. The foundation of calculation and analysis of the MRI perfusion is on the time-intensity curves. Another advantage of the MRI perfusion study is that it gives a high sensitivity and specificity. For example, in cardiac stress perfusion tests, the sensitivity and specificity are of 89% and 87%, respectively (*11*). However, the disadvantages of MRI perfusion difficult in a clinical setting are moderately long acquisition time (30 – 45 min), heartbeat sensitivity, and restriction in patients with metal implants.

1.4.3 Computed Tomography (CT) Imaging

1.4.3.1 CT Physics

The first CT scanner was developed in 1972 by Godfrey Hounsfield, and now this modality has become an essential radiological technique applied in a wide range of clinical cases. X-rays are used in CT to generate cross-sectional, two-dimensional images of the body. An X-ray tube rapidly rotates by 360 °around the body, and the

transmitted radiation is then detected by an array of sensitive radiation detectors located on the gantry around the patient (**Figure 3**).

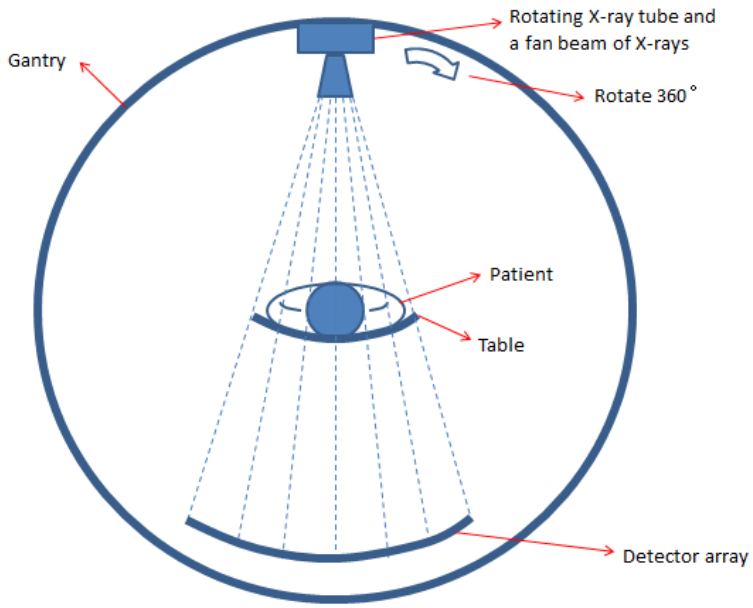

Figure 3. CT structure.

Images are generated through reconstruction, an inverse problems mathematical technique, from multiple X-ray projections to reproduce the internal structures of the body. Essentially, the patient is linearly scanned by the X-ray beam and a shadow image, referred to as "projection" or "attenuation profile", is produced. A further rotation of the X-ray tube and the detector by a small angle renders another shadow image. This procedure is repeated many times until the patient has been scanned for a 180 degree rotation. The data obtained from CT scanner is modeled with Radon Transform. The Radon Transform allows to create film images of objects, and the inverse problems (inverse Radon Transform) allows converting Radon Transform back into attenuation profile to reconstruct the body from the scanning data. The attenuation profiles are

processed by the image processor, and each attenuation profile is subjected to kernel, which is a mathematical high-pass filter, to correct the blurred image and produce overshoot and undershoot at the edges of the patient. The profiles then pass through a mathematical operation of convolution and are further added up to produce a sharp image. The creation of the images is accomplished by overcoming superimposition of structures and presenting slight differences in tissue contrast.

The CT image does not show attenuation values directly, but does show the CT number—Hounsfield Units (HU), the relative electron density of tissues (*25*).

$$HU = 1000 \times (\frac{\mu - \mu_w}{\mu_w}) \quad (1)$$

Where μ is the attenuation coefficient and μ w is the attenuation coefficient of water. Attenuation coefficients depend on electron density of tissues.

A contrast (tracer) can be applied to enhance the imaging presenting in some certain areas through the blood flow. The contrast is usually injected intravenously. There are many kinds of contrast used in CT imaging, and the most common one is an iodine-based contrast. The principle of contrast enhancement is based on the photoelectric interaction of the x-rays with the iodine atoms. A contrast (iodine)-enhanced CT imaging has always been performed at 80 KV, instead of the conventional 120-140 KV. The determination of the tube voltage is because it is closer to the K-edge of iodine, which is 33.2 KeV (*26*). K-edge refers to a sudden increase in the attenuation of photons that occurs at an energy level just above the binding energy of the K shell

electron of the atoms interacting with the photons. These energy levels cause an increase photoelectric absorption (*27*). A maximum iodine signal can be obtained if the mean beam energies straddle the K-edge of iodine (*28*). The selection of this kilovolt (80 KV) can reduce the administered radiation dose to the patient as well as increase the contrast signal (*29*).

1.4.3.2 CT Perfusion Studies

CT has evolved into a reliable imaging modality for non-invasively measuring tissue perfusion, given the rapid acquisition time, its ability to be nearly unaffected by physiological noise—like heartbeat rate. An important role of CT perfusion study is to anatomically and functionally assess tissue abnormality. In addition, another important advantage of CT perfusion is the linear relationship that the change in attenuation, which is expressed as HU, is directly proportional to the concentration of the contrast material (*30*). This linear relationship potentially facilitates semi-quantitative measurement of perfusion.

The CT perfusion can be divided into qualitative study and semi-quantitative study. The qualitative technique utilizes the visual perception of the different attenuation values to distinguish hypoperfused areas from normal tissue areas. The advantage of this method is that it can provide both anatomical and functional assessment of perfusion in a single test with significantly reduced radiation dose and decreased contrast injection. However, the accuracy is not ideal. The signal attenuations in the organ represent the

relatively accurate perfusion level only if the image is acquired during the contrast maximal enhancement. The optimal visualization, with high qualities of both view and time, is difficult to acquire. Furthermore, the contrast arrival times in the ischemic or infarcted areas are significantly delayed compared to that of the normal areas. Another disadvantage is that the visualization of the contrast enhancement is largely affected by image artifacts arising from motion and beam hardening. A true defect should be consistent in all the image phases, but with only one signal test, it is hard to tell the persistency.

The modern approach for CT perfusion is dynamic CT imaging, in which sequential images are obtained over a defined period of time to trace the kinetics of contrast bolus in the blood pool and tissues. In the dynamic CT perfusion study, imaging is started to be performed during the first pass of contrast bolus traversing through the tissue microvasculature. The areas with normal perfusion uptake higher contrast and present brighter images than the ischemic areas with reduced perfusion. The principle is similar to that of DSC-MRI, and one compartment irreversible model is used. The HU changing over time allows the creation of the enhancement curves for the tissue, region of interest or individual pixels.

1.5 Arterial Input Function (AIF) Determination

1.5.1 Dynamic Evaluation Curves (DEC)

The dynamic evaluation curves represent the tracer tracking in a certain region along the dynamic imaging sequence. The specific name for DEC depends on the particular meaning presented by pixel intensities from each imaging modality. For PET imaging, the dynamic evaluation curve is the time-activity curve (PET-TAC); for MRI imaging, it is the time-intensity curve (TIC); and for CT imaging, it is the time-attenuation curve (CT-TAC). In all the imaging modalities, the dynamic evaluation curves involve the tracer kinetics of baseline, wash-in, wash-out and steady state (**Figure 4**). However, the presenting of them varies with imaging modalities, imaging protocols and tracer properties. For example, the time-intensity curves generated from DSC-MRI shows negative contrast enhancement (**Figure 5A**), while the CT-TACs and PET-TACs present the positive contrast enhancement—showing peaks. For the diffusible tracers, the wash-out process is displayed as clearing-up. However, the non-diffusible tracers will be trapped into the tissue, and therefore, the wash-out process cannot show up in tissues (**Figure 5B**).

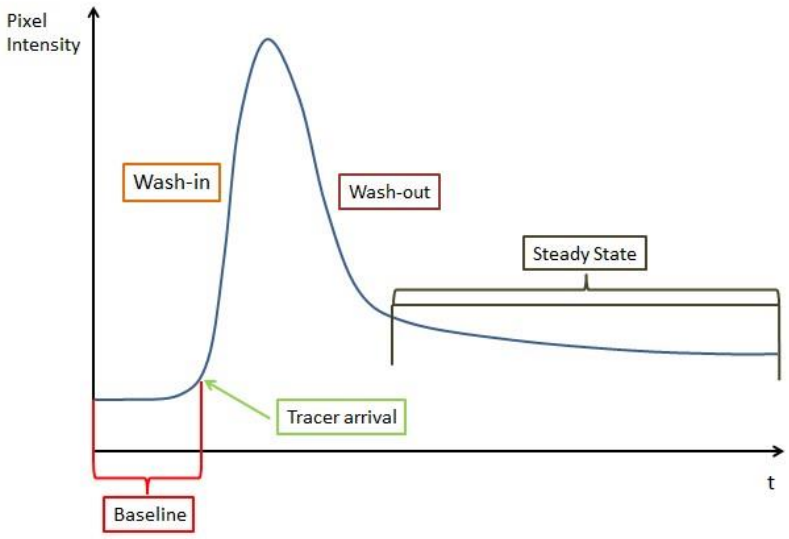

Figure 4. A general presenting of a dynamic evaluation curve.

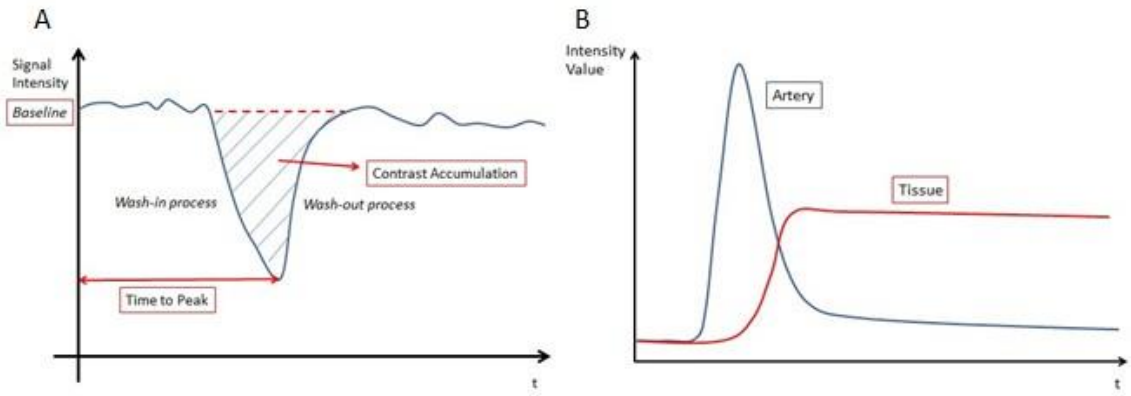

Figure 5. Two cases of dynamic evaluation curves. A. Dynamic evaluation curve for DSC-MRI; B. Dynamic evaluation curve for non-diffusible tracer kinetics in tissue and artery.

The dynamic evaluation curves are utilized in generating perfusion parametric maps to demonstrate the blood distribution and contrast clearance rate, which are shown by tissue blood flow (TBF), blood volume (TBV) and mean transit time (MTT). TBF is defined as the volume of blood moving through a given vascular network in the tissue

per unit time, with units of milliliters of blood per 100g of the tissue per minute (ml/min/100g). TBV is described as the total volume of flowing blood within the vascular network, with units of milliliters of blood per 100g of the tissue (ml/100g). MTT is defined as the average transit time of all blood elements entering the arterial input and leaving at the venous output of the vascular network, measured in seconds (s) (*31, 32*). A relationship exists among these three parameters:

$$\mathrm{TBV} = \mathrm{TBF} * \mathrm{MTT} \quad (2)$$

Therefore, once two parameters are obtained, the other one can be simultaneously calculated.

1.5.2 Perfusion Quantitative Analysis

The quantitative analysis—TBF, TBV, and MTT—of tissue perfusion relies on dynamic evaluation curves by using maximum slope (upslope) model, model-based deconvolution mathematical modeling and trapped-tracer model, which are tracers and modality dependent.

1.5.2.1 Maximum Slope Method

Maximum slope analysis is also called upslope analysis, which means to compute perfusion maps from the maximum slope of DECs of the tissue. This method is usually applied in MRI and CT perfusion studies.

The computation process is based on four general assumptions. First, a perfusion tracer is neither metabolized nor absorbed by the tissue through which it traverses. Second, the maximum slope method is based on Fick's Principle of conservation of mass to a given region of interest (the tissue studied) (*31*). The essence of the principle is on the basis of one-compartment model, and is generally defined as the amount of a substance in a compartment at any moment in time yields to the integral over time of the net rate of flow of the substance into the compartment. The net rate of flow is equal to the difference between inflow and outflow (**Figure 6A**). In the perfusion study, the substance is the contrast agent, and the inflow is the contrast flowing inside the artery, while outflow is the contrast flowing inside the vein. The net flow is the contrast within the tissue (**Figure 6B**).

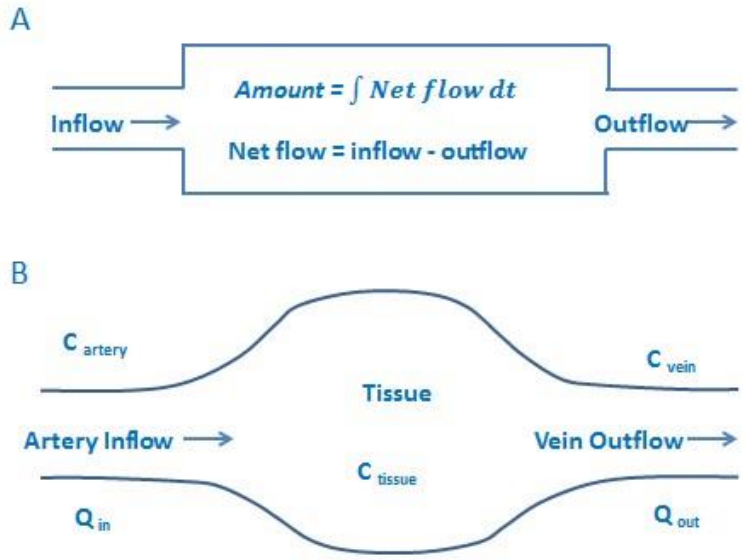

Figure 6. The model for Fick principle of conservation of mass (A) and the associated one-compartment model for tissue perfusion studies. In (B), C_{artery}, C_{vein} and C_{tissue} are the contrast concentrations in the artery, vein and tissue, respectively. Q_{in} and Q_{out} are the blood flows, with contrast included.

In this assumption, there is only a single inflow (artery), a single outflow (vein), no delays (instantaneous bolus injection), and no dispersion (one pathway of blood). The third assumption is that perfusion is an incompressive fluid dynamic process, which means that inflow equals to outflow, corresponding to the interested tissues

$$Q_{in} = Q_{out} = Q \tag{3}$$

Where Q_{in} (velocity/time) and Q_{out} are the flow-in and flow-out blood flows, with contrast included.

According to the law of conservation of mass, it comes to

$$M(t) = C_{tissue} \times V = Q \times \int_0^T [C_{artery}(t) - C_{vein}(t)]\, dt \tag{4}$$

Where C_{artery} (mass/volume), C_{vein} and C_{tissue} are the contrast concentrations in the artery, vein and tissue, respectively. M (t) is the accumulated mass of contrast at a moment in time. V is the volume of the tissue.

The equation of mass conservation can be simplified as

$$M_{accumulation} = M_{in} - M_{out} \tag{5}$$

The mass of accumulated contrast yields to the difference between the mass of wash-in contrast and the mass of wash-out contrast.

The forth assumption is that the maximal mass accumulation of the contrast within the tissue occurs when the perfusion process turns into an irreversible one-

compartment model—this means that the concentration of the contrast inside the blood flow of the vein yields to zero ($C_{vein} = 0$). And the equation (4) turns out to be

$$C_{tissue} \times V = Q \times \int_0^T C_{artery}(t)dt \quad (6)$$

TBF is the flow per unit tissue volume, and thus

$$TBF = Q/V = \frac{dC_{tissue}/dt}{C_{artery}} \quad (7)$$

At this time, mass accumulation is the maximum, and since the general blood flow, Q, will not change, the concentration of the contrast inside artery will be the maximum

$$C_{artery}(t) = C_{artery\_max} \quad (8)$$

At the same time, in equation (6), since the flow Q, volume V, and the concentration C_{artery} are constant, dC_{tissue}/dt must also be constant. This means that

$$\frac{\partial^2 C_{tissue}}{\partial t^2} = 0 \quad (9)$$

Therefore, in this moment, the concentration of the contrast inside the tissue is in the status of being maximum upslope

$$\frac{dC_{tissue}}{dt} = maximum \quad (10)$$

In sum, based on the assumptions aforementioned, it turns out the equation that demonstrates that the rate of contrast accumulation will peak when the arterial concentration is maximal.

$$\left(\frac{dC_{tissue}}{dt}\right)\max = TBF \times (C_{artery})max \tag{11}$$

Hence, TBF can be represented as the ratio of the maximum slope of tissue DECs to the maximum arterial concentration.

Tissues contain the vasculature, cells and the interstitium, and TBV measures fractional vascular volume—the volume of distribution.

$$TBV = \frac{V_{vasculature}}{V_{vasculature} + V_{interstitium} + V_{cells}} = \frac{V_{vaculature}}{V_{tissue}} \tag{12}$$

Since the perfusion process does not count contrast absorption and metabolism, all the contrast inside the tissue only exists in microvasculature surrounding or in the tissue

$$C_{tissue} \times V_{tissue} = C_{vasculature} \times V_{vasculature} \tag{13}$$

According to the law of conservation of mass, the amount of the contrast flowing from the artery into the microvasculature in the tissue does not change.

$$M(t) = Q \times \int_0^T C_{artery}(t)dt = Q \times \int_0^T C_{vasculature}(t)dt \tag{14}$$

Based on the equations of (12), (13), (14), it turns out

$$TBV = \frac{\int_0^T C_{vasculature}(t)dt}{\int_0^T C_{tissue}(t)dt} \quad (15)$$

This is an ideally simplified method to calculate TBV. However, in fact, some corrections need to be considered: ρ, tissue attenuation, which varies by tissues, and CH, a correction factor to adjust the difference between arterial and microvasculature hematocrit (*31, 33*). The more accurate calculation to get TBV is demonstrated in the equation (16).

$$TBV = \frac{CH}{\rho} \times \frac{\int_0^T C_{vasculature}(t)dt}{\int_0^T C_{tissue}(t)dt} \quad (16)$$

Since the two correction numbers are not easy to obtain, researchers always use equation (15) to get the estimated TBV, and results are well shown.

MTT is either measured from the first detection of contrast to the contrast wash-out point, or calculated from equation (1) (*31, 34*). The calculation from equation (1) is more accurate since the detection of the contrast wash-in and wash-out is not easy.

Compared to other methods, the maximum slope method is simple, and thus the speed of calculation of perfusion parameters is high. The maximum slope method yields relative, rather than absolute, perfusion assessment. It is both efficient and accurate. Another advantage is that this analysis method only requires imaging to just a portion of the DEC, reducing the radiation exposure. However, a high rate of contrast injection-as

high as 10 ml/s-is required to satisfy the assumption of no venous outflow. In clinical practice, it is hard to achieve this high injection rate. Therefore, it is utilized in preclinical studies, instead of routinely achieved in clinical practice (*31*).

1.5.2.2 Model-Based Deconvolution

Generally speaking, this model used for perfusion quantification is based on the principles of tracer kinetics for non-diffusible tracers (*1*). It utilizes the two-compartment model that besides the contrast flowing into the capillary bed of the tissue, it also remains in the intravascular space (*35*). However, the calculation still obeys the assumptions of Fick Principle of conservation of the mass, one inflow (artery) and one outflow (vein), and non-absorbable and non-metabolized. This model can be applied in MRI and CT perfusion studies.

The concentration of the contrast agent inside the tissue can be defined in terms of three functions (*1, 31, 32*):

1) Transport function, h (t): the probability density function of tissue transit time through the given volume of interest at the moment t in time, with the condition of an ideal instantaneous bolus injection. This function relies on the vascular structure and blood flow inside and presents the distribution of the transit time over an individual voxel.

2) Residue function, R (t): the fraction of injected tracer that still remains in the

tissue voxel of interest at the moment t in time, following an ideal instantaneous unit bolus injection. R (t) is unitless and equals one when t equals zero.

3) Arterial input function (AIF), C_{artery} (t): the concentration of contrast in the blood feeding areas (usually arteries) to the voxel of interest at time t.

The residue function R (t) represents an intermediate quantity and is defined as

$$R(t) = \begin{cases} 1 - \int_0^t h\,(\tau)d\tau\,, for\ t \geq 0, \\ 0, for\ t < 0. \end{cases} \quad (17)$$

The residue function R (t) only relies on the hemodynamic properties of the voxel of interest. It demonstrates an abrupt rise due to the instantaneous injection of the contrast, followed by a plateau of duration that yields to the minimum transit time through the voxel of interest. The contrast agent will leave the each voxel of interest gradually over time, rather than instantaneously, due to the various transit times within the capillary bed. As a result, the residue function R (t) decreases gradually from one to zero. **Figure 7** represents the examples of a transport function h (t) and the corresponding residue function R (t). The function h (t) is usually modeled by a gamma variate model (*36*).

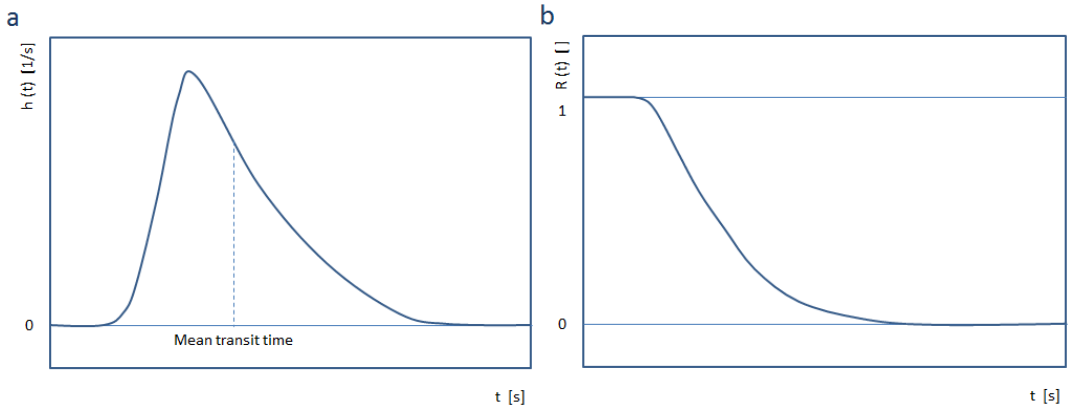

Figure 7. Examples of the transport function h (t) with the mean transit time included and the corresponding residue function R (t).

The tissue DECs, in fact, present the combination of the AIF and the inherent tissue properties (*31*). Thus, the impulse effect caused by the instantaneous contrast injection into the AIF needs to be removed via deconvolution, a mathematical method, to derive R (t). It turns out to be the formulation of the indicator-dilution theory (*35*).

$$C_{tissue}(t) = \frac{\rho}{CH} \times TBF \times \left[C_{artery}(t) * R\ (t)\right]$$

$$= \frac{\rho}{CH} \times TBF \times \int_{\tau}^{t} C_{artery}(\tau) \times R(t-\tau)d\tau \qquad (18)$$

Where "*" is the convolution operator, ρ is the tissue attenuation, CH is the correction factor for the microvasculature hematocrit. C_{tissue} and C_{artery} are the concentrations of the contrast inside the tissue and the blood feeding areas, respectively and can be measured directly from the DECs.

For the interpretation of this equation, in an ideal situation, the concentration of the contrast in the blood feeding areas, C_{artery}, is a superposition of consecutive contrast

injection C_{artery} (τ) dτ at time τ, and the concentration of the contrast that still remains in the voxel of interest at time t will be proportional to C_{artery} (τ) R (t - τ) dτ. Therefore, the total concentration of the contrast inside the voxel of interest is the integral of all the contributions over time (*1*). In order to compute TBF, the term TBF ·R (t) should be isolated via deconvolution. At the time t = 0, R (0) = 1, and TBF is obtained.

TBV can be obtained by equation (15). As for the calculation of MTT, apart from equation (1), another method can be used. By the definition of the transport function h (t), MTT is the ratio of the first moment of the transport function to its zeroth moment (*1*).

$$MTT = \frac{\int t \times h(t) dt}{\int h(t) dt} \quad (19)$$

1.5.2.3 Trapped-Tracer Model

In the model of completely (approximately 100% first pass) trapped radiotracers, the blood flow can be calculated according to the fact that after the radiotracers are injected into cardiac output directly (the left ventricle or atrium), they are distributed to the individual organ/tissue in proportional to the blood flow to that organ. Therefore, the blood flow can be determined through the radioactivity distribution in the tissue (*37*).

$$F\ (mL/min) = C.O.(mL/min) \times (A_0/A_t\ ) \quad (20)$$

Where F is blood flow, C.O. is the cardiac output, A_0 is the radioactivity of the tracers accumulated in the tissue, and A_t is the radioactivity of the tracer injected as total.

Tissue perfusion is determined by blood flow per gram of the tissue, which is then given by the **equation (21)**.

$$TBF\ (mL/min/g) = C.O.(mL/min) \times [(A_0/m_0\ /A_t\ )] \quad (21)$$

Where A_0 / m_0 presents the radioactivity concentration of the tracer in the measured tissue.

However, cardiac output is difficult to measure at exactly the same time as the sample, so "reference sample technique" is usually used to replace the direct cardiac output measurement. In the microsphere study, when the microspheres flow to the organ, the arterial blood is withdrawn simultaneously at a rate of S (mL/min). The total activity of the withdrawn blood sample is labeled as A_s. The perfusion of the organ becomes to the **equation 22**.

$$TBF = S \times [A_0\ /\ m_0\ /\ A_s] \quad (22)$$

1.5.3 Arterial Input Function Determination

The quantitative analysis of the parametric perfusion maps relies on accurate determination of AIF, which describes the concentration of the tracer in the blood pool within blood feeding areas to the voxels of interest at a certain time. In simpler words, AIF is the dynamic evaluation curve of blood feeding (mostly arterial) areas. Currently, most researchers select AIF areas manually, by visual inspection of the anatomy in the regions containing the blood pool. The manual selection process requires specially trained operations, and the results vary with observers. Moreover, the complicated

structures in some tissues—such as brain—make the detection of the AIF areas difficult due to the scattered distribution of arteries. In addition, the selection of the global AIF in 3D is even more complex because researchers have to select in each single slice and combine them together, which easily loses consistency in the entire 3D volume and causes large time and labor expenses. The automated process of finding the AIF, on the other hand, can reduce time and labor consumption, and more importantly, remove the inherent inter-operator variability and inconsistency in parallel experiments, or when comparing changes in follow-up studies during treatment therapy.

There are several algorithms already developed that can automatically extract an AIF in perfusion studies (*38-40*). Briefly described, an AIF is selected by looking at various characteristics of an image voxels' time-intensity curves, such as peak height, peak width, wash-out time and wash-in process (*41-43*), and followed with cluster analysis, group independent component analysis and curve fitting analysis. In these studies, pre-knowledge of estimated AIF location is needed, and the technologies are based on spatial difference between AIF areas and tissues. Therefore, most of the studies are specific to certain tissues analysis, and they are only particularly used in a single imaging modality. In addition, so far, most of studies focus on MRI perfusion studies, and very few studies work on the automated determination of an AIF from CT and PET perfusion studies. Accordingly, it would be advantageous to develop a method for the automatic selection of an AIF widely used for any imaging modalities and broadly

applied in any tissue studies. To achieve this goal, more physiological conditions of organs should be involved to compromise the modalities differences.

1.6 Research Objectives and Thesis Outline

1.6.1 Research Objectives

In this study, we develop an algorithm to pick an AIF automatically by classifying the characteristic parameters of each image pixel' dynamic evaluation curve between blood feeding areas and tissues. The selected AIF is used in producing parametric perfusion maps displayed for assisting diagnosis of physiological changes of a patient. It has six innovation points.

First, this approach takes more physiological conditions into consideration and combines the modalities physics into the results. It is self-adjusted and tissue-independent. Therefore, it is able to be used for any imaging modalities among CT, PET and MRI and applied in any tissues with minimal adjustment due to the different functionalities of varied organs.

Second, the AIF determination by the manual selection is normally executed in one slice, while our automated method selects an AIF from the entire 3-D volume at one time, which increases the efficiency and consistency.

Third, this automatic generation requires interaction with physicians for physiological phase determination. And this requirement for the phase determination will not vary with operators. Therefore, the automated process is able to maintain inter-operator consistency.

Fourth, this technology is based on pixel-wised characteristics analysis, and therefore despite the scattered distribution of the blood supply areas, the selection of AIF pixels is still efficient and effective.

Fifth, this technology transfers a multi-dimensional problem into several 2-D plots for later analysis, reducing the overall complexity.

Lastly, we will test the algorithm in both CT and PET to realize both semi-quantitative analysis and quantitative analysis. The accurate relationship between PET data and microsphere data will be built, through which the accuracy of using PET perfusion is determined.

1.6.2 Thesis Outline

Chapter 2 describes the technical development of the algorithm, including the flow chart and how it is developed step by step. A dynamic evaluation curve for each pixel in each slice of imaging data is produced to extract characteristic parameters. The characteristic parameters can include time to peak, maximum slope, and maximum

enhancement. In some cases, the characteristic parameters being extracted can further include wash-out slope and time to wash-out. Based on the extracted parameters, pattern recognition and classification can be carried out.

Chapter 3 is a case study—CT myocardial perfusion study—to investigate the effectiveness and efficiency of the algorithm. The background is introduced first, with the estimated AIF areas included. Following is the description of the experiment procedure. A quantitative analysis is carried out to assess the performance of our algorithm.

Chapter 4 is case study—PET abdominal perfusion study. In this study, the slightly modified algorithm is applied. The backgrounds of PET studies and microsphere study, which is the current "Gold Standard" for perfusion studies, are introduced. Following is the description of the experiment procedures. Quantitative comparison between microsphere studies and PET imaging studies is performed for assessing the consistency and accuracy of the algorithm. Manual selection of AIF and automated selection that we develop are compared to evaluate the effectiveness of the algorithm.

CHAPTER II

TECHNICAL DEVELOPMENT

2.1 Flow Chart

A general process for presenting data obtained from a perfusion study involves taking data obtained from imaging a tracer injected into a patient and presenting the dynamic information as a parametric image associated with anatomy. As previously described, selecting the AIF areas is an important step in obtaining quantitative measurements of blood flow through a region of interest.

Figure 8 shows a process flow for perfusion analysis in which an AIF selector can operate. Referring to **figure 8**, imaging data from an imaging modality such as MRI, CT, or PET can be input to an automated AIF selection module for selection of the AIF areas. Once the selection of the AIF is obtained, a parametric perfusion map can be generated and the map output for display.

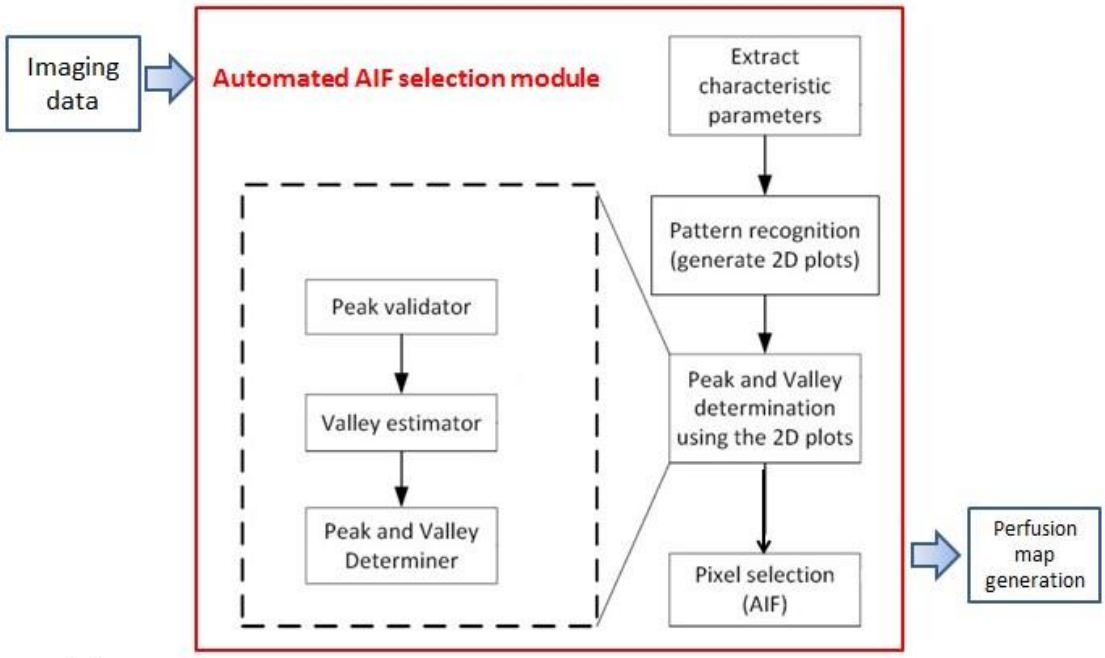

Figure 8. Flow chart illustrates the process flow for perfusion analysis in which an AIF selector can operate.

Inside the automated AIF selection module, imaging data is received and may undergo a pre-processing step. The imaging data contains information of position (slice number), time point (in a time series), and pixel coordinates (e.g. x and y positions). The pre-processing step may be any suitable filtering or processing of data received from an imaging modality, for example, de-noising smoothing techniques or curve-fitting techniques may be applied.

A dynamic evaluation curve for each pixel in each slice is produced to extract the desired characteristic parameters to determine perfusion information about a subject. The characteristics parameters include the three parameters of time to peak, maximum slope,

and maximum enhancement. In the more detailed characteristic parameters selection, two more wash-out parameters should be included: wash-out slope and time to wash-out.

Based on the extracted parameters, pattern recognition is performed to identify relationships between extracted characteristic parameters. The identified relationships are used to classify datapoints of the imaging data for automatic tissue segmentation and AIF area determination. The pattern recognition includes generating two-dimensional plots based on the extracted parameters. The 2-D plots includes a plot of maximum slope vs. time to peak (S vs. T); maximum enhancement vs. time to peak (E vs. T); and, optionally, wash-out slope vs. time to wash-out (W vs. T).

Peak and valley determination is made with respect to the 2-D plots, including a peak validator, a valley estimator, and a peak and valley determiner. The data on 2-D plots can be processed by the peak validator to obtain potential peaks and the valley estimator to obtain potential valleys. The potential peaks and valleys are then used to determine the real peaks and valleys (as opposed to peaks and/or valleys associated with local minimum noise or other artifacts) in the peak and valley determiner. The resulting datapoints are used to select the pixels indicating AIF areas.

Lastly, the selected AIF areas are used to generate parametric perfusion maps for display and analysis.

2.2 Characteristic Parameters Extraction and 3-D Map Generation

2.2.1 Features Selection—Phantom Study

To determine the characteristic parameters of the DEC for the AIF area, we developed a perfusion phantom to mimic blood wash-in (to the tissue) and wash-out processes, which are critical to derive DECs for the dynamic evaluation. In this step, only CT scan is performed due to its low cost and fast acquisition. There is not much difference in using various modalities, because as mentioned before, we are trying to look for the characteristic parameters existing among the dynamic evaluations of all the modalities. In the preliminary study, the phantom was used to build a simplest model to help understand the complicated process better. The use of the phantom eliminates the metabolism process that occurs in the live bodies, since metabolism should not be considered when studying about perfusion. In addition, the use of this phantom reduces the sacrifice of animals.

The design of the phantom is briefly described (**Figure 9**): a catheter with a diameter of 5 mm was used to mimic an artery, and therefore the change of contrast inside the catheter reflected the blood flow inside arteries. A polyurethane open-cell sponge with around 30 ppi porosity was utilized to mimic the tissue. A power injector, infusing iodine as a contrast and followed by flushing out the tracer with saline, helped the wash-in and wash-out processes.

Figure 9. The phantom was scanning using CT.

The CT-TAC for the AIF areas and the CT-TAC for the surrounding tissues in the phantom study are shown in **figure 10A**. In agreement with the hypothesis, the CT-TAC for the AIF areas clearly presents the characteristics features—the highest maximum enhancement, shortest time to peak and sharpest maximum slope—compared to the CT-TAC in the surrounding parts. Compared to the real tissue perfusion, the contrast enhancement in the phantom study stays for a much longer time since there is no natural bloodstream to clear out the contrast quickly. In addition, there is no suitable wash-out process existing in the phantom study. However, even though this preliminary phantom study cannot represent the real tissue function, we particularly chose the early time points with less physiological process involved in both real tissues and the phantom to obtain the characteristic parameters to increase the accuracy. In an ideal tissue perfusion condition, the CT-TACs will be displayed like in **figure 10B**, which illustrates parameters.

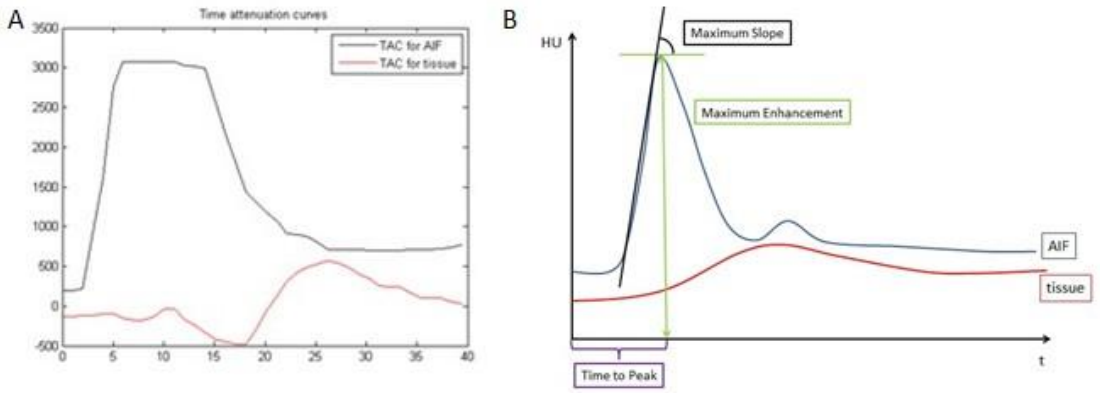

Figure 10. CT-TACs of the AIF areas and that of the surrounding tissues. A: CT-TACs in the phantom study. Blue: AIF; red: tissue. B: Examples of TACs in an ideal tissue perfusion study, with three parameters annotated. Blue: AIF; red: tissue.

The above three parameters are the general characteristics for AIF, but in some cases, only these three characters are not enough to differentiate the AIF from tissues. At this point, we need to find more characteristics for AIF so as to make our technology more solid. For example, if the tracer is completely trapped by the tissues, then this relationship between AIF and the curve of tissues is shown in **figure 11**. There is no wash-out process existing in the tissue. In this case, the wash-out parameters, wash-out slope and wash-out time, can also be considered as characteristics of AIF.

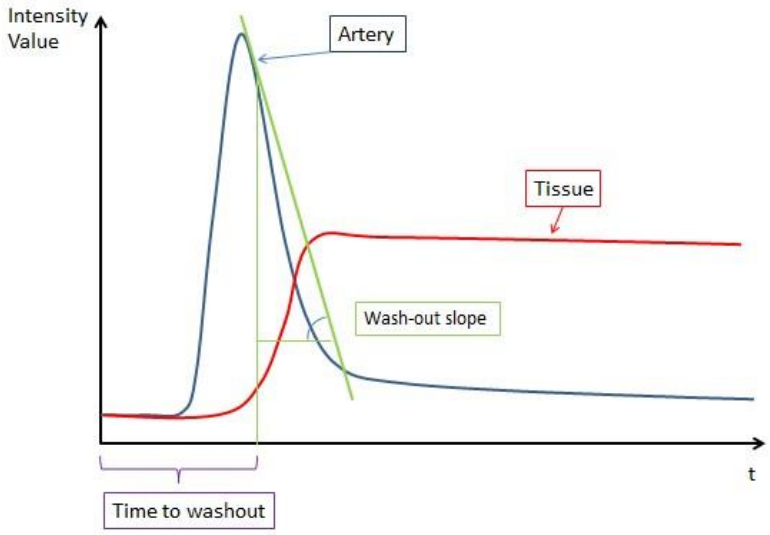

Figure 11. CT-TACs in the case of non-diffusible tracers that are used, with two more characteristic parameters annotated: wash-out slope and time to wash-out. Blue: artery; red: tissue.

2.2.2 Characteristic Parameters Extraction

The 4-D imaging perfusion data, containing the information of position (slice number), time point (in time series), and pixels coordinates (x, y positions), were pre-processed using smoothing techniques. The smoothing techniques can be averaging, curve fitting or interpolation. In this study, interpolation and averaging were used. The DEC for each pixel in each slice was produced to calculate the first three parameters: maximum enhancement, maximum slope and time to peak (**Figure 12**).

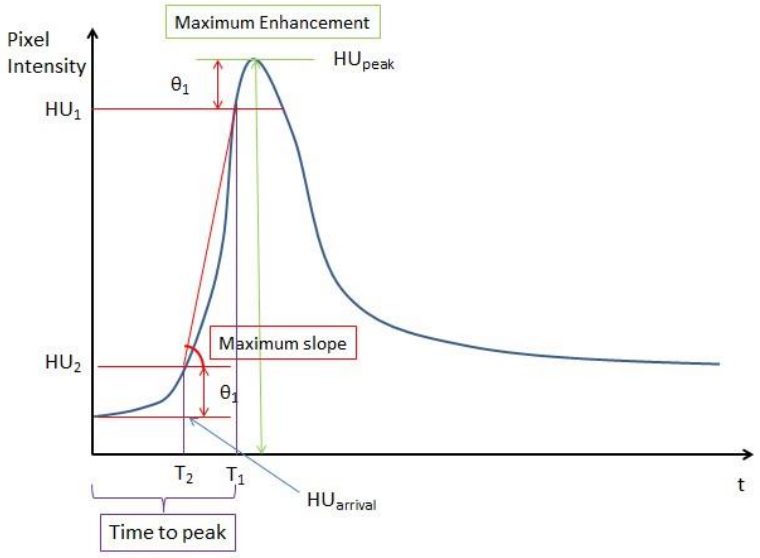

Figure 12. The process of three characteristic parameters—maximum enhancement, maximum slope and time to peak—extraction and calculation.

As illustrated in **figure 12**, $HU_{arrival}$ is the value of the change in attenuation (e.g., Hounsfield Unit) at the point of arrival of the tracer (or "bolus") and HU_{peak} is value of change in attenuation at point of the maximum enhancement.

To address system noise that may exist in a CT system, the calculations using CT imaging perfusion data can include thresholds such as a peak-dependent threshold θ_1 to minimize negative affects to the determination of the maximum slope of a CT-TAC. Thus, the maximum slope can be given as:

$$\frac{HU_1 - HU_2}{T_1 - T_2}, \text{ where} \tag{23}$$

$$HU_1 = HU_{peak} - \theta_1 \tag{24}$$

$$HU_2 = HU_{arrival} + \theta_1 \tag{25}$$

$$\theta_1 = \alpha * HU_{peak}, \quad 0 < \alpha < 1 \tag{26}$$

An optimal value of α can be determined by selecting a steady and characteristic upslope. HU_1 and HU_2 are values of changes in attenuation at the two points selected by threshold θ_1, and T_1 and T_2 are the corresponding time slices.

The time-to-peak is the time at which a change in attenuation reaches the second point selected by the threshold θ_1 that is temporally closer to the maximum enhancement (e.g., at HU_{peak}).

Since the integrate of these three characteristic parameters of time to peak, maximum slope and maximum enhancement represents an uniform change trend, which contains useful information, the absence of any of these means an random signal. Therefore, if a pixel's time-attenuation curve does not show all of the three characteristic parameters, then the pixel can be ignored as being either too noisy for calculation or as being in background of image (and not containing useful information).

For the case that needs one step further, with wash-out process included, the DEC for each pixel in each slice was also used to calculate wash-out slope and time to wash-out (**Figure 13**).

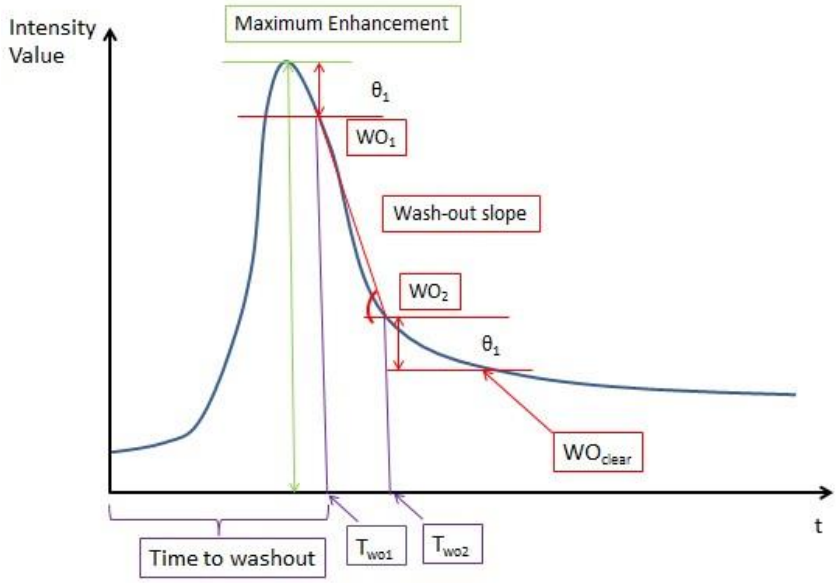

Figure 13. The process of two characteristic parameters—wash-out slope and time to wash-out—extraction and calculation.

Referring to **figure 13**, the wash-out parameter can be calculated in a manner similar to the determination of maximum slope, but on the side corresponding to the tracer being cleared (e.g., the wash-out process). The calculations can use the peak-dependent threshold θ_1 to minimize negative effects to the determination of the wash-out slope of the CT-TAC by using the peak-dependent threshold θ_1 to select two points, the gradient of which is an estimation of the wash-out slope. In particular, the gradient (e.g., the wash-out slope) is given as:

$$WO_{slope} = \frac{|WO_2 - WO_1|}{T_{wo1} - T_{wo2}}, \text{ where} \tag{27}$$

$$WO_1 = I_{peak} - \theta_1 \tag{28}$$

$$WO_2 = WO_{clear} + \theta_1 \tag{29}$$

I_{peak} is the intensity value (or the associated unit for the particular imaging modality) at the point of maximum enhancement, and WO_{clear} is the value at the point where the tracer is cleared up (this value may represent where the tracer is completely cleared up). WO_1 and WO_2 are the values at the two points selected by threshold θ_1 and T_{wo1} and T_{wo2} are the corresponding time slices (e.g., the time values in the acquisition time serial). Time to wash-out can be the time when the dynamic evaluation curve reaches WO_2.

2.3 Pattern Recognition: Multi-Dimension to 2-D Plots

Including the wash-out process, five characteristics parameters should be analyzed, and it would be hard to perform five-dimensional analysis for the classification. To solve this problem, several 2-D relationships were generated in respect with the five parameters for analysis. In this case, we transferred the multi-dimensional problems to several 2-D plots, and this is one of the key concepts for the entire algorithm. Three curves were generated (**Figure 14**): Maximum slope vs. Time to peak (S vs. T) (**Figure 14A**), Maximum enhancement vs. Time to peak (E vs. T) (**Figure 14B**), and optional, Wash-out slope vs. Time to wash-out (W vs. T) (**Figure 14C**).

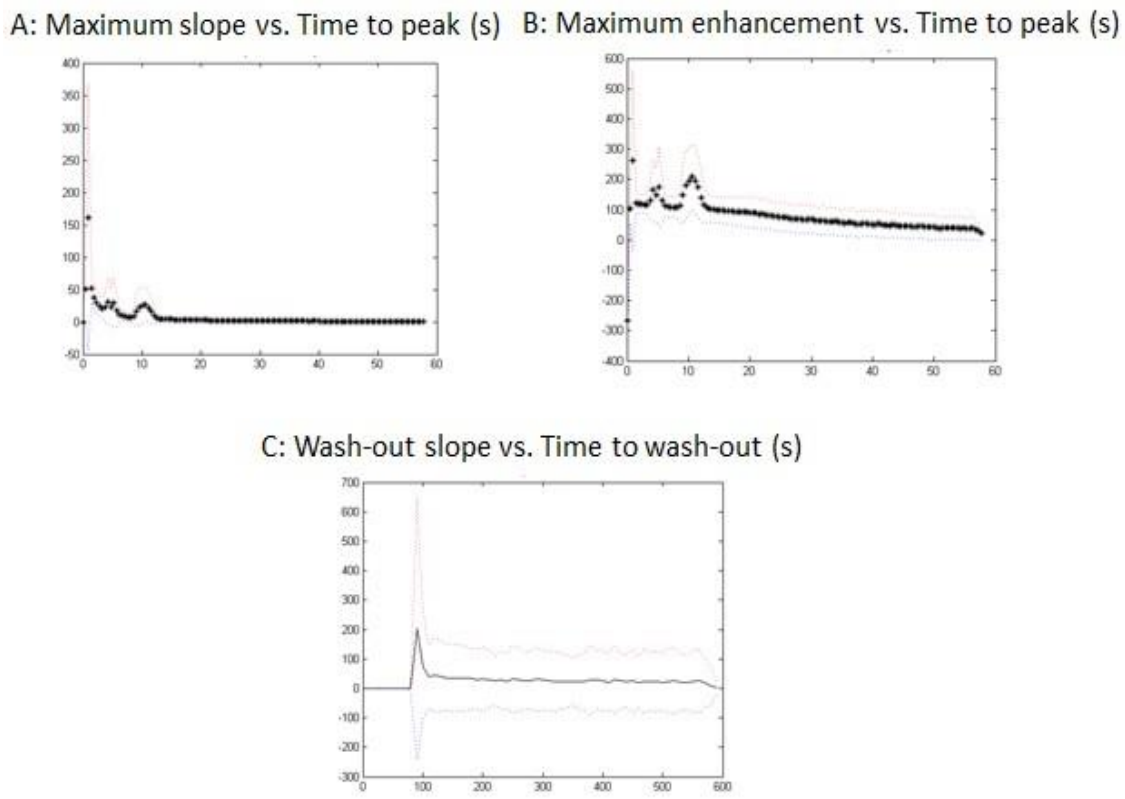

Figure 14. 2-D plots presenting Maximum slope vs. Time to peak (S vs. T) (A), Maximum enhancement vs. Time to peak (E vs. T) (B), and optional, Wash-out slope vs. Time to wash-out (W vs. T) (C).

The pixels that have the same time points were used to generate the curves. For example, the S vs. T curve was generated by extracting all the pixels that have the same time points—time to peak—and taking the average of the slopes of the dynamic evaluation curve of those selected pixels. The black lines or dot lines are the mean values for each time, red lines or dot lines are mean plus standard deviation and blue lines are mean minus standard deviation. Starting now, physiology analysis started to be involved, and the real image data taken from animals was used to the later analysis. The data from the first two curves (S vs. T and E vs. T) were generated from CT myocardial

perfusion study, and the ones from the third curve (W vs. T) were from PET abdominal perfusion study. Regardless of modality, the patterns are similar, because the physics of the kinetic transport is similar, only the measurement method changes.

The three 2-D plots clearly present particular patterns: parabolas or peaks. Each parabolas or peaks represent a physiological phase. Since the S vs. T curve and E vs. T curve are not independent, they show a similar pattern. In fact, they have a linear relationship. Therefore, once the patterns of S vs. T curve are analyzed, those of E vs. T curve are indicated. In this case, only S vs. T was chosen to perform the later analysis.

In the S vs. T (also in the E vs. T) curve, there are two parabolas, gradually ascending and then descending. The formation of parabolas means some pixels during this time to peak period have very steep slopes (and very high enhancements). According to the analysis before, these areas are usually blood pool areas. When evaluating the physiological process in this experiment, the physiological phases vary case by case. In this trail study, myocardial CT perfusion imaging was performed to test blood flow in the myocardium. The tracers were injected through a vein, and therefore the first blood pool areas are the right ventricle and the associated venous system. The second blood pool areas contained in the second parabola are left ventricle and the associated arterial system. When considering the AIF, the blood feeding areas are inside the second parabola. The number of the parabolas, referred to physiological phases varies with tissues due to the variable physiological processes in different tissues. For

example, in the liver, there might be two peaks: arterial phase and venous phase. The number can also change based on the scan phases we are imaging. Therefore, the emergence of different numbers of phases relies on the tissues and imaging protocol. Because the variables are known before a perfusion study, the particular pattern can be known. In such case, by selecting the specific pattern can this automated proceed simultaneously, and the patterns are not varied with operators.

It should be understood that before the first parabola, the scattered points represent bones and interference tissues (usually with fluid (not blood) inside). The sharp slopes and high enhancements are due to the high attenuation caused by bones and some tissue fluids. Before the tracer washes in, this noise weighs more. However, once the tracer washes in, the dynamic change of tracer dominates.

In the W vs. T curve, there is one peak. The formation of peaks, instead of parabolas, is due to the much longer acquisition of PET imaging (due to rapid transition between peaks) than that of CT imaging. This peak contains the information of the areas that have wash-out process. Since in this experiment, a non-diffusible tracer was used, only blood pool areas have wash-out process. Therefore, the AIF areas are presented in this peak area. The same thing as in the S vs. T curve, number of the phases depends on the tissues and imaging protocol, and it can be known before a perfusion study.

In order to realize the automated determination of AIF areas, automatically recognizing the locations of physiological phases and the tracer arrival point for each physiological phase is the key. In other words, we need to recognize valleys and peaks/parabolas on the 2-D plot curve.

Figures 15, 17, 19 and 21 show detailed process flow diagrams of an example method of selecting AIF areas. It includes the steps of initialization, peak validation, valley estimation, peak & valley determination and AIF determination. Since the operation processes are similar among the three curves (S vs. T, E vs. T and W vs. T), only S vs. T is selected for describing the operation process.

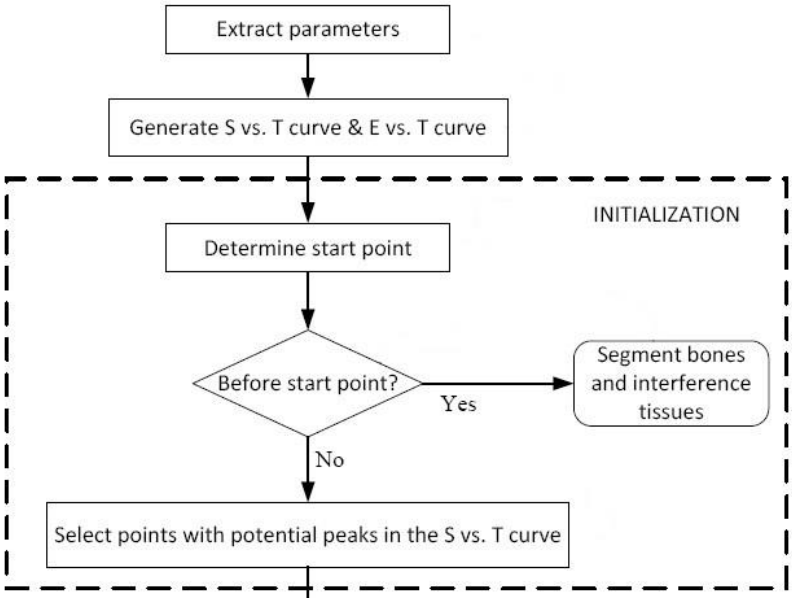

Figure 15. Initialization step of the automated process.

Referring to **figure 15**, an initialization process is performed to segment pixels indicating bones and interference tissues. To segment (i.e., remove) bones and

potentially interference tissues, a threshold θ_2 can be set to provide an absolute number limit for the first derivative of the S vs. T curve based on the principle that bones and interference tissues show sharp slopes. To find the start point (the bolus arrival point of the first peak) (**Figure 16A**), a zero-crossing method can be used. For some imaging modalities, such as CT, the start point is located in the first valley. Therefore, bones and interference tissues can be automatically segmented by setting the time restriction before the start point (**Figure 16B**). Once the start point begins, the dynamic change of the tracer dominates and the later process can be performed.

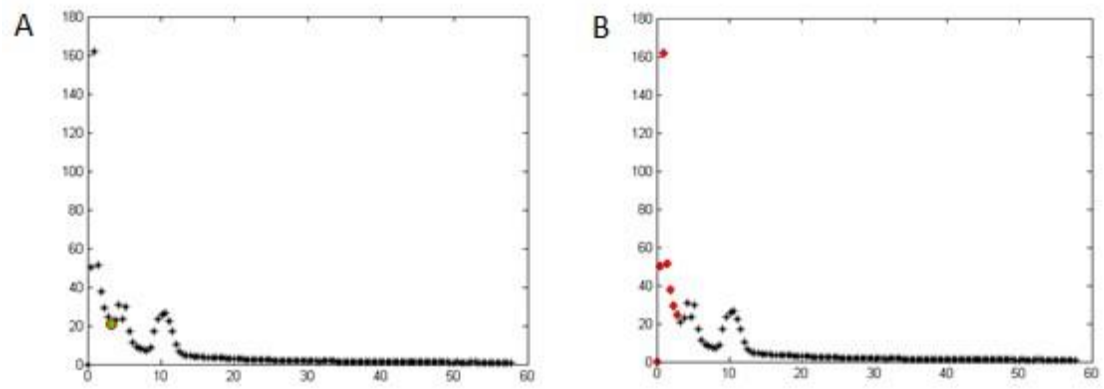

Figure 16. Initialization process. A. start point; B. datapoints indicating bones and interference tissues segmentation. Label: x-axes are times (s), and y-axes are slope value.

Then it comes to the peak validation process to find peak candidates (**Figure 17**).

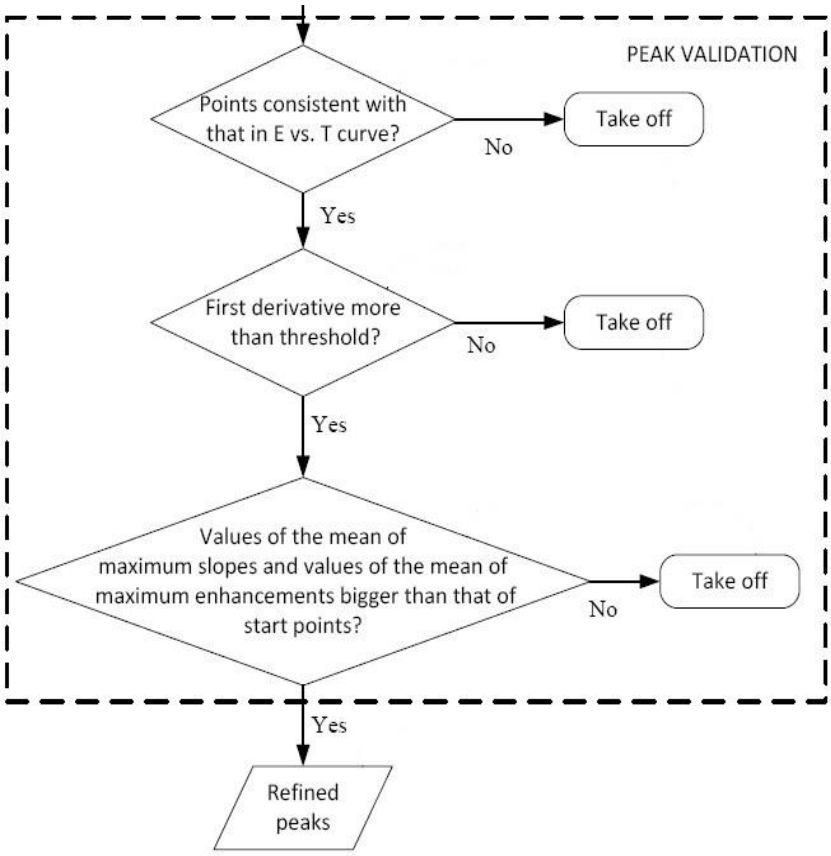

Figure 17. Peak validation step of the automated process

From the start point, the potential peak selection uses the zero-crossing method by looking for downward zero-crossings in the first derivatives of the S vs. T curves. Once the points are selected in the S vs. T curve, peak validation can be carried out. As mentioned before, the E vs. T curve has linear relationship with the S vs. T curve, and they should keep a consistency for each physiological phase. By this way, random noise can be eliminated. Therefore, a determination is made as to whether the selected points indicative of potential peaks in the S vs. T curve are consistent with that in the E vs. T curve (**Figure 18 A&B**). If a point is not consistent between the S vs. T curve and the E

vs. T curve, then the point is removed from being indicated as a peak. If the point indicative of a potential peak in the S vs. T curve is considered consistent with that in the E vs. T curve, then a determination is made as to whether the first derivative of the curve at the point is more than a threshold (θ_3). This threshold is provided to remove small peaks, which may be indicative of noise or other signals.

In some cases, small recirculation peaks exist that vary with the amount of the tracer in the scanning. In order to remove very small recirculation peaks that can be neglected the values of the mean of maximum slopes and the values of the mean of maximum enhancements should be bigger than those at the start points, respectively. Accordingly, a determination can be made whether the mean values at the points are bigger than that of the start points. If the values are not bigger, then the point can be removed.

The results of peak validation provide data regarding the refined peaks (**Figure 18C**).

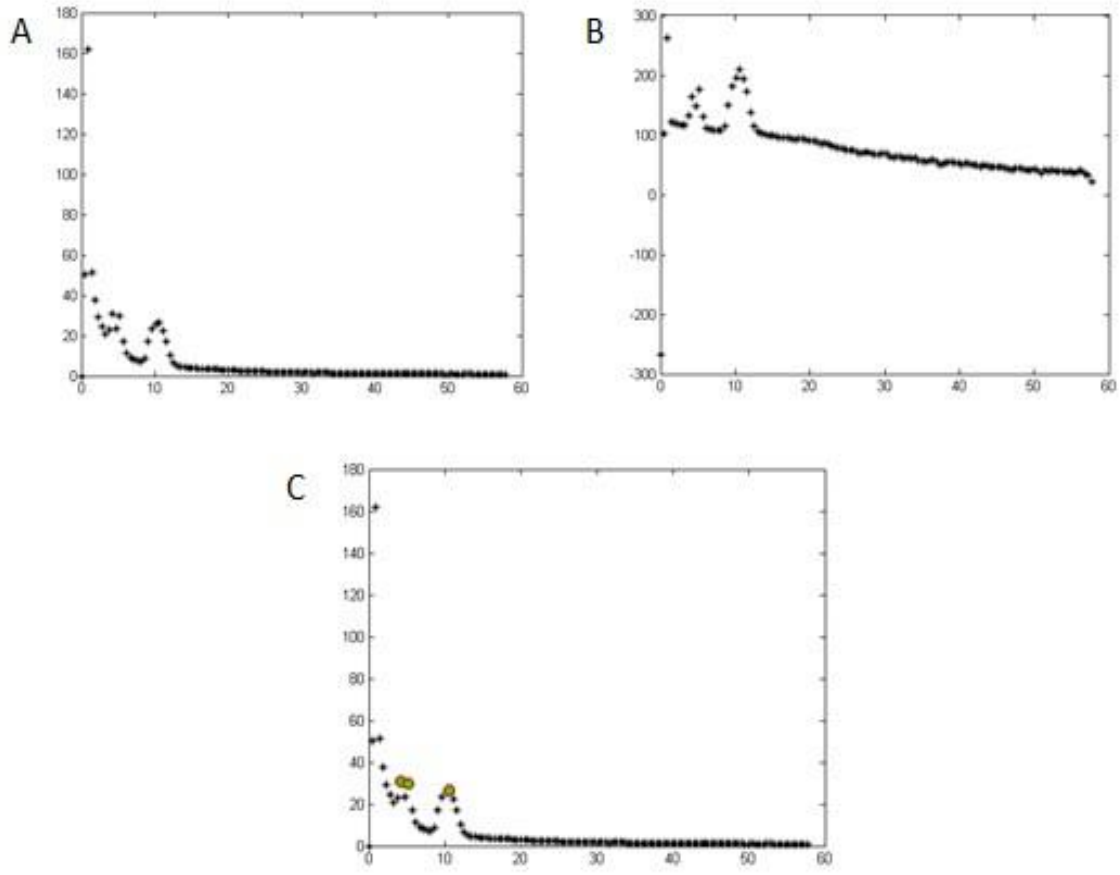

Figure 18. Peak validation process. A, B: an example S vs. T curve (A) and E vs. T curve (B), respectively. C: refined peaks/peak candidates indicated in the green points. Label: x-axes are times (s), and y-axes are slope values (A), enhancement values (B) and slope values (C), respectively.

The step of valley estimation (**Figure 19**) is to look for refined valleys which potentially are the tracer arrival point for each physiological phase.

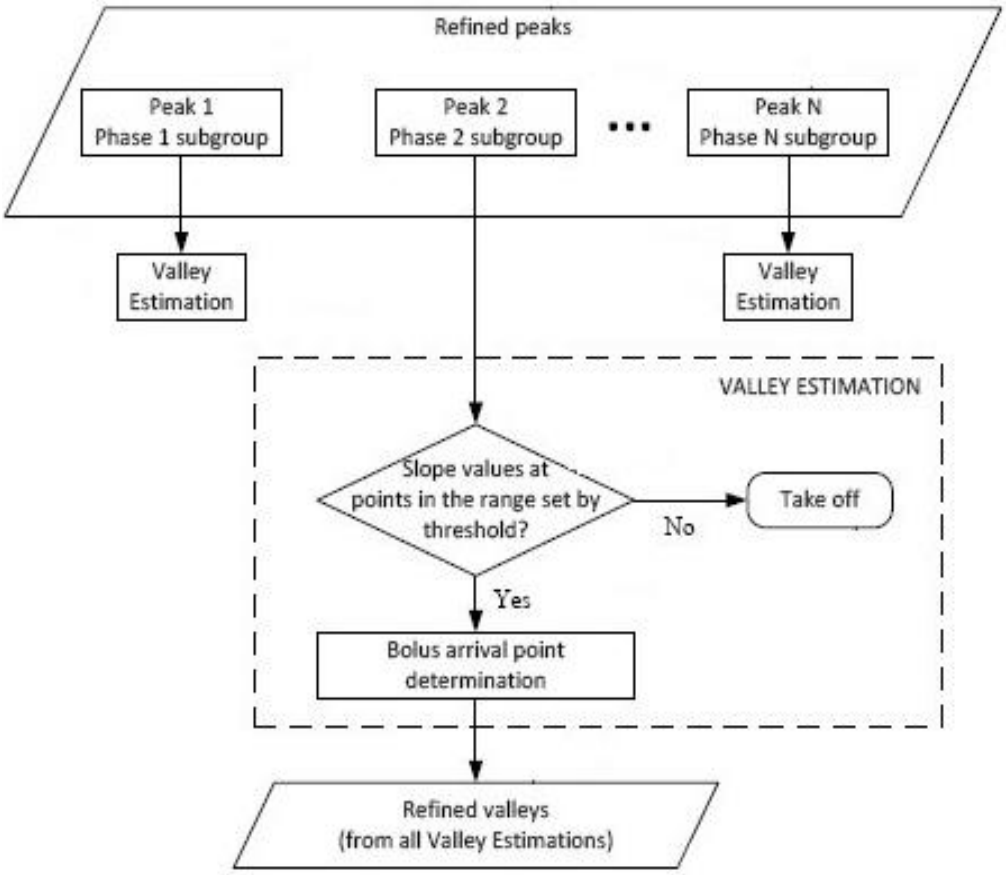

Figure 19. Valley estimation step of the automated process.

The potential valleys are determined by the upward zero-crossing method. For each physiological phase (presenting as a parabola), there is one valley and one peak. A subgroup is assigned for each peak candidate/refined peak in the data regarding the refined peaks. A subgroup contains all the potential valleys having time to peaks between that of the peak (with which the subgroup is assigned) and that of the previous peak. For example, the peak candidate Peak 1 can have a phase 1 subgroup assigned that

contains a collection of points of potential valleys between the start point and the first peak (with the start point included). The peak candidate Peak 2 has a phase 2 subgroup assigned that contains a collection of points of potential valleys between the first peak and the second peak. This arrangement continues for all peak candidates through Peak N, which is assigned a phase N subgroup containing a collection of points of potential valleys between the previous peak (e.g., N-1) and its peak (**Figure 20A**).

Valley estimation is then carried out with in each subgroup. Since the tracer arrival point for each phase is generally among the few lowest valleys in each subgroup, a peak-dependent threshold θ_4 is used to obtain the valley range. A determination is then made to whether the slope values are within the range set by the threshold. The arrival time point for each peak candidate is the last valley within the valley range assigned to the phase. The threshold θ_4 is used to remove small valleys that should be neglected. The threshold θ_4 and valley range R_{valley} can be given as:

$$\theta_4 = \beta * S_{peak} \tag{30}$$

$$R_{valley} = S_{lowest} + \theta_4 \tag{31}$$

S_{peak} is the mean of the maximum slopes in the range containing the peak point, S_{lowest} is the lowest mean of the maximum slopes among all the boxes in this subgroup, and β is a variable for setting the threshold. An optimal determination of the threshold θ_4 is to ensure that the valley range will not cover the points in the upgrade part of the S vs. T curve, and at the same time, to remove the small and noisy valleys.

If the slope value is not within the range R_{valley}, the point can be removed; however, if the slope value is within the range, a determination of the tracer arrival point can be made and the results of the valley estimations for each subgroup can provide the data regarding the refined valleys (**Figure 20B**).

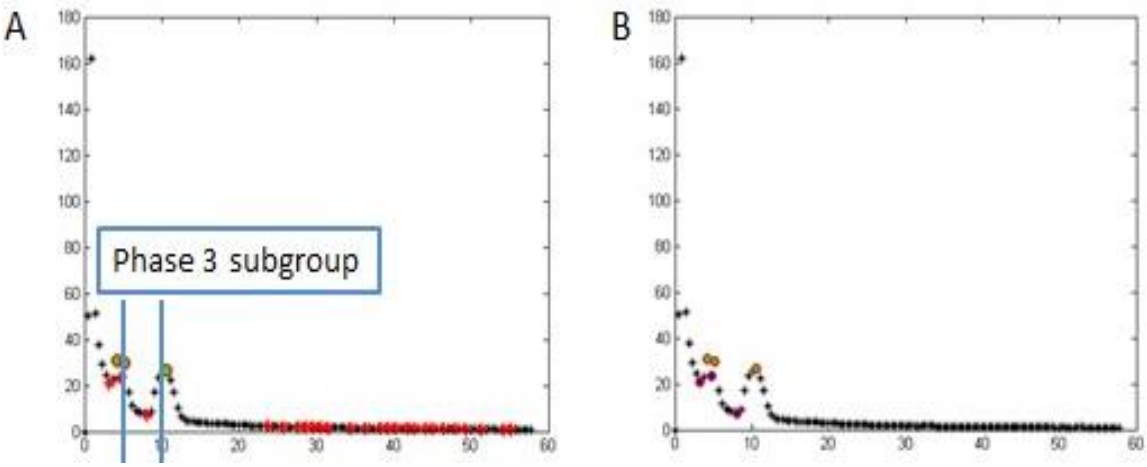

Figure 20. Valley estimation process. A. an example of Peak 3 subgroup assignment (red points: potential valleys; green points: peak candidates); B. refined valleys (purple points) and refined peaks (green points). Label: x-axes are times (s), and y-axes are slope value.

Figure 21 illustrates peak & valley determination using.

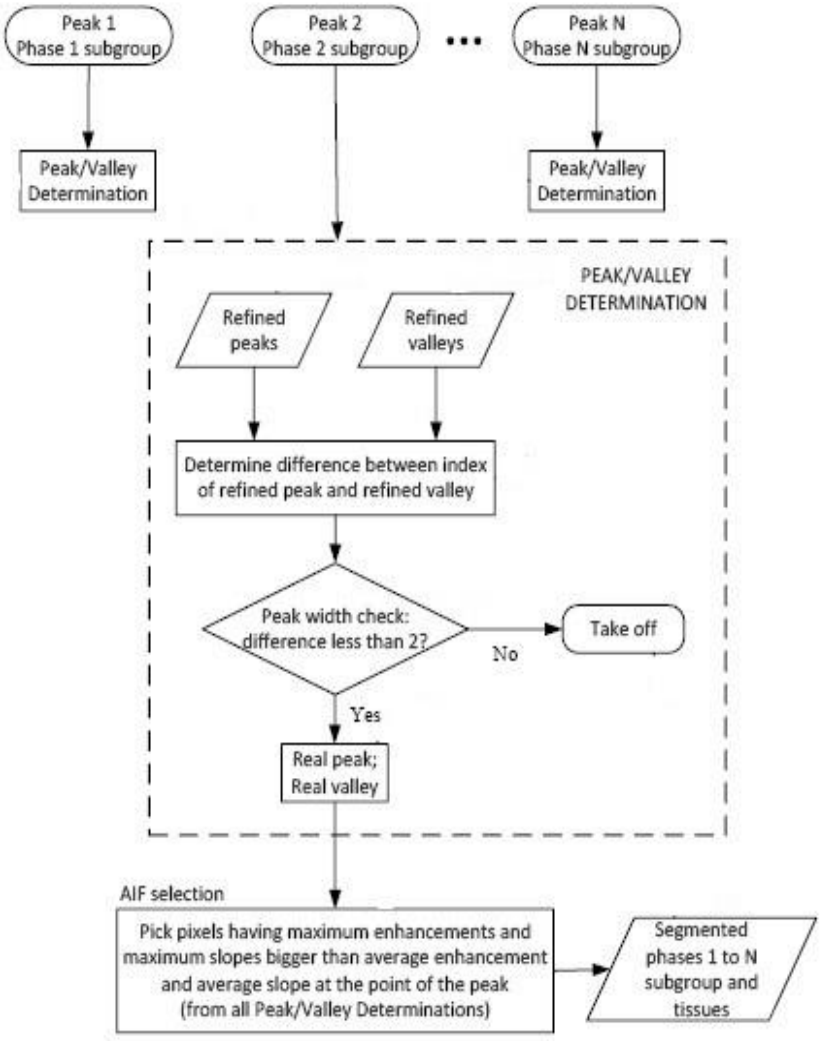

Figure 21. Peak & valley determination step of the automated process.

The refined peaks and refined valleys obtained through the peak validator and valleys estimator are used to determine the phases having real peaks and valleys. Each phase subgroup has its associated peaks and valleys determined. The difference between the index of a refined peak and refined valley can be determined using the refined peaks

and refined valleys for the phase 2 subgroup. The "index" refers to the coordinates of the points on the plots. A peak width threshold is used to ensure that the peak and the valley are not nearby each other, since in the physiological term, any change will not be that rapid. In this case, a width threshold may be 2 time segments. A determination is then made whether the index difference is less than 2. If the peak width is less than this threshold, the point can be determined to be a real peak or a real valley (**Figure 22**).

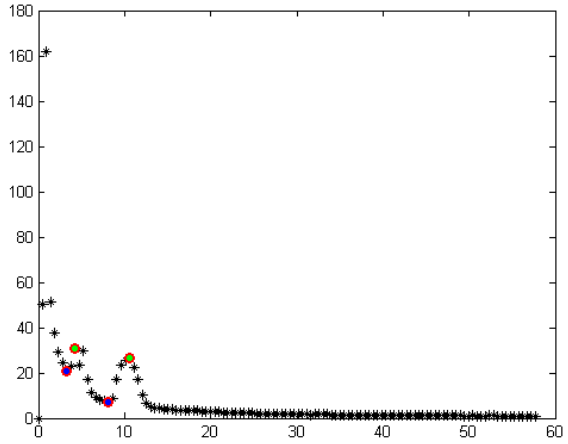

Figure 22. The result showing selected real valleys (purple points) and real peaks (green points). Label: x-axis is time (s), and y-axis is slope value.

By using the automatically determined phases with detected peaks and valleys, and on the basis of the physiological condition of the tissue, the phases containing AIF can be selected (**Figure 23**). Since the general tissue perfusion is also present in the AIF phase, the AIF can be determined by performing calculations refining the blood pool. The maximum enhancement and the maximum slope of an AIF are generally higher than that of tissues, and these two variables depend on the amount of tracer and the injection rate. In the general situation, the pixels that are in the AIF areas are the ones with the

maximum enhancements bigger than the mean enhancement at the point of the peak in the AIF phase, with the condition that the maximum slopes are bigger than the mean slope at the same point. Accordingly, AIF selection is carried out by picking pixels having maximum enhancements and maximum slopes bigger than the average enhancement and average slope at the point of the peak. The results of AIF selection provide segmented tissues. In an optional term, when consider wash-out process, the AIF selection further includes calculating wash-out slope and selecting the sharpest wash-out slope, which is determined to be bigger than the average wash-out slope at the point of the peak on the W vs. T curve; and calculating time to wash-out and selecting the shortest time to wash-out. The additional computations can be optional, depending on the type of tracer and the size of blood feeding areas undergoing the perfusion studies. The optional computations are usually included when trappable tracers are being used for the perfusion studies.

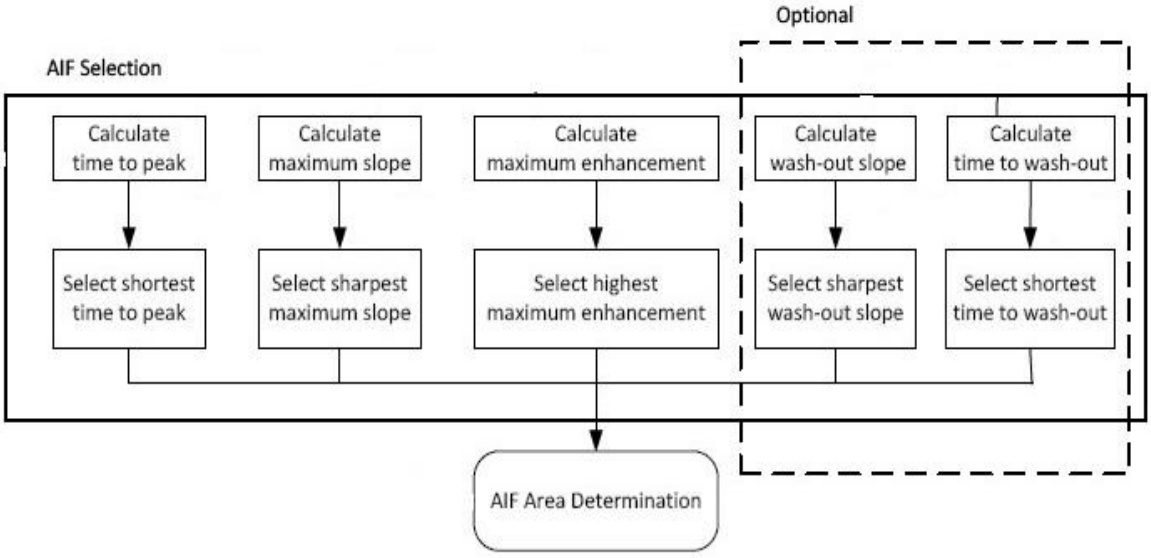

Figure 23. AIF determination step of the automated process.

For example, when blood feeding areas are large, such as the area of the left ventricle and arteries (as compared to myocardium – which also does not indicate a high uptake of tracer), the difference between blood pool areas and tissues with respect to maximum slope and maximum enhancement stands out.

In contrast, when blood feeding areas are very small, especially when the uptake of the tracer in some tissues, such as kidney, is too large to provide a clearly distinguishable difference between arteries and such tissues, it can be difficult to determine the appropriate maximum slope and the maximum enhancement. A non-diffusible tracer may be biologically trapped by certain tissues. Thus, inside blood pool areas, a non-diffusible tracer behaves similarly to a diffusible tracer. However, for the certain tissues, the non-diffusible tracer can become completely trapped by the tissue. In such cases, the tracer cannot be washed out from the tissue. It should be noted that the maximum enhancements of tissues are not necessarily lower than those of arteries.

Examples of such studies include cerebral perfusion analysis and abdominal perfusion analysis. For these cases, the wash-out process which is more distinguishable than the maximum slope and the maximum enhancement is extracted to execute the pattern recognition and determine the appropriate AIF areas. For the wash-out parameters extraction, the peak validation can be carried out in a similar manner as with the S vs. T and E vs. T curves. For example, zero-crossings in the first derivative that exceed a threshold are searched.

An automated AIF selector is presented that is applicable to many imaging modalities and tissue types with slight variations according to the physics of an imaging modality and tracer properties. For example, PET imaging is different from CT imaging in that there is less interference from bones and fluid. In particular, unlike the CT imaging data affected by the bones and fluids resulting in large attenuation, the start point (the tracer arrival point of the first peak) in the PET imaging data does not appear like a valley, but simply is an initial position for the following peak. This point can be obtained by looking for the first derivative that exceeds a threshold. Peaks and valleys are easier to be picked by simply looking for downward (for peaks) and upward (for valleys) zero-crossings in the first derivative that exceed another threshold. Due to less noise involved, the automated determination of peaks and valleys in PET studies can be simplified to omit steps for the noise removal.

The example of resulting AIF is shown in **figure 24**. It clearly demonstrates that AIF involves the tracer kinetics of baseline, wash-in, wash-out and steady state. A recirculation occurs due to the use of a slightly large amount of tracer injected.

This automated AIF determination technique replaces the conventional spatial classification method with physiological and functional classification method. In other words, it not only utilizes mathematical thinking, such as classification, dimension reduction and pattern recognition, but also takes more physiological considerations and explanations involved. In such way, physicians are able to understand and use this

technique in their perspectives. In addition, it does not require pre-knowledge of expected location of AIF areas, as the spatial classification does. Furthermore, this technology is based on pixel-wised characteristics analysis, and therefore despite the scattered distribution of the blood supply areas, the selection of input function pixels is still efficient and effective. Also, this technology is very straightforward; the dimension reduction on the multidimensional problems into several 2-D plots questions simplifies the entire calculation and analysis procedures. Last but not least, the process of noise removal in the procedure of "Peak and valley determination using the 2-D plots" is very robust, because it was developed based on CT signals, in which more background noises exist compared to PET and MRI signals. In this way, this technique can be used in perfusion calculations from both CT and PET, and might be extended to MRI.

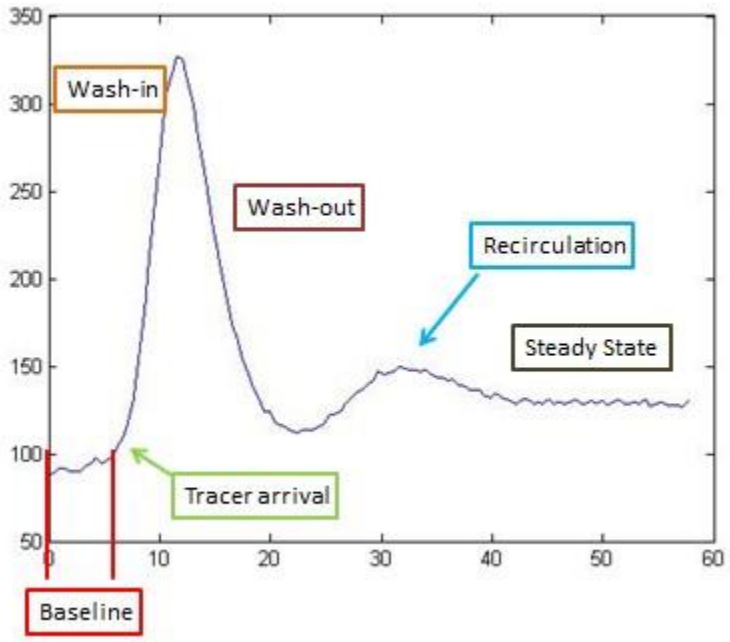

Figure 24. An example of resulting AIF. X-axis is time (s), and y-axis is in the unit of HU (Hounsfield Unit).

CHAPTER III

CASE STUDY—MYOCARDIAL CT PERFUSION

3.1 Introduction

3.1.1 Coronary Artery Disease

Coronary artery disease (CAD) is a leading cause of death in the developed world and the most common cause of mortality in the United States. CAD is a type of disease in which blood supply to the myocardium—heart muscle—is reduced due to narrowing in coronary arteries. The clinical problems associated with CAD are chest pain and myocardial infarction (MI) that causes heart attacks. The reduction in coronary blood flow results in absence of nutrition and oxygen exchange, and the state of oxidative stress would affect cardiac functions, such as heart rate, systolic wall stress and contractility. Each year, it is estimated of around 1.2 million Americans suffer MI clinically, and a further 195,000 cases of silent MI occurs each year (*44*).

In order to maximize the medical management in CAD, research has been directed to the early detection, risk stratification and identification of CAD. It is important in non-invasive assessment of MI using medical imaging techniques because the imaging modalities are able to simultaneously provide both anatomical and functional assessment of MI. MI is presented by decreased myocardial perfusion, which refers to capillary-level blood flow in the myocardium.

3.1.2 Medical Imaging Used for Myocardial Perfusion Studies

In the past decades, the functional imaging of myocardial perfusion has been mainly dominated by nuclear imaging techniques—SPECT and PET—as the clinical gold standard. They show very high diagnostic accuracy with a specificity ranging from 87% - 94% and a sensitivity ranging from 85% - 90% (*11*). However, the costs associated to the two modalities are moderately high, and the two techniques still fall short of enabling quantification of transmural differences in the myocardial perfusion. Semi-quantitative measurement of myocardial perfusion using the MRI technique has been widely studied in research settings, with the sensitivity of 89% and the specificity of 87% (*11*). It does not require exposure to ionizing radiation and has greater flexibility of anatomical coverage. However, no metals should be involved in MRI imaging, since metal-based materials can interfere with magnetic fields. Additionally, MRI imaging requires a longer acquisition time. CT perfusion is capable of simultaneously providing both anatomical and functional assessment of myocardial infarction and its advantages of rapid acquisition time, nearly unaffected by heartbeat rate and the linear relationship between the attenuation and the concentration of the contrast will facilitate the quantitative measurement of hemodynamic parameters.

3.1.3 AIF Addressed for Myocardial Perfusion Analysis

To assess myocardial perfusion, the region of interest (ROI) that is selected as AIF for perfusion calculation is set either on the aorta (*30*) or on the left ventricle (*45*). However, AIF should be positioned in all the areas that feed blood into the tissues of

interest rather than only the aorta or left ventricle. **Figures 25 (A, B)** shows the 3-D heart external structure and blood supply areas.

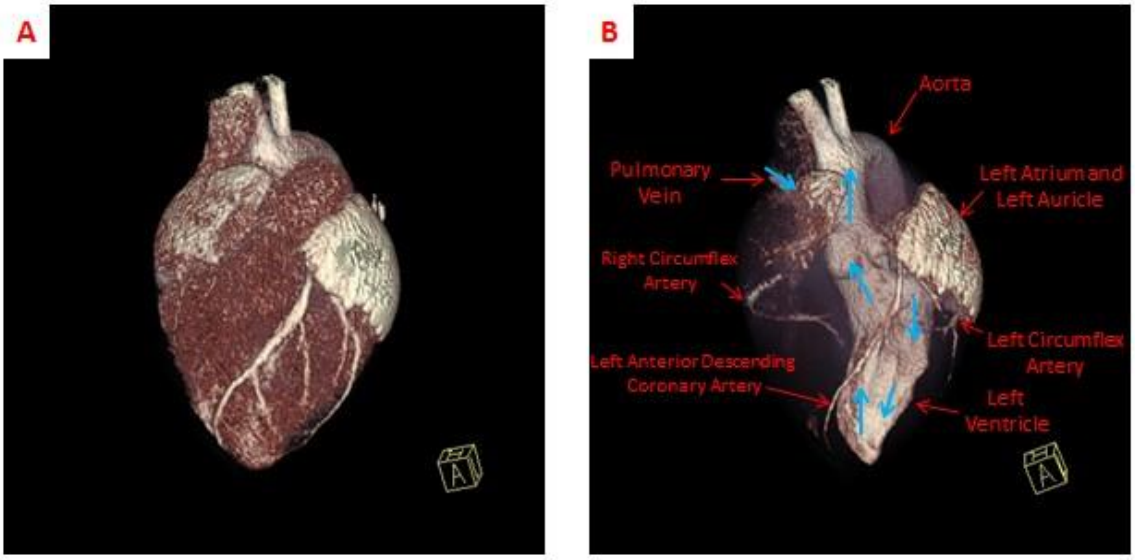

Figure 25. Heart structure (A) and cardiac blood pool and the myocardial blood supply (B). In the figure of B, the red arrows present the blood pool for supplying the myocardium; the blue arrows represent sequential blood flow: pulmonary vein → left atrium → left ventricle → aorta → coronary arteries.

Generally, the circulatory system in the body can be divided into either pulmonary circulation or systemic circulation. Deoxygenated blood returns from the body through the systemic venous system into the two major veins, the cranial and the caudal vena cava, which terminates in the right atrium. From the right atrium the deoxygenated blood is pumped to the right ventricle and subsequently into the main pulmonary artery. The main pulmonary artery quickly bifurcates into the right and left pulmonary arteries, which supply their respective lungs. Blood subsequently passes through the pulmonary capillaries where gas exchange occurs and continues into the pulmonary veins, left atrium, left ventricle and aorta. The coronary arteries supply the

myocardium and originate at the proximal part of the aorta. The major arteries of the coronary circulation are the left coronary artery, which divides into left anterior descending and circumflex branches, and the right coronary artery. Both of them originate at the base of the aorta, and lie on the surface of the heart, referred to as the epicardial coronary vessels. These arteries distribute blood flow to different regions of the myocardium and are classified as heart end circulation because they are the only blood supply source for the myocardium. Coronary artery disease is always caused by the blocked coronary arteries, and the damage of any of these three arteries will lead to critical outcomes.

Based on the above described system, the pulmonary veins, left atrium, left ventricle, aorta and the arterioles (the last small branch of the arterial system from where the blood is released into the capillaries) are considered AIF areas. The direct blood supplies for the myocardium are coronary arteries, however, only coronary arteries to be the AIF can cause significant underestimation of the arterial TAC due to partial volume averaging (*46*). The current technologies will only pick the left ventricle or aorta, because they need pre-knowledge of where the AIF areas are located.

3.2 Materials and Methods

3.2.1 Animal Preparation

In this example, a pig weighing 50 kg was used as a model of myocardial ischemia and reperfusion in this study after approval from Institutional Animal Use and

Use Committee (IACUC). Myocardial infarction was induced by using cardiac catheterization to occlude the blood flow of the left anterior descending (LAD) coronary artery for 90 minutes. CT scans were performed prior to and after the intervention.

3.2.2 Tracer Validation

The key for the quantitative analysis is how to transfer the value from the modality—CT number to the concentration of the tracer. In this study, iodine (Omnipaque 350) was used as the tracer for dynamic evaluation of perfusion. As aforementioned, the CT perfusion technique is based on the linear relationship that the change in attenuation is directly proportional to the concentration of the tracer material (*30*). To validate the relationship between the concentrations of iodine with CT number, a phantom study was performed. Five centrifuge tubes were filled with 15 ml sheep blood sample (heparin was used to prevent blood clotting) containing iodine with the concentrations of 0%, 1%, 5%, 10% and 15%. The contained iodine in each tube was mixed well with blood using glass rod. It should be noted that the mixing process should not cause bubbles inside, since bubbles have an influence on the later imaging. The five centrifuge tubes were arranged in parallel and placed on the bed of CT scanner. The CT scan was performed using 80 KV of voltage and 120 mAs of current.

3.2.3 CT Scan Imaging Protocol

The CT scan was performed with a 128-slice CT multi-row detector CT (MDCT) scanner (Biograph mCT, Siemens, Knoxville, USA) with a gantry rotation time of 300

ms. The tracer of iodine (Omnipaque 350) was infused through the vein at a rate of 4 ml/s. In the before-infarcted study, the amount of tracer used was 12 ml, and the after-infarcted study, the amount was 24 ml. The difference in tracer amount is used to test the tracer-dependency of the automatic AIF selection algorithm. For both of the studies, a saline chaser of 64 ml at the same injection rate as that of tracer was utilized for wash-out process. The scan was started 2 s after the initiation of the tracer injection and continued for 70 s such that the tracer can move through the entire heart. It was located through the entire heart. Twenty four slices of images were obtained with 3 mm slice thickness. The image protocol was performed at 80 KV due to the photoelectric effect for 80 KV photons, which are closer to the "k-edge" of iodine (*31*). Based on this kilovolt, the constant milliampere-second was set to be 120 mAs. Values for effective radiation dose were calculated by multiplying the dose-length product with a conversion factor ($k = 0.014$ mSv/mGy ×cm).

After imaging, a cardiac phase of 52% was selected for both before-infarcted and after-infarcted studies to achieve the least motion and artifacts, and also to contain both left ventricle and right ventricle. A medium-smooth convolution kernel (B30f) was chosen to ideally reflect the iodine content in the myocardium. The axial images obtained by cine mode scan were reconstructed into 3600 images and a beam-hardening correction was applied in the reconstruction kernel to prevent beam-hardening artifacts that mimic the appearance of myocardial perfusion defects.

3.2.4 Algorithm Implementation

In this case, the blood feeding areas are large, the difference between blood pool areas and tissues with respect to maximum slope and maximum enhancement easily stands out. Three characteristic parameters—maximum slope, maximum enhancement and time to peak—are sufficient to differentiate the AIF areas from other tissues.

In the "characteristic parameters extraction and pattern recognition" step, we set α yield to 0.3 to give us a steady and characteristic upslope. In the "automated determination of AIF and segmentation of tissues" step, based on the principal of bones and interference tissues showing big attenuation, we set the threshold θ_2 that was used to take off those tissues as 100. The slope derivative threshold θ_3, which was used for removing small peaks, is set to be 3. To set threshold θ_3, the variable β was determined as 0.1, so that the valley range was enough for taking off the small and noisy valleys without covering the points in the upgrade.

Since different amounts of tracers were used before and after the infarction, the AIF determination strategy needs to be changed a little bit. "Maximum enhancement" is an absolute number change, and the larger amount of tracer would cause a much bigger enhancement showing in the E vs. T curve. However, "maximum slope" is a relative number change, and the larger amount of tracer will not affect the appearance of S vs. T curve too much. Accordingly, in the before-infarcted study, the pixels are picked with the maximum enhancements bigger than the mean enhancement at the point of the peak

in the arterial phase, whereas in the after-infarcted study, the pixels are picked with the maximum enhancements bigger than the mean plus standard variation of the enhancement at that point. For both studies, the AIF pixels selection are under the same condition that the maximum slopes are bigger than the mean slope at the point of the peak in the arterial phase.

3.2.5 Perfusion Maps Generation

Once AIF was selected, perfusion parametric maps were generated for each slice (each position). To obtain the perfusion maps, the maximum slope method was used. Again, myocardial blood flow (MBF) is computed as the ratio of the maximum slope of tissue TACs to the maximum arterial concentration.

To make the perfusion parametric maps clearly show how blood flow distributes over the entire block of the tissue, we used OsiriX Imaging Software to reconstruct 3-D volume for perfusion maps.

3.3 Results and Discussion

3.3.1 Characteristic Parameters Extraction and Pattern Recognition

Through the characteristic parameter calculation algorithm, the three parameters were extracted: maximum enhancement, maximum slope and time to peak. After the 3-D parameter maps were converted into two 2-D plots (S vs. T curve and E vs. T curve), the patterns for both curves were presented clearly (**Figure 26 (A, B, C and D)**).

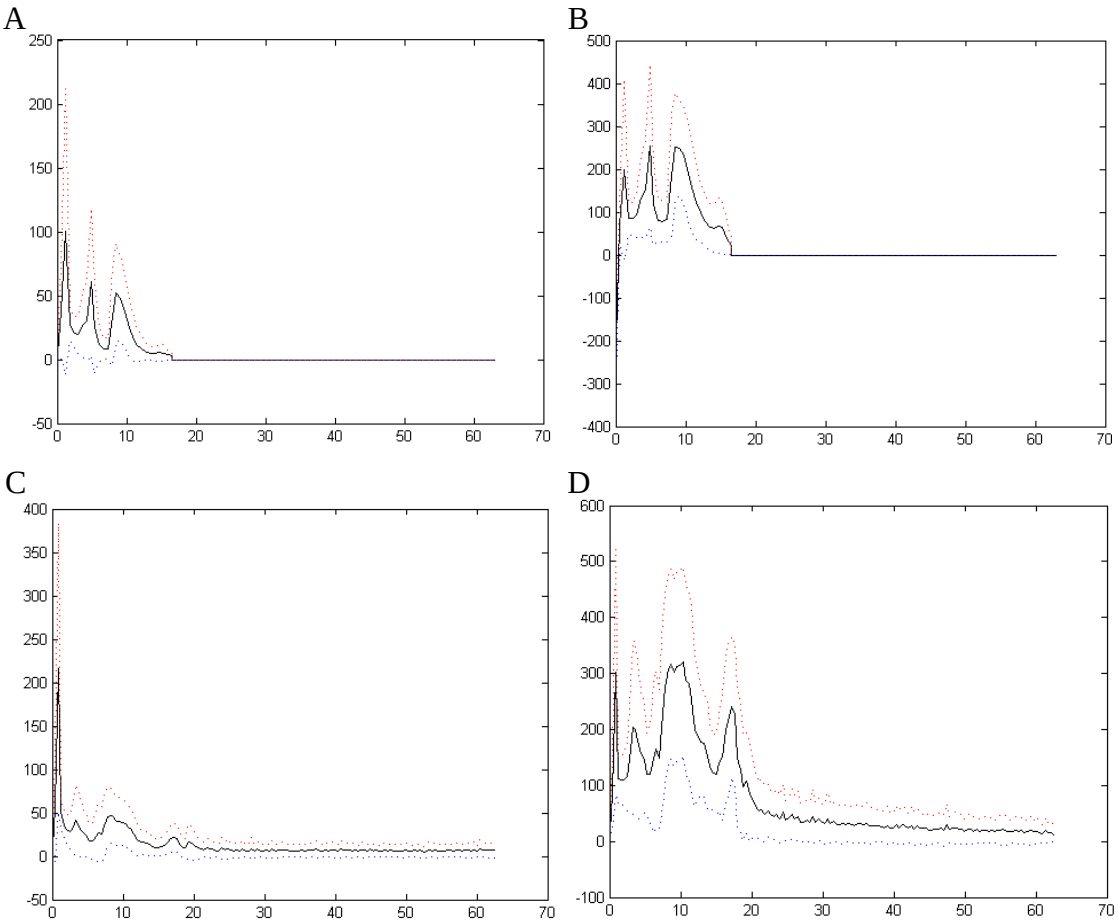

Figure 26. The 2-D plots—S vs. T curves (A, C) and E vs. T curves (B, D) for both before-infarcted study (A, B) and after-infarcted study (C, D).

On both S vs. T and E vs. T curves, the very sharp peaks or valleys that occur before the tracer arrives are caused by bones and interference tissues with fluid (not blood) inside. After the tracer arrival, since the tracer was infused from the vein, the first peak (or parabola) represents the contrast enhancement of the right ventricle and the associated venous phase. The second peak (parabola) demonstrates the contrast enhancement of the left ventricle/atrium, pulmonary veins, the aorta and its branches. The third peaks on both curves in the after-infarcted study are associated with the blood

recirculation to the right ventricle. However, in the before-infarcted study, the third peaks are not obvious because the amount of the tracer injected was half of that in the after-infarcted study. Therefore, the occurrence of the third peaks is tracer-dependent. AIF is not computed by recirculation, or the effect is too small to consider.

3.3.2 Automated Determination of AIF and Segmentation of Tissues

The automated processes for selecting peaks and valleys for both studies are shown in **figure 27**. Refined by the threshold requirements and the consistency features, two phases (right ventricle phase and left ventricle phase) or three phases (recirculation phase added) are automatically determined. No matter how many phases there are, the second phase mainly shows the blood pool in the left ventricle and associated major arteries, which are candidates for AIF. Throughout the process, the AIF is accurately and automatically selected. Using the similar method in the first phase, right ventricle and the associated major arteries are automatically segmented.

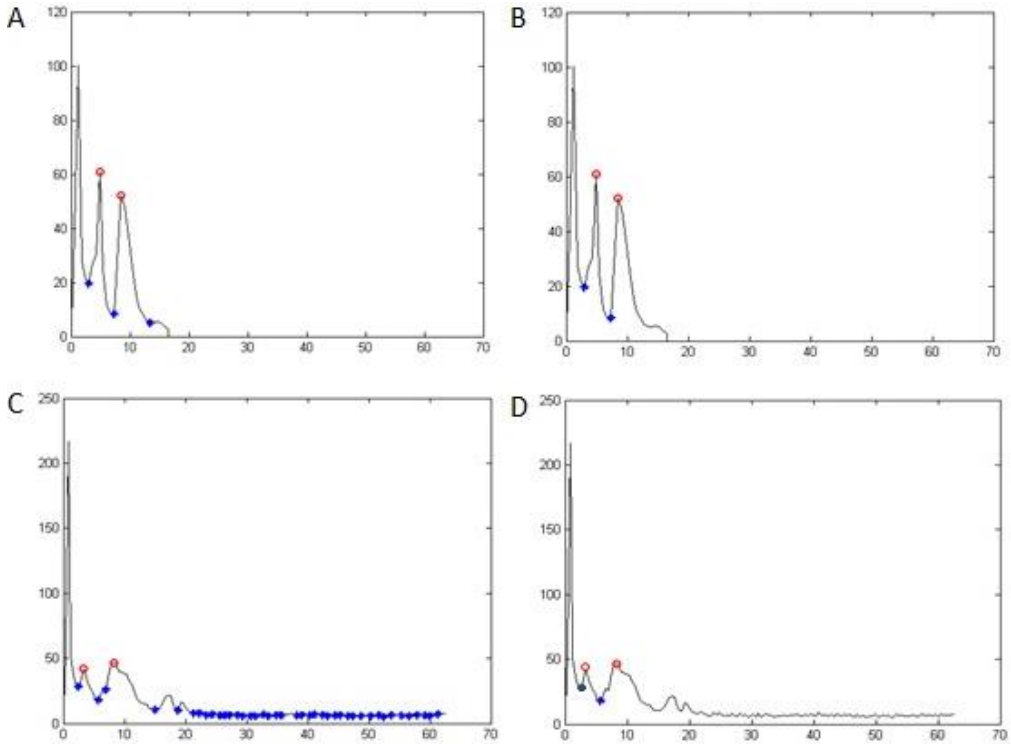

Figure 27. Automated process for the myocardial perfusion study. A and B show the automated selection of potential peaks and valleys, and real peaks and valleys for the before-infarcted study; C and D present that for the after-infarcted study. Label: x-axes are times (s), and y-axes are maximum slope values.

The results of the automated AIF selection are shown as binary images in **figure 28 (C, D)**. In both studies, the AIF pixels are located in the blood pool in pulmonary vein, left atrium, left ventricle, aorta, and the branches of aorta and pulmonary vein, which are blood supply areas to coronary arteries to feed the myocardium. Even the blood supply areas blocked by some parts of myocardium can be selected accurately. Despite the scattered distribution of the blood supply areas, the selection of AIF pixels is more efficient and more accurate than the manually selected ones. The average TACs of all selected AIF pixels (**Figure 28 (E, F)**) are smooth, which represents the uniform patterns of the bolus wash-in and wash-out processes in both studies.

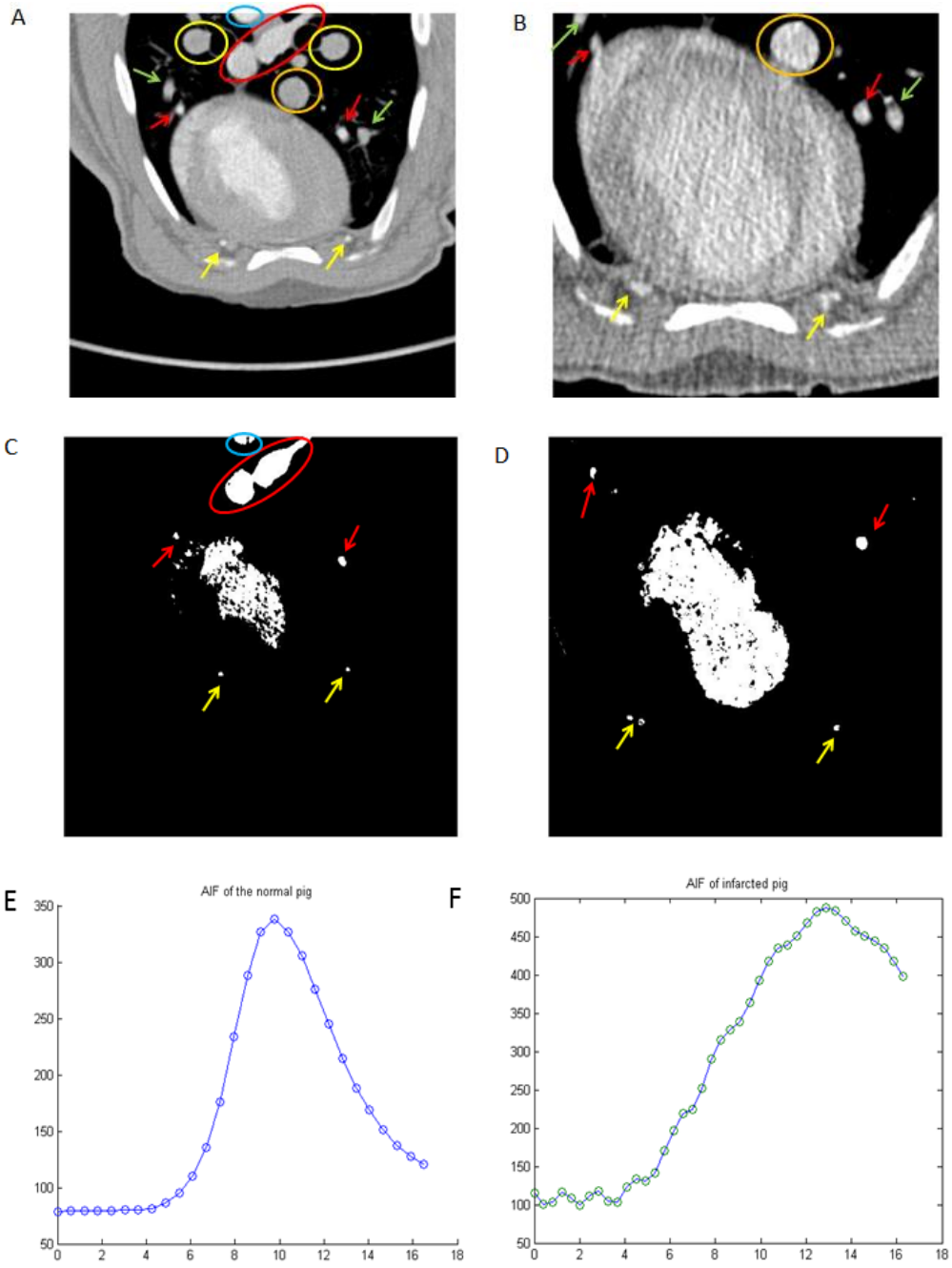

Figure 28. The resulted AIFs binary images (C, D) by the automated determination and the associated TACs (E, F) (x-axis: time (s); y-axis, HU) of AIFs, corresponding to the original anatomical images (A, B). A, C, E are in the before-infarcted study, and B, D, F are in the after-infarcted study. In the figures, blue circle: aorta; red circle: pulmonary vein; yellow circle: pulmonary artery; orange circle: postcaval vein; red arrow: small branches of pulmonary vein; green arrow: pulmonary arteriole branches; yellow arrow: sternal artery (originate from aorta).

The AIFs in both before and after infarcted studies are only presented within the first 16 seconds, because only wash-in process was taken into consideration in this case and the shortened time duration could display the changes much clearly. Both AIFs hit 350 HU at the same time and the maximum enhancement of the after-infarcted study is higher. It matches the tracer administration: the total amounts of tracer are different, but the infusion rate is the same.

3.3.3 Perfusion Maps and Quantitative Analysis

The perfusion maps were generated, as shown in **Figure 29 (A, B)**, to show the myocardial blood flow and distribution. By visually comparing the before (**Figure 29A**) and after (**Figure 29B**), it can be seen that there is normal enhancement in the inferoseptal wall, and dramatically reduced perfusion in the anterolateral wall, which is also much thinner. The 3-D perfusion volume (**Figure 29 (C, D)**) is reconstructed from series of perfusion 2-D maps to anatomically and functionally assess myocardial physiological conditions.

The quantitative analysis was performed by drawing a region of interest (ROI) along the anterolateral wall as infarcted areas and a ROI along the inferoseptal wall as non-infarcted areas in both before-infarcted and after-infarcted studies, and taking the average perfusion values for comparison. The two corresponding ROIs are in the same size. In the before-infarcted study, the ratio of the perfusion values of infarcted and non-infarcted areas is 1: 1. While in the after-infarcted study, the ratio is 1: 1.45 (**Table I and**

Table II). It indicates that the blood flow on the anterolateral wall was dramatically blocked in the after-infarcted study. It matches the experiment design, because the left anterior descending (LAD) coronary artery that was occluded is along the anterolateral wall. By comparing the ratios change, the quantitative analysis can be realized. We could not use the absolute number change to perform the quantitative analysis, because the absolute number change in perfusion values will be affected by many factors, like physiological change of myocardial cause by catheterization. In this study, before and after infarction, the non-infarcted areas have different absolute perfusion values. The possible explanation is that after the LAD was occluded, less blood flowed through the anterolateral wall. In order to keep the heart function normal, the heart pumped much harder, so that more blood would be pumped to the aorta to supply for the myocardium. Therefore, the perfusion value in the non-infarcted areas is higher in the after-infarcted study than that in the before-infarcted study. The perfusion values of infarcted areas in before and after the infarcted studies are similar, which means that the heart is still hard working to remain the function of the anterolateral wall, but this continuously hard beating will lead to the later heart failure.

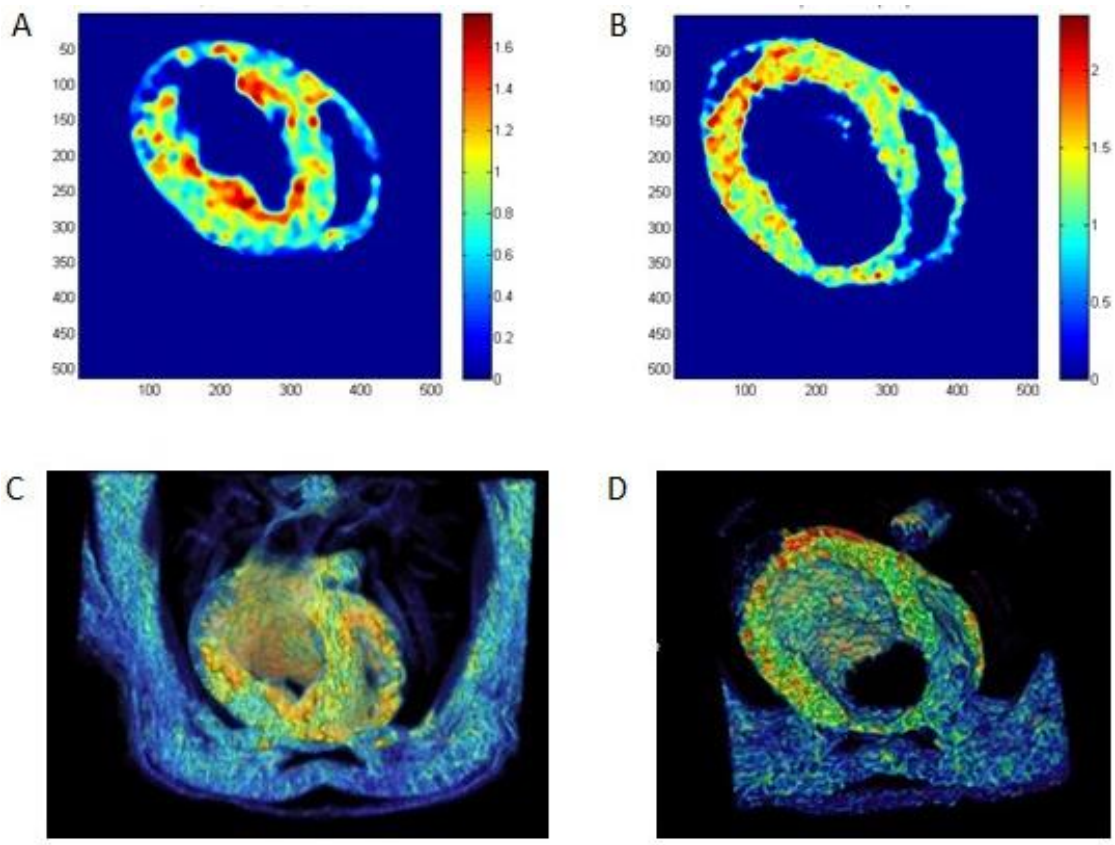

Figure 29. The perfusion maps (A, B), and the associated 3-D perfusion volumes (C, D). A, C are in the before-infarcted study, and B, D are in the after-infarcted study.

Table I. Quantification in the before-infarcted study

Areas	Perfusion values (ml/100g/min)
Infarcted areas	96 +/-20
Non-infarcted areas	97 +/-20

Table II. Quantification in the after-infarcted study

Areas	Perfusion values (ml/100g/min)
Infarcted areas	91 +/-20
Non-infarcted areas	132 +/-20

CHAPTER IV

CASE STUDY—PET ABDOMINAL PERFUSION

4.1 Introduction

4.1.1 PET Imaging in Gastrointestinal (GI) Perfusion

Positron emission tomography (PET) is one of the ideal methods to quantify the tissue perfusion because of its noninvasive property and the ability to accurately describe the distribution of radionuclides within the body, with absolute PET number reflecting the tracer concentrations. PET perfusion studies can be applied in many organs, especially in myocardium, and it becomes one of the "Gold Standard" methods to assess the cardiac perfusion studies. However, so far, no one employs PET scan in abdominal perfusion studies. Abdominal perfusion studies require more sensitive and accurate measurements because of the much more complicated structure in the abdomen than the cardiac structure. We believe that different cardiac outputs will result in different distribution and perfusion inside the abdomen, with kidneys, upper gastrointestinal (GI) and lower GI included. In this study, we plan to test our idea.

4.1.2 ^{62}Cu-PTSM as PET Tracer

PET perfusion can be measured accurately with tracers such as oxygen-15-labeled water ($H_2{}^{15}O$) and 13N-ammonia (*47*), however, they can only be produced by cyclotron, to which most PET center have no direct access. Generator-produced tracers, such as ^{82}Rb-chloride and ^{62}Cu, are widely used for the estimation of blood flow.

Although ^{82}Rb-chloride has been successfully and extensively used in the detection of coronary artery disease (*48*), the short half-life of it, which is 1.3 min, prevents it from being an ideal tracer for PET perfusion studies. Furthermore, ^{82}Rb-chloride is easily influenced by the metabolic activities of organs, making the quantification more difficult.

^{62}Cu-labeled pyruvaldehyde bis (N-4-methylthiosemicarbazone) copper (II) (PTSM) is a lipophilic perfusion tracer. The ^{62}Cu isotope has 100% positron decay and a physical half-life of 9.7 min, which is ideal of the PET instrumentation (*49*). ^{62}Cu-PTSM is highly extracted and retained in cells and organs. The mechanism of ^{62}Cu-PTSM entrapment in cells is involved with diffusion of it across the cell membrane with subsequent reduction of copper (II) to copper (I) by ubiquitous intracellular sulfhydryl groups. The reductive decomposition is able to bind nonspecifically to intracellular macromolecules, and hence, becomes trapped (*47, 50*). All the advantages make this compound promising for clinical use in quantitative measurement of tissue blood flow.

The most significant difference from the properties of iodine-based tracers in CT scans and PET based ^{62}Cu-PTSM is that this compound is completely trapped biologically by tissues. Therefore, except for the blood feeding areas—aorta and artery branches in the abdomen, there is no wash-out process existing in the tissues.

4.1.3 Dynamic PET Imaging Reconstruction

The quantitative analysis for PET abdominal perfusion studies is sensitive to the imaging reconstruction process. Dynamic PET imaging is acquired as a collection of a series of time frames over adjacent time intervals. The data of each frame is reconstructed independently and used to form a set of images (*51*). The selection of adjacent time intervals gives a set of acquisition times. The longer acquisition time means longer scans with good counting statistics. However, it compromises the temporal resolution, leading to the loss of some important information. The shorter acquisition time, on the contrary, preserves the temporal resolution, but bring in too much noise due to insufficient counting statistics. In this case, some important information is obscured by noise. Moreover, shorter acquisition time results in more data within a certain time, which increases burden of data processing and requires more memory. In perfusion studies, the extraction of AIF requires data precise enough to form PET-TACs that are used to differentiate arterial blood and tissues. The quantitative measurement involves accurate AIF and stable data for the steady-state of tissues. An optimal reconstruction method should provide detailed information during the perfusion process and sufficient counting statistics at the steady period.

In this study, we test our algorithm in a different image modality (PET) on a distinct tissue (abdomen) using dissimilar tracers (^{62}Cu-PTSM) with completely different properties. Also, in order to find the optimal reconstruction protocol for PET abdominal

perfusion measurement, we iteratively refined the reconstruction protocols to optimize method.

4.2 Materials and Methods

4.2.1 Animal Preparation

Three adult 60-80 kg ovine were used for the PET abdominal perfusion studies after approval from Institutional Animal Use and Use Committee (IACUC). Different cardiac outputs (blood flow output from left ventricles) were controlled using an implanted left ventricle assist device (LVAD). The animals were implanted with a centrifugal continuous flow LVAD in the left ventricular apex to the descending aortic position. The controlling modes are baseline (LVAD off, named mode 1), low continuous flow (LVAD flow 2.5 L/min, mode 2), high continuous flow (LVAD flow 4 L/min, mode 3), low induced pulse flow (LVAD flow 2.5 L/min, mode 4) and high induced flow (LVAD flow 4 L/min, mode 5). The intestinal and renal blood flows were measured using microsphere and PET Scan techniques.

4.2.2 Microsphere Measurement

The microsphere studies were performed 20 minutes before each PET scan. Different colored microspheres were injected into the left ventricle during the five modes. Gold, samarium, ytterbium, europium and terbium color microsheperes were used in the five modes—baseline, low continuous flow, high continuous flow, low

induced pulse flow and high induced flow—respectively. The intestinal and renal tissue biopsies were harvested for the microsphere analysis after the study is terminated.

4.2 3 ^{62}Cu-PTSM Preparation

The Zn-62/Cu-62 generator, from Proportional Technologies (Houston, TX), was used to prepare ^{62}Cu-PTSM. The generator was eluted 20 minutes earlier before the PET studies started, in order to maintain the radioactivity of the ^{62}Cu-PTSM.

In order to test the optimal radioactivity of the ^{62}Cu-PTSM in the abdominal perfusion studies, two ovine studies (Study 1 and Study 3) were performed in the days when the generator arrived and one another studies (Study 2) were executed in the next days.

4.2.4 PET Scan Imaging Protocol

PET/CT scans were performed using Siemens Biograph mCT (Siemens Molecular Imaging, Tennessee, US). The scanner is equipped with 128 slice molecular CT and high resolution time-of-flight (TOF) PET with extended field-of-view (FOV). The subjects were positioned in head first-supine (HFS) orientated in the scanner. CT scans were implemented first through the whole body to optimize the region of interest, which locates from right kidney to small intestines, followed by PET scans.

In Study 1 and 2, the PET scans were performed over 8 minutes. 221 slices of images were obtained with 1 mm slice thickness. In the Study 3, the PET scans were performed over 10 minutes. Two hundred and twenty two slices of images were obtained with 1 mm slice thickness. The differences in the slice number and scan duration would have no influence on the final results. In three studies, the ^{62}Cu-PTSM was infused into the left ventricle through a peripheral intravenous tube around 30 seconds later after the PET scans started. A 3-D Gaussian filter with a full-width-half-maximum response of 5.0 mm was used as the kernel convolution for the later reconstruction. After each scan, the subjects were left inside the scanner for 40 minutes in order to let the radionuclides decay and be cleared out.

4.2.5 PET Imaging Reconstruction

In this experiment, we iteratively refined the reconstruction protocols to optimize method. First, through the entire study, the images were acquired at 30 sec/frame, in order to achieve a good counting statistics and also save memory space. Second, the images were acquired at 10 sec/frame. Even though this reconstruction method took more memory space, detailed information might be able to be obtained. These two methods were used for looking for physiological process information: the durations of baseline (delay for tracer injection), perfusion process and steady state. According to the results from these methods the perfusion process occurs from 30 sec (varies a little bit from study to study) to 3 min; and then the regions of interest enter into steady states. Accordingly, the third reconstruction (named adaptive reconstruction) method was

developed: during the first 3 min, images were acquired at 5 sec/frame, and in the rest of the process, the acquisition was obtained at 1 min/frame. The reason for the development of this reconstruction protocol is that we were trying to extract detailed information during the perfusion process, and remain a good counting statistics during the steady state. One step further, the fourth reconstruction method (named adaptive detail reconstruction) was developed for remaining more detailed information: during the first 30 seconds, images were acquired at 10 sec/frame; from 30 seconds to 3 min, images were acquired at 3 sec/frame; and in the rest of the process, the acquisition was obtained at 1 min/frame. This reconstruction method could remain more detailed information during the perfusion process. However, to save some memory, the acquisition was obtained at 10 sec/frame during the first 30 seconds before tracer washed in.

4.2.6 Algorithm Implementation

In abdominal perfusion studies, blood feeding areas are very small, especially the uptake of the tracer in kidney is too large to provide a clearly distinguishable difference between arteries and kidneys. It is difficult to determine the appropriate maximum slope and the maximum enhancement. As mentioned before, the ^{62}Cu-PTSM is completely trapped biologically by tissues when it is injected into the body. Therefore, unlike the behavior inside arteries or blood pool areas, the ^{62}Cu-PTSM experiences no washout process in the tissues. To address this scenario, the additional computations involving wash-out process were included in the algorithm for automated AIF selection.

Since reconstruction determines the dynamic evaluation performance, the four types of reconstruction affect the strategy of algorithm implementation. According to the results from the reconstructions (see the "Results and Discussion" in "reconstruction"), the data from the reconstruction of 10 sec/frame is optimal to be used in automated AIF selection.

In the "characteristic parameters extraction and pattern recognition" step, we set α yield to 0.3 to give us an optimal threshold θ_1 for both wash-in parameters and wash-out parameters calculation. The five parameters were extracted: maximum enhancement, maximum slope, time to peak, wash-out slope, and time to wash-out. Three 2-D plots were generated: S vs. T curve, E vs. T curve and W vs. T curve. In the "automated determination of AIF and segmentation of tissues" step, the slope derivative threshold, enhancement derivative threshold and washout derivative threshold were chosen based on the requirement that small noise should be removed completely. According to our imaging protocol, the tracers infused process happened within 4 min, and after that, the tracers were either cleared up by the arterial system or trapped by tissues. They kept steady state during the rest of the scanning period. Therefore, all the automated calculation was executed only in the time period from 0 min to 4 min.

4.2.7 Perfusion Maps Generation

Once AIF was selected, perfusion parametric maps were generated for each slice location. To obtain the perfusion maps, the trapped radiotracers model was applied.

Referring to the equation used in microsphere study,

$$Perfusion\ (mL/min/g) = S\ (mL/min) *\ \ [(A_{tissue}/m_{tissue}\ /A_{artery}\ )] \quad (32)$$

Where S is withdrawn rate, A_{tissue} / m_{tissue} presents the radioactivity concentration of the tracer in the measured tissue, and A_{artery} is the total activity of the withdrawn blood sample.

This radiotracers trapped model can also be used in PET perfusion studies, but needs some modification. The typical PET data represents the tracer concentration, with the unit of Bq/mL—for example. In addition, in terms of withdrawn process, it depends on if the blood sample would be taken for the reference sample or cardiac output would be applied. In this study, neither blood sample was withdrawn nor cardiac output was captured (it is hard to calculate). A perfusion calculation method only using PET imaging was developed. **Figure 30** illustrates the sampling example from PET perfusion for both AIF areas and tissues. Since AIF is the DEC of blood feeding areas, which describes dynamics of blood sampling. Since the unit of PET number is Bq/mL, the sampling rate s is 1 ml/(1min/sample interval).

The tracer total activity in arterial sampling is the integral of radioactivity of all the sampling points (showing in the black dots in Figure 30) along the time period from tracer arrival to tracer clear-out. Due to the complexity and more techniques involved—like curve fitting—in the integral operation, we could use sum to digitize the sampling to

replace integral operation. Then, the calculation process of the total activity of tracer in arterial sampling is

$$A_{artery} = \int_{arrival}^{clear} C_{artery} dv$$

$$= \sum_{arrival}^{clear} C_{artery} * \text{dv} \quad (33)$$

Where dv = 1 ml, and C_{artery} is obtain from the PET number directly. Similarly, the calculation process of the activity of tracer in tissues is

$$A_{tissue} = \int_{arrival}^{trapped} C_{tissue} dv \quad (34)$$

Since tissue is acting like an integrator because it is taking tracer in and not giving it up. In such way, $A_{tissue} = C_{tissue,}$ when C_{tissue} is taken from a point at steady state (shown in **figure 30**). m_{tissue} is calculated from the equation

$$m = \rho \times V \quad (35)$$

Since we are taking the unit volume sample, V equals 1 ml. The density of a tissue in general is approximately like water, which is 1 g/ml. In such way, m_{tissue} yields to 1 g. Consequently, the perfusion calculation only by PET imaging can be achieved.

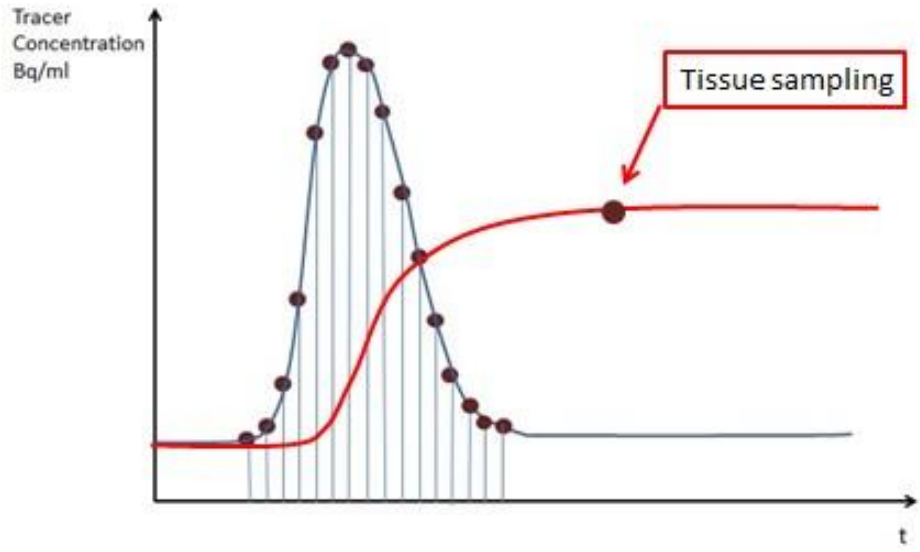

Figure 30. Sampling example from PET perfusion for both AIF areas and tissues. Blue line: AIF; Black dots on the blue line: blood sampling; Red line: DEC of tissues; Black dots on the red line: tissue sampling.

In this study, the sample rate is 6 ml/min, since we sampled at the rate of 10 sec/min. During the wash-out process, because some free copper ions mix well with blood and stay with the blood or be trapped by lumen, the steady state of AIF is not going down to zero as expected. However, these copper ions will not flow into tissues with other blood. To avoid the overestimation of blood sampling, the data from AIF after the maximum enhancement was normalized based on the principle that the steady state should be at zero.

4.2.8 DICOM File Generation and Workstation Use

The calculated perfusion maps were written into Digital Imaging and Communications in Medicine (DICOM) files for importing into Syngo Workstation

(Siemens Medical Solution, Tennessee, USA) for the further analysis. DICOM is a standard in the radiology imaging for the exchange of images and the related information. A single DICOM file contains a header—storing the information about the patient's information, imaging protocol, study description, etc.—and all the image data (pixel data). When we process the data to generate perfusion maps, we deal with the image data. When it comes to importing data into the workstation, we need to deal with the header. There are four hierarchies for the header: 1. Patient; 2. Study; 3. Series; 4. Image. The image contains more detailed information—slice and frame.

To write the perfusion maps into the specific DICOM files correctly, we need to make sure the patient and study remain the same as their originals. A new series should be created for each perfusion study. Since the perfusion maps are static, rather than being dynamically acquired, the series type should be changed from "dynamic" to "whole body". The related parameters, such as frame information, unique identification number and service-object pair, would also be changed. To display the perfusion maps with their original values, the "Rescale Slope" and "Rescale Interception" were set to be 1 and 0, respectively. The image reconstruction factors were set accordingly.

The perfusion maps in DICOM files were imported into the workstation, and fused with original CT whole body images, so that the positions of the hot spots displayed in the PET perfusion maps could be identified.

4.3 Results and Discussion

4.3.1 Reconstruction

Figure 31 (A, B) presents the reconstruction results of one of the studies with 30 sec/frame reconstruction method and 10 sec/frame reconstruction method, respectively. Since the AIF area has higher concentrated tracer, it is supposed to have higher maximum enhancement and sharper maximum slope. However, in the result from 30 sec/frame reconstruction, the maximum enhancement of the AIF area is much lower than that of kidneys. It is due to partial time effect; it is averaging over a long period of time so information in the high frequency is lost. Compared to the 30 sec/frame reconstruction, the result from the 10 sec/frame reconstruction is much better, which matches our expectation: the AIF area has the highest maximum enhancement, steepest maximum slope; kidneys have very high maximum enhancement due to the largely trapped tracers; the maximum enhancement and maximum slope of other tissues are not that high. In addition, the wash-out process only exists in the AIF area. However, the 10 sec/frame reconstruction method is not perfect. Some detailed information is still missing if we were not sampling at a perfect time. In other words, partial time effect might still exist in this reconstruction method.

The results from 30 sec/frame and 10 sec/frame reconstruction methods indicate that the tracer started to wash in at the time of 30th second, and the perfusion process started from the 30th second and ended up with 3rd min. The rest of the scanning duration is the steady state.

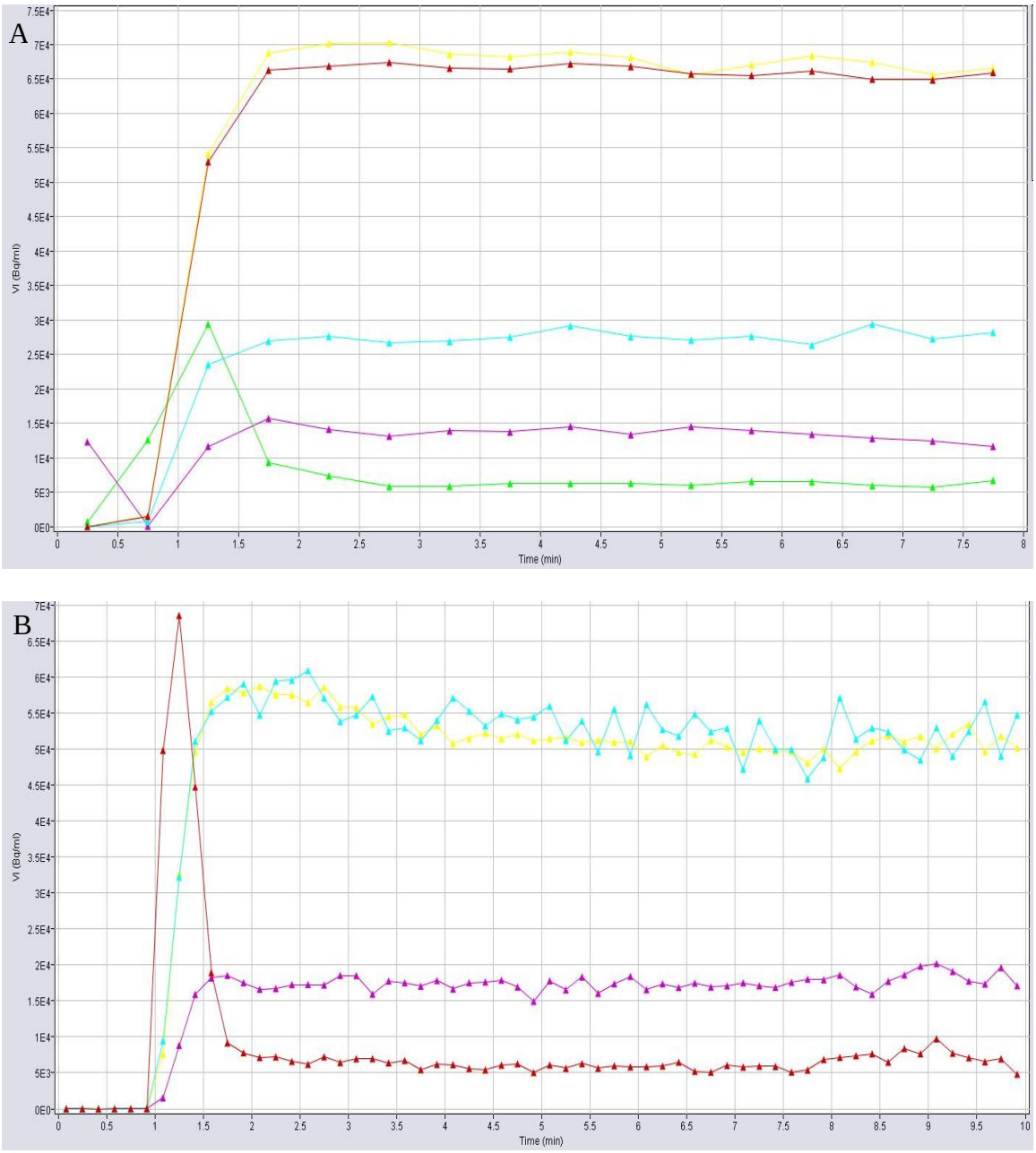

Figure 31. Reconstruction results of 30 sec/frame (A) and 10 sec/frame (B). A: green line: AIF; red and yellow lines: kidney; blue and purple lines: tissue. B: red line: AIF; blue and yellow lines: kidney; purple line: tissue.

Figure 32 (A, B) illustrates the results from the adaptive reconstruction method (5 sec/frame (0-3 min) + 1 min/frame (3-10 min)) and adaptive detail reconstruction method (10 sec/frame (0-0.5 min) + 3 sec/frame (0.5-3 min) + 1 min/frame (3-10 min)). The detailed information is preserved well in both results, but the adaptive detail one is better: the maximum enhancement of the kidneys is not supposed to be identical to that of the AIF area, but should be a little lower due to the mass of kidney tissues. However, adaptive reconstruction gives the result that the maximum enhancements of the kidney and the AIF area are almost the same. It might be because of the noise domination. Even though detailed information can be preserved in both reconstruction methods, the counting statistics is poorer than ideal. More noise domination means less useful information presentation. Detailed information of AIF is good for the later perfusion calculation, and therefore, the adaptive detail reconstruction could provide proper data for perfusion calculation.

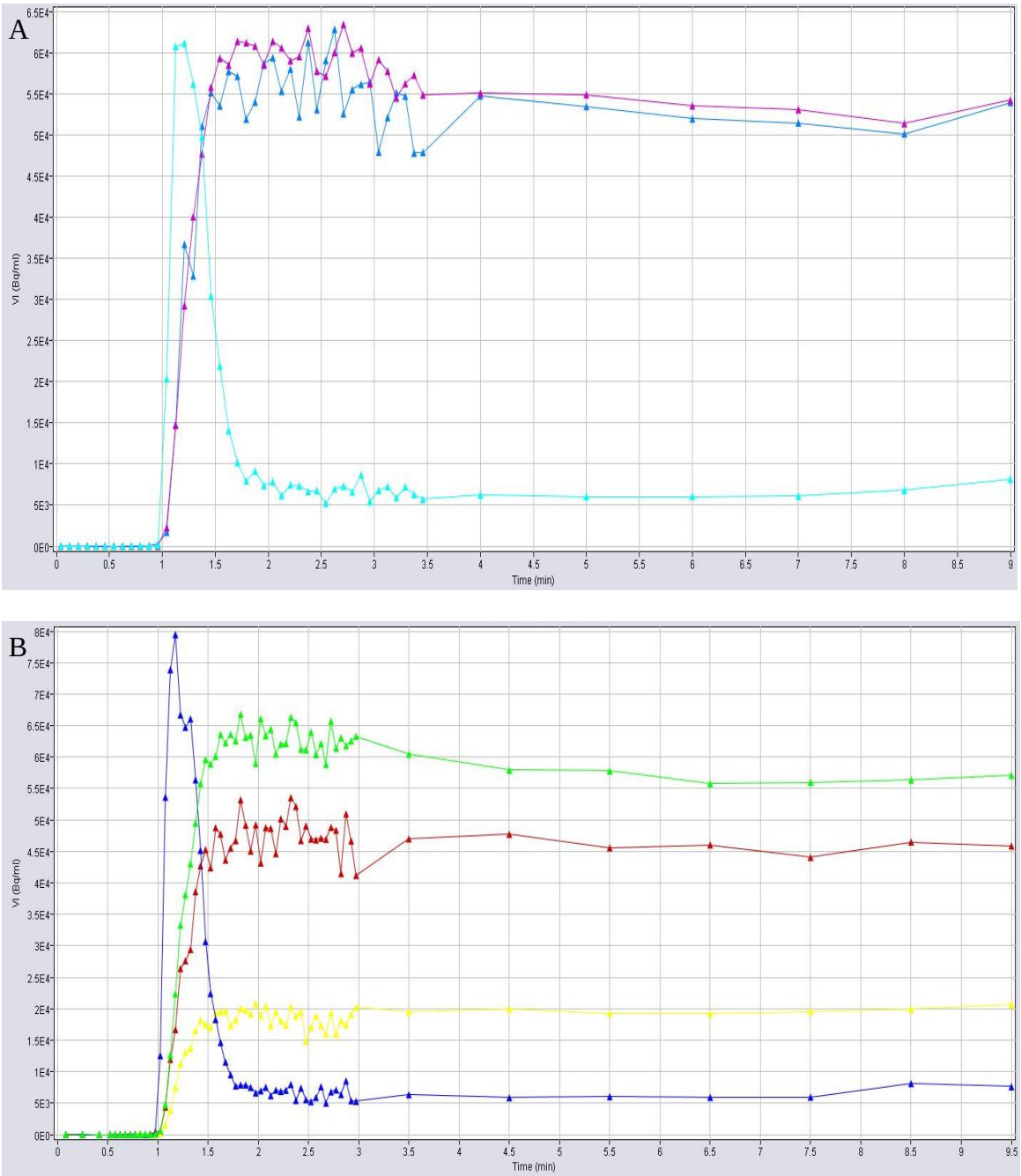

Figure 32. Reconstruction results of adaptive (A) and adaptive detail (B). A: light blue line: AIF; purple and blue lines: kidney. B: blue line: AIF; green and red lines: kidney; yellow line: tissue.

4.3.2 Characteristic Parameters Extraction and Pattern Recognition

According to the results from the last step, the 10 sec/frame reconstruction is better than the 30 sec/frame one. Additionally, the adaptive detail reconstruction is better than the adaptive one. In this step, 10 sec/frame and adaptive detail reconstruction methods were performed. Through the characteristic parameter calculation algorithm, we extracted five parameters: maximum enhancement, maximum slope, time to peak, washout slope and time to washout. Three 2-D plots were generated: S vs. T curve, E vs. T curve and W vs. T curve.

Only S vs. T curves of both studies, as shown in **Figure 33 (A, B)**, were picked for comparison. Compared to the S vs. T curve of the adaptive detail reconstruction study, the curve of the 10 sec/frame reconstruction study displays much clear patterns, and it is easy to differentiate the physiological phases. Accordingly, in terms of implementing the automated AIF selection algorithm, 10sec/frame reconstruction is better. However, if accurate quantitative analysis in perfusion studies is needed, more detailed information should be preserved. In such case, adaptive detail reconstruction is the optimal. According to the results, the 10 sec/frame reconstruction method is more suitable for automated AIF selection, since it makes the physiological phases on the 2-D plots easier to differentiate. The adaptive detail reconstruction method (10 sec/frame (0-0.5 min) + 3 sec/frame (0.5-3min) + 1min/frame (3-10min)) is good for perfusion calculation. Even though the counting statistics of this reconstruction method is poor, detailed information is able to be preserved.

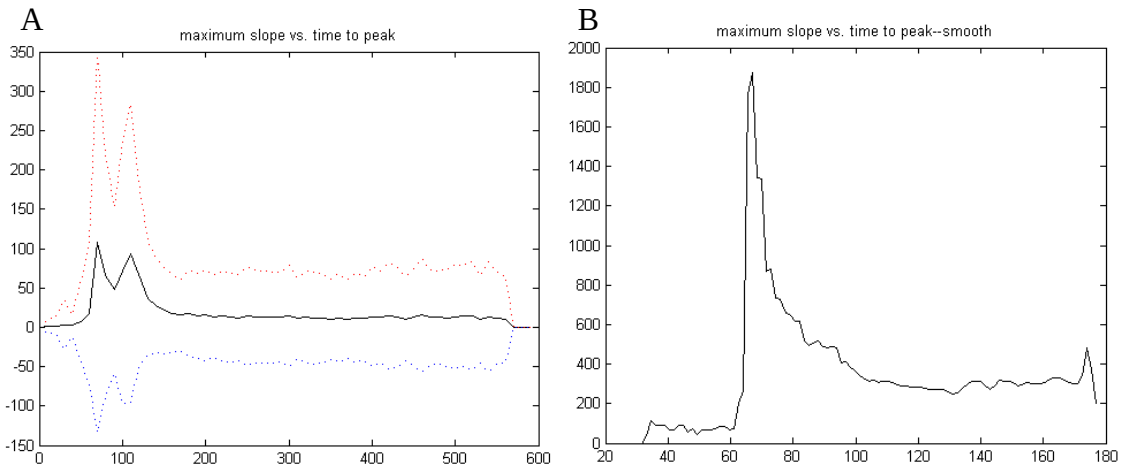

Figure 33. S vs. T curves of the data from 10 sec/frame reconstruction (A) and from adaptive detail reconstruction (B). Label: x-axes are times (s), and y-axes are maximum slope values.

In this step, only data from 10 sec/frame reconstruction was performed. The patterns, as what we described before, are presented clearly (**Figure 34**). As shown in the **Figure 34 (A, B)**, there are two peaks on both the S vs. T curve and E vs. T curve. The abdomen region was scanned from the right kidney (top) to the small intestines (bottom). Kidneys have very high metabolic activity. The tracer was wash into the AIF region first. Therefore, the first peak represents the arteries and the associated branches, and the second is a result of tracer in the kidneys. As shown in **figure 34C**, on the W vs. T curve, since only the arterial phase has the wash-out process, the single peak during the perfusion process is the expression of the AIF area in general. Another peak on the W vs. T curve is around the end of curve, which is around the time of 9 min. It is due to physical decay of copper-62. Tissues do not have wash-out process. The system mistakes the physical decay to be wash-out. Since the decay behavior is very uniform, and our threshold is the maximum enhancement-dependent, the "times to wash-out"

should be close to each other. The shown peak means an accumulated time that "wash-out" (actually decay) occurs. It should not be considered because it is out of perfusion process.

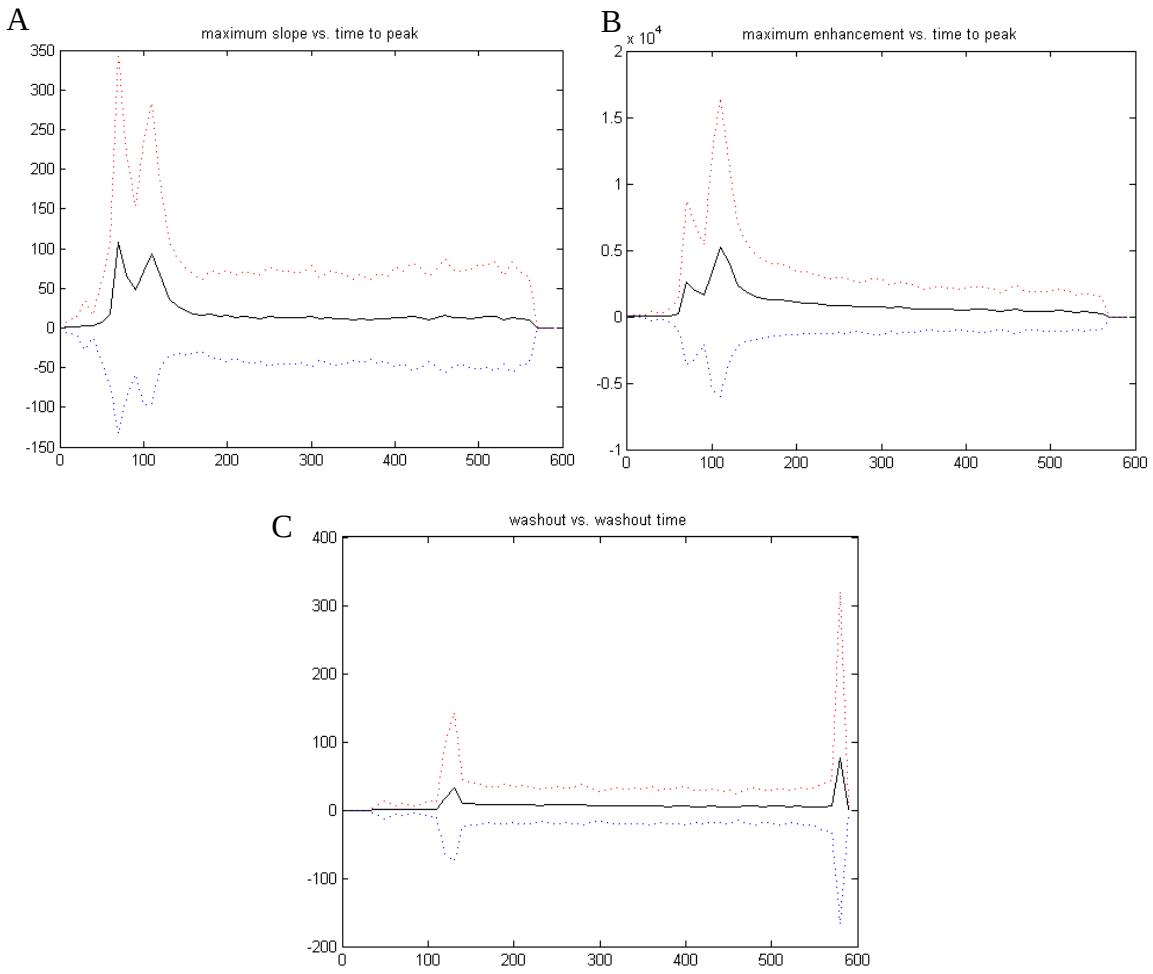

Figure 34. The 2-D plots: S vs. T curve (A), E vs. T curve (B) and W vs. T curve (C). Label: x-axes are times (s), and y-axes are maximum slope values (A), enhancement values (B) and wash-out slope values (C), respectively.

4.3.3 Automated Determination of AIF

The automated processes for selecting characteristic points are shown in **figures 35-37**. The arteries and kidneys phases were accurately selected.

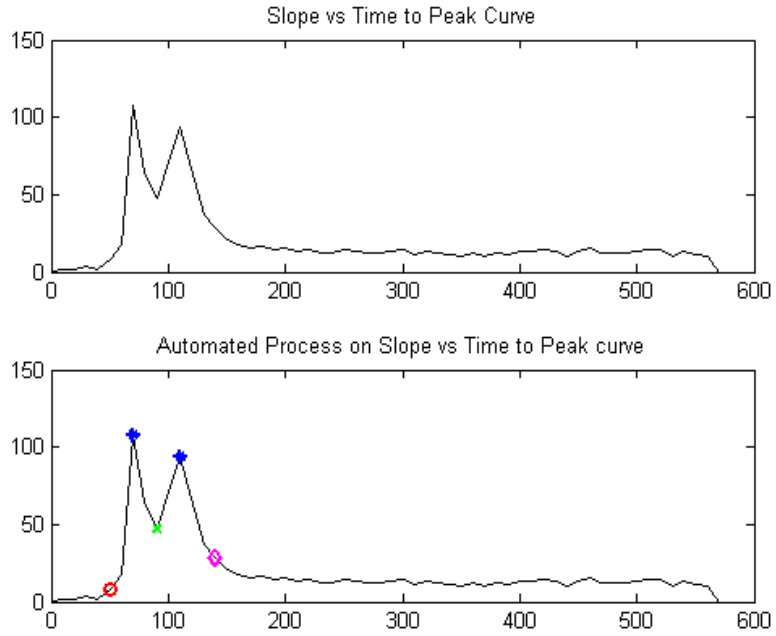

Figure 35. Automated process for S. vs. T curve. Label: x-axes are times (s), y-axes are maximum slope values.

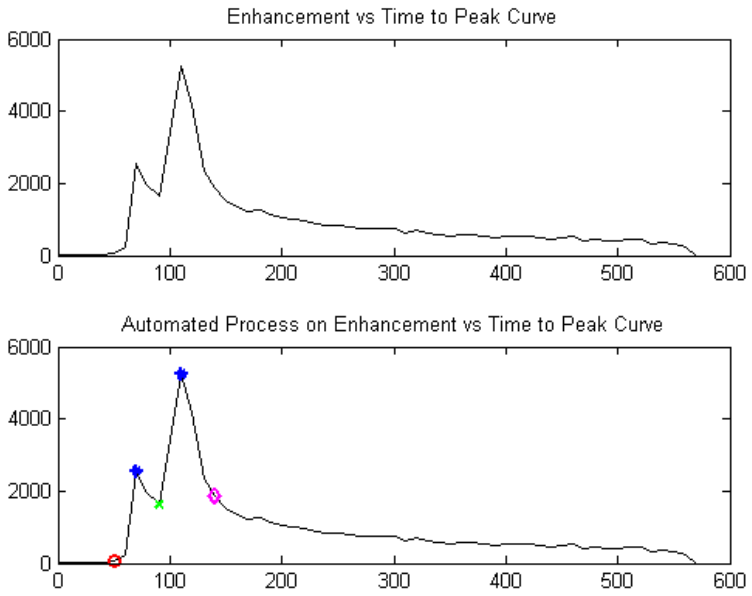

Figure 36. Automated process for E vs. T curve. Label: x-axes are times (s), y-axes are enhancement values.

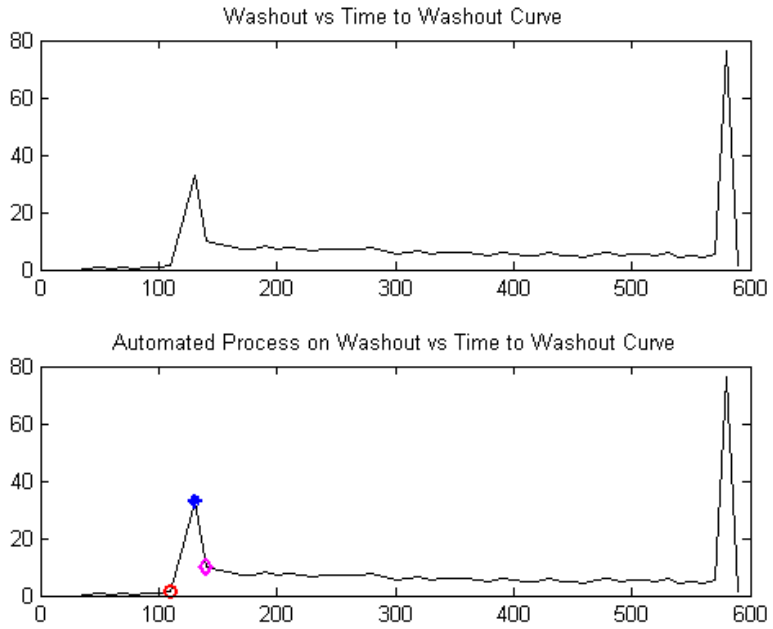

Figure 37. Automated process for W vs. T curve. Label: x-axes are times (s), and y-axes are wash-out slope values.

To pick the AIF, the results from the three plots were integrated. The selected pixels satisfied the following requirements: the maximum enhancement is bigger than the mean enhancement at the point of the peak (in the phase of interest) on the E vs. T curve, the maximum slope is bigger than the mean slope at the point of the peak on the S vs. T curve, and the wash-out slope bigger than the mean wash-out slope at the point of the peak on the W vs. T curve. These selected pixels further meet the time requirements where the time to peak associated with these pixels are within the peaks (in the phases of interest) on both E vs. T curve and S vs. T curve, and the time to wash-out is within the single peak on the W vs. T curve.

The result of the automated detection of AIF pixels is shown in a 3-D binary image in **figure 38**. An intact and clear arterial system is shown in this figure: a main artery originated from aorta and then distributed into two branches, which are femoral arteries. This artery system is the blood feeding areas for the entire abdomen.

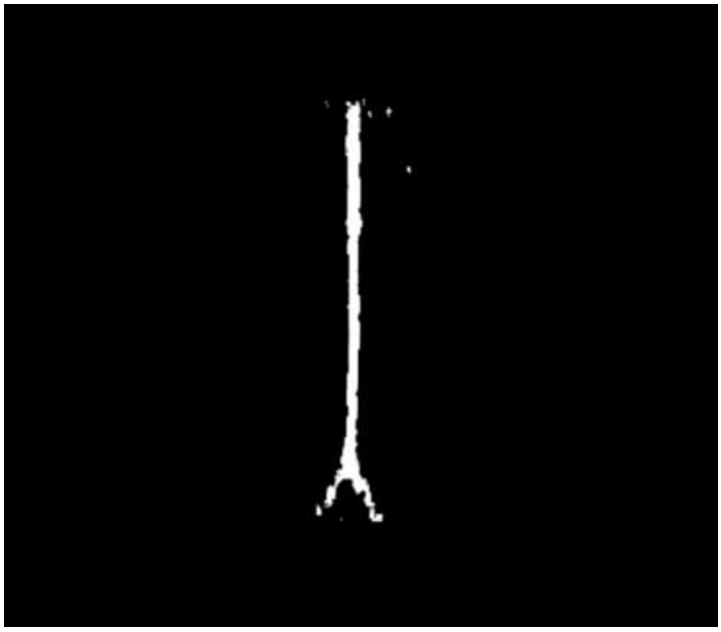

Figure 38. 3D AIF region—femoral system

The average PET-TAC, as shown in **figure 39A**, of the AIF pixels is smooth and represents the uniform patterns of the tracers wash-in and wash-out processes. When applied the data from the adaptive detail reconstruction on the selected AIF areas, the transferred PET-TAC is shown in **figure 39B**. The maximum enhancement of the transferred PET-TAC is much higher than that of the original one, which means that more detailed information is preserved. In addition, more sampling provides higher accuracy. The modified PET-TAC, as shown in **figure 39C**, is the one with the normalized data to avoid the effect brought by free coppers staying inside lumen.

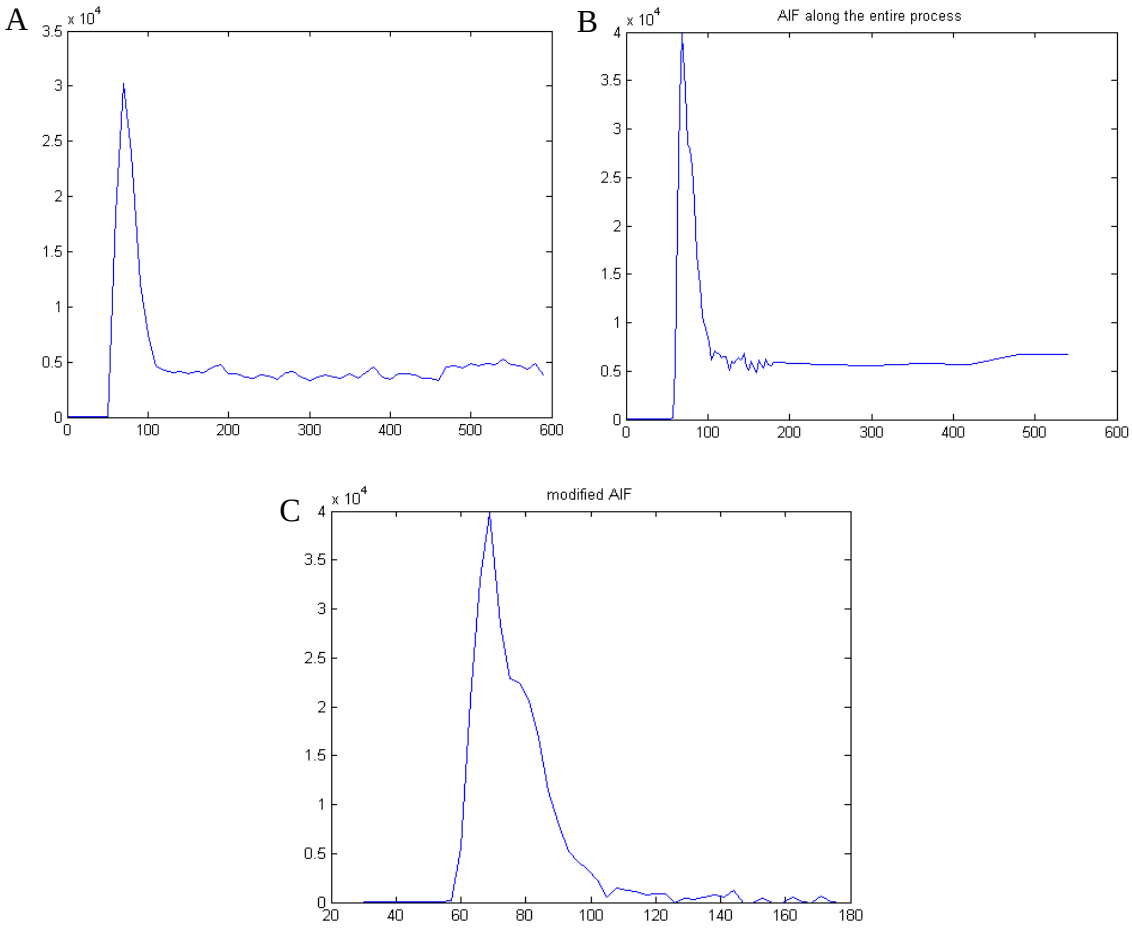

Figure 39. PET-TACs of AIF areas. A is from the data from 10sec/frame; B is from the data from adaptive detail; C is the modified TAC based on B. Label: x-axes are time (s), and y-axes are radioactivities.

4.3.4 Perfusion Maps and Fused Perfusion Maps with CT Anatomy Images

Figure 40 (A, B) shows the generated perfusion maps of the kidneys and upper GI. Perfusion values of lower GI are too low to be detected. **Figure 41 (C, D)** shows the fused perfusion maps with CT anatomy images that are corresponded with original CT whole body images, as shown in **figure 41 (A, B)**. The registration of the two modalities provides the information for both anatomy and functionality of the tissues.

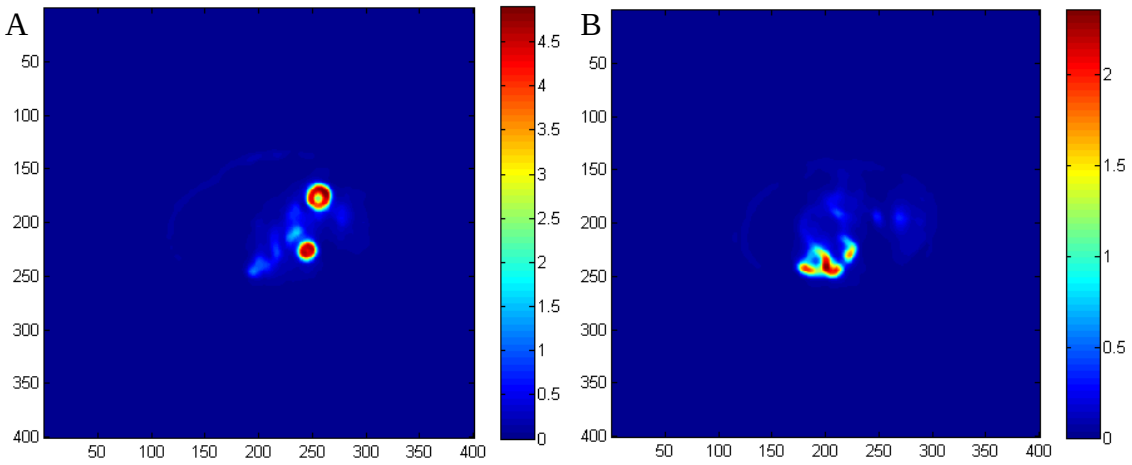

Figure 40. Perfusion maps showing kidneys (A) and upper GI (B).

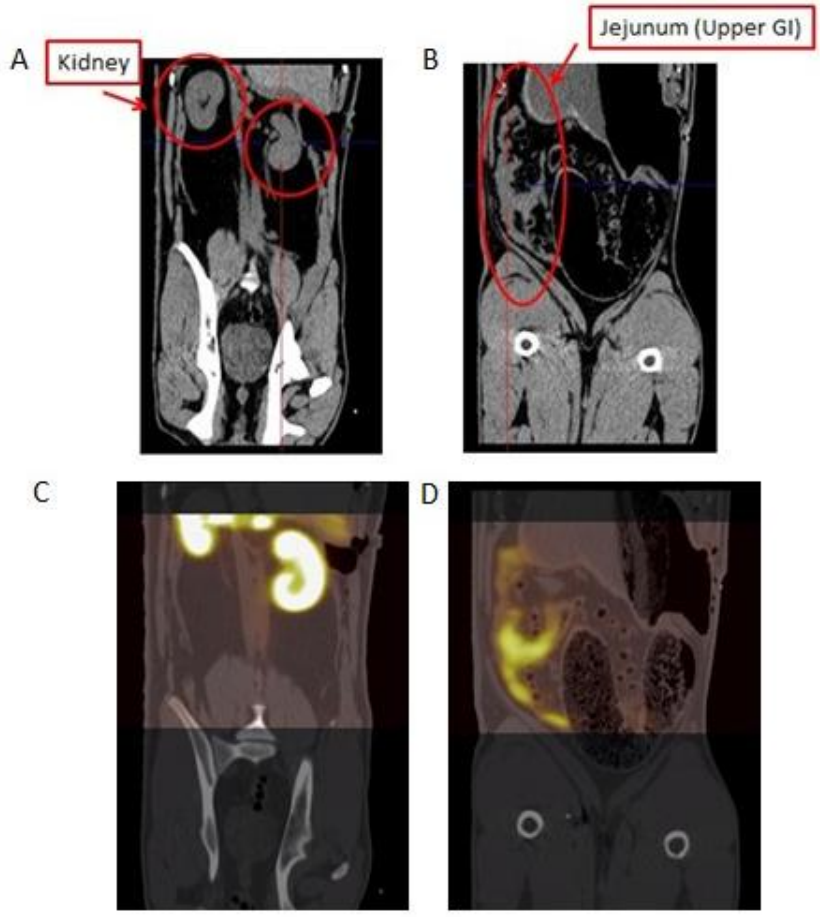

Figure 41. Fused perfusion maps showing kidneys (C) and upper GI (D) with CT anatomy, and the corresponding original CT whole images (A, B).

4.3.5 Quantitative Analysis for Microsphere and PET Imaging Studies

To evaluate the consistency and effectiveness of this algorithm used in PET imaging, two methods of quantitative analysis were performed. Since very low radioactivity of tracers was applied in Study 2, the counting statistics were not sufficient to get an accurate measure, therefore, only perfusion data from Study 1 and Study 3 were used.

The first method is to test if the microsphere data matches with PET data. Bars were used to present PET data range and an individual data to present microsphere data, because even in a single organ, the perfusion distribution is different through all the spots. However, only a small spot was harvested for microsphere measurement, but it is hard to tell the location of the spot where the biopsy was taken. On the contrary, PET imaging scanned the entire organ, and the perfusion values of all the spots in this organ could be collected. Therefore, we can conclude that if the microsphere data is located inside the range of the PET data, the PET data is accurate.

The comparison of PET data and microsphere data is shown in **figure 42 (A, B, C and D)**. The edges of the bars in PET data represent 75% (top) and 25% (bottom) percentiles of the perfusion values of an organ. The upper limit (shown as the highest line) is the maximum value of the perfusion, and the low limit (shown as the lowest line) is the minimum value of the perfusion. The red lines inside the bars are mean values. Some mean values are not in the middle of the bars because the perfusion distribution of

an organ does not match the normal distribution. Microsphere data is shown as an arrow with values denoted.

In the Study 1, all the perfusion values measured from microsphere studies are filled inside the bars of the corresponding PET data. In the Study 3, most of the microsphere data matches well with PET data except for mode 3 and mode 4. The microsphere data is so extraordinary high that it is illogical. It would be highly abnormal if a tissue could perfuse at the rate of 15 ml/min/g. It is likely that there were some problems with the catheters when performing blood sampling. This is a weakness of microsphere measurements.

The results indicate that the algorithm of automated AIF selection in PET perfusion studies provides consistency in quantitative analysis. It is relatively accurate and not easily affected by the technique itself. On the contrary, even though microsphere measurement might offer the most accurate results if this technique is performed in a perfect way, the technique is somewhat inconsistent and ineffective.

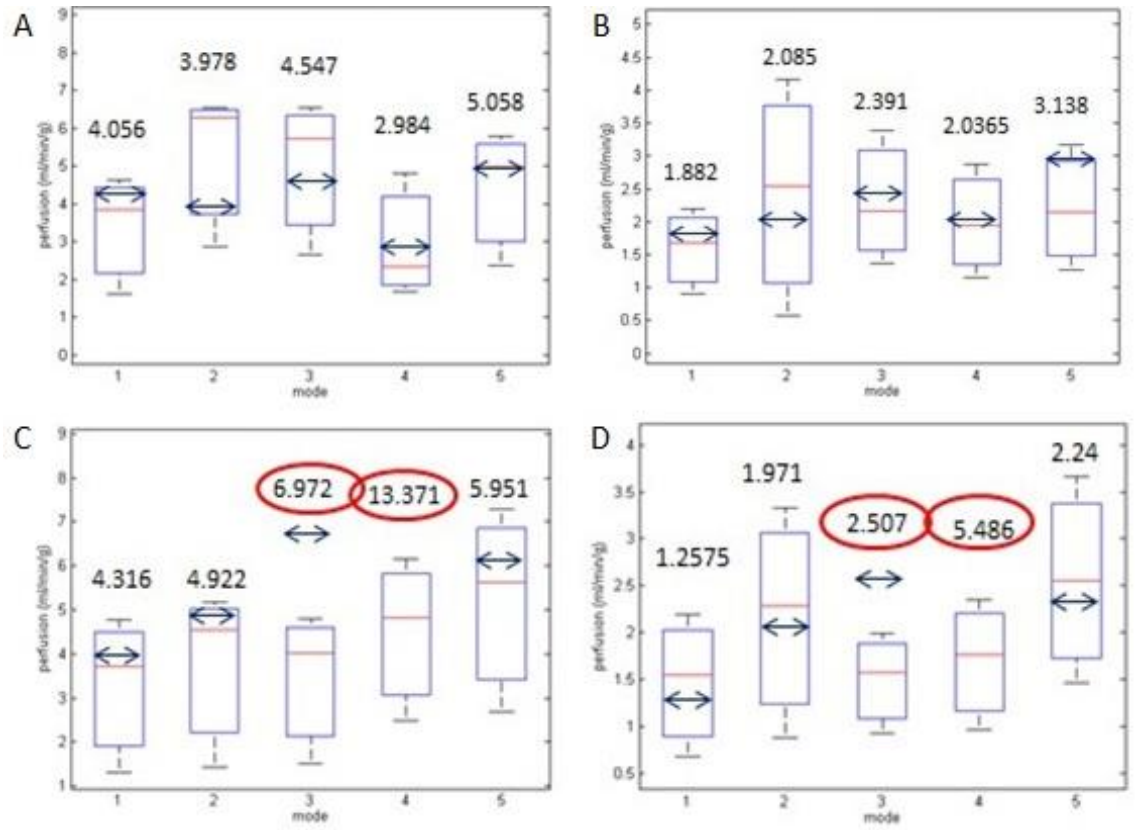

Figure 42. The comparison of PET data and microsphere data in Study 1 and Study 3, with modes of 1, 2, 3, 4 and 5. A: Study 1 kidney perfusion values; B: Study 1 upper GI perfusion values; C: Study 3 kidney perfusion values; D: Study 3 upper GI perfusion values. PET data ranges are shown using bars, and microsphere data is shown using arrows. The red circles are suspect numbers.

The second method is to detect the trend of perfusion changes when different control modes for cardiac outputs were applied. The first method roughly assesses the effectiveness of the algorithm and the PET imaging in perfusion studies. The second method is to detect the subtle changes in tissue perfusion brought by the blood flow controlling (mode 1, 2, 3, 4 and 5) using PET imaging. To evaluate this, the tissue perfusion trend detected from PET imaging is compared with that from microsphere data. **Figure 43 (A, B)** presents the comparison of microsphere data and PET data in averaged

perfusion values through all the studies of kidneys (**Figure 43A**) and upper GI (**Figure 43B**), and **Figure 43 (C, D)** illustrates the comparison of microsphere data and PET data in perfusion values of kidneys (**Figure 43C**) and upper GI (**Figure 43D**) only in Study 3. The most suspiciously abnormal data, like the super high perfusion values in microsphere studies, was removed. The Study 3 was selected only as an example.

Figure 43 (A, B) indicates that different cardiac outputs result in varied tissue perfusions. However, the change trends in the tissue perfusions corresponding to each blood flow controlling mode from PET data and microsphere data are not identical. According to the **figure 43 (C, D)**, the change trend in tissue perfusions from PET data in Study 3 is similar to that from microsphere data, but still not exactly the same. It also demonstrates the change trends in tissue perfusions in different PET imaging studies are not identical. The blood distribution to an organ varies with cardiac outputs and also differs with animals.

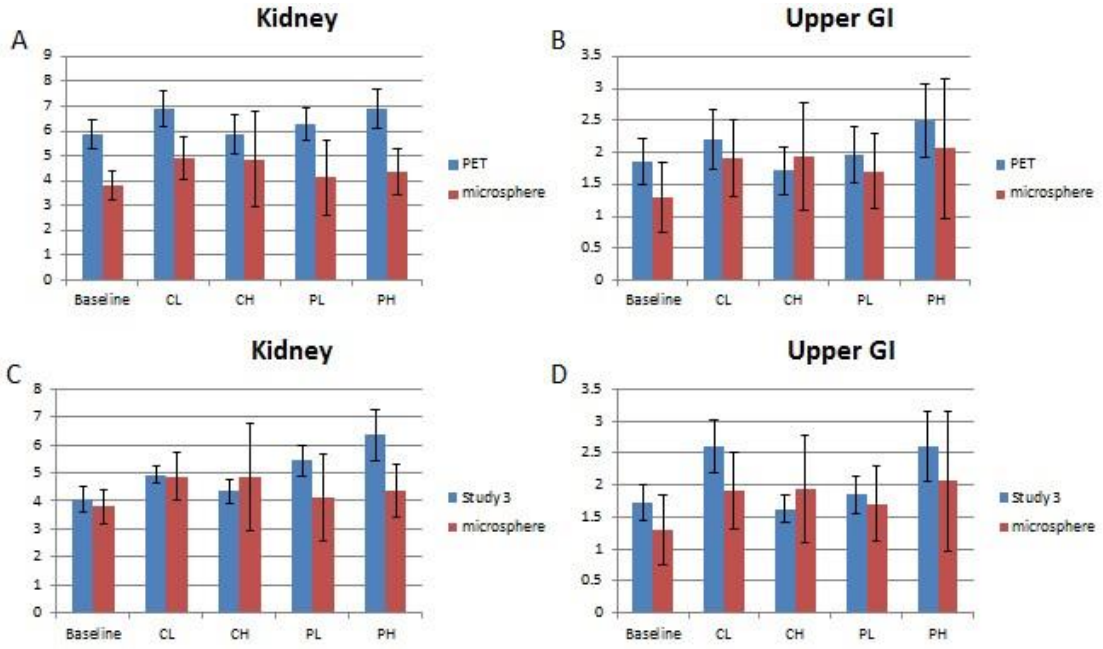

Figure 43. The comparison of PET data and microsphere data in trend detection. A, B: the comparison of microsphere data and PET data in averaged perfusion values through all the studies of kidneys (A) and upper GI (B); C, D: the comparison of microsphere data and PET data in perfusion values of kidneys (C) and upper GI (D) only in Study 3.

The methods to measure the standard deviations for microsphere studies and PET imaging studies were not exactly the same. Only two microsphere biopsies were harvested for each organ, and biopsy spots were far from each other. Each standard deviation of microsphere data for each organ was calculated from the data of the organs from all the animals. The microsphere results show that the standard deviation relative to the mean is high, so the confidence interval is not wide. Since a confidence interval is used to indicate the reliability of an estimate. A bad confidence interval indicates the confidence range cannot capture a true population parameter of the given samples. Therefore, it is not appropriate to say that the change trend shown in the microsphere

data is correct. The reason causing this problem is that even though microsphere measurement in perfusion studies is the "Gold Standard" study, it is subject to the technique itself. PET perfusion studies can provide perfusion values from both a single point and the overall value of an organ. The standard deviation for each organ was calculated by drawing a ROI with 20 pixels contained on each animal and averaging the standard deviations for all the animals. The PET imaging data gives shorter error bars, which means that the standard deviation relative to the mean is low. Accordingly, PET imaging can provide more consistent results.

4.3.6 Comparison Studies between Automated Selection and Manual Selection of AIF

Inveon Research Workplace (IRW, Siemens Healthcare, U.S.A.) was used to realize the manual selection of AIF. Femoral artery was selected by drawing a 3-D cylinder to cover the entire blood vessel. The resulting AIF is shown in **figure 44A**. Then we changed a slice and used the same method select femoral artery, but made the cylinder a little smaller. The cylinder was still inside the femoral artery. Another resulting AIF is shown in **figure 44B**. In fact, the two drawn cylinders are almost the same. However, the maximum enhancement of the first AIF is 4E4 Bq/ml, and that of the second AIF is 7.5E4 Bq/ml, which is twice of that of the first AIF. The resulting perfusion number calculated from the second AIF drawing might be twice of that from the first AIF drawing. The results indicate that slight change in selecting the AIF region might cause a big influence in the result. The slight change happens between operators with operators, and slice with slice even one person operates. On the contrary, the

automated AIF selection remains consistency in the entire study, because the automated AIF selection is able to give the AIF areas in three dimensions at one time, and the selection slice by slice is not necessary. In addition, the automated AIF selection reduces inter-operator variation, since the only input for the AIF selection is to choose the physiological phase that contains AIF region, and this phase is known, according to which study is performing (such as myocardial study and abdominal study), before the scan.

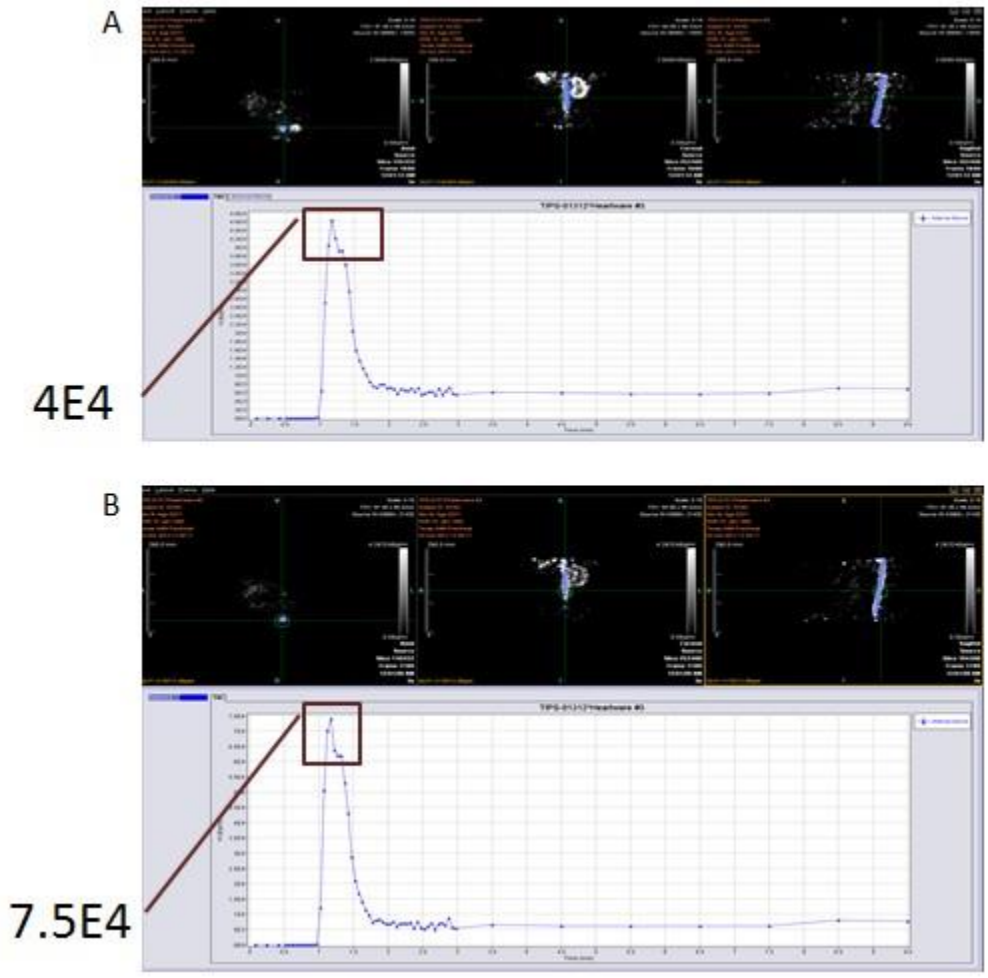

Figure 44. Resulting AIFs with the first manual selection (A) and the second manual selection (B).

CHAPTER V

CONCLUSION AND FUTURE WORK

In this study, a technique for performing automated determination of arterial input function (AIF) areas was developed. Briefly described, imaging data acquired from imaging modalities is used for extracting characteristic parameters (maximum enhancement, maximum slope, time to peak, and optional, wash-out slope and time to wash-out). The extracted parameters were converted to a plurality of 2-D plots. The 2-D plots include a plot of maximum slope vs. time to peak (S vs. T); maximum enhancement vs. time to peak (E vs. T); and, optionally, wash-out slope vs. time to wash-out (W vs. T). Pattern recognition is performed to identify the physiological phases on 2-D plots. Through automatically finding peaks and valleys of each phase on the plurality of 2-D plots, the AIF areas and some other tissues can be determined.

This technique/algorithm was tested in CT myocardial perfusion studies and PET abdominal perfusion studies. In the CT myocardial perfusion study, perfusion parametric maps were generated based on the automatically determined AIF areas, and quantitative analysis on infarcted and non-infarcted areas was performed. In the PET abdominal perfusion study, perfusion parametric maps were generated based on the automated AIF selection, the comparison between PET data and microsphere data was performed, and the comparison between automated selection and manual selection of AIF areas was also

implemented. From the results in this study, some conclusions are made for this technique.

First, this automated AIF determination technique replaces the conventional spatial classification method with physiological and functional classification method. In other words, it not only utilizes mathematical thinking, such as classification, dimension reduction and pattern recognition, but also takes more physiological considerations and explanations involved. In such way, physicians are able to understand and use this technique in their perspectives. In addition, it does not require pre-knowledge of expected location of AIF areas, as the spatial classification does.

Second, the technique is applicable to different modalities. It functions well in both CT and PET imaging in tissue perfusion studies. Since the dynamic evaluation curves are used as a basis for the technique and the curves from the imaging modalities of PET, CT and MRI behave similar, this technique can be extended to MRI, as well.

Third, this technique is effective on many tissues. Even though some slight changes are needed case by case in terms of tissue physiology, the central algorithm remains the same when implemented in both myocardial and abdominal perfusion studies. Accordingly, this technology can be used in varied tissue perfusion studies, minimally modified with physiological phase selection.

Fourth, the technique is efficient and effective. It is based on pixel-wised characteristic analysis, and therefore the resolution of generated perfusion maps would be good. The automated selection of AIF areas is performed through the entire 3-D volume at one time, instead of selecting the AIF areas in 2-D slices manually. In such case, it reduces time and labor consumption. The results from the generation of parametric perfusion maps indicate that this technique is effective.

Fifth, this algorithm provides consistent results. The comparison between PET imaging data and microsphere data, and the comparison between automated selection and manual selection of AIF areas demonstrate that this automated AIF selection technique provides more consistent results than microsphere measurement and manual AIF selection.

As for future work, the algorithm should be tested in MRI perfusion studies and even in ultrasound perfusion studies. As mentioned before, this algorithm might be effective in both imaging modalities, since they are also based on dynamic evaluation curves. The potential differences would be in the resolutions of parametric perfusion maps which are controlled by the imaging systems. The pre-processing techniques of the raw data acquired from the imaging might be different. For the long acquisition time, interpolation will be used; for the poor counting statistics, smoothing will be utilized; for large noise, curve fitting might be applied.

In addition, since this algorithm was developed using MATLAB, and this technique is based on pixel-wised operation, the calculation is slow. It would be much better if this algorithm can be transferred to C++ or Java to improve the function pace.

Lastly, more animal studies and more tissue perfusion studies are needed for testing this technique. It also needs to be evaluated in liver perfusion studies because the liver system is different from other organs, and it has two blood input paths: the arterial path and the venous path. It would be beneficial if this algorithm could differentiate these two blood input areas, and provide accurate perfusion maps.

REFERENCES

1. Thomas DL, Lythgoe MF, Pell GS, Calamante F, Ordidge RJ. The measurement of diffusion and perfusion in biological systems using magnetic resonance imaging. *Phys Med Biol.* Aug 2000;45(8):R97-R138.

2. Gottrup F. Physiology and measurement of tissue perfusion. *Ann Chir Gynaecol Fe.* 1994;83(3):183-189.

3. Gunn RN, Gunn SR, Turkheimer FE, Aston JAD, Cunningham TJ. Positron emission tomography compartmental models: A basis pursuit strategy for kinetic modeling. *J Cerebr Blood F Met.* Dec 2002;22(12):1425-1439.

4. Tofts PS. Modeling tracer kinetics in dynamic Gd-DTPA MR imaging. *Jmri-J Magn Reson Im.* Jan-Feb 1997;7(1):91-101.

5. Patlak CS, Blasberg RG. Graphical evaluation of blood-to-brain transfer constants from multiple-time uptake data. Generalizations. *J Cereb Blood Flow Metab.* Dec 1985;5(4):584-590.

6. Patlak CS, Blasberg RG, Fenstermacher JD. Graphical evaluation of blood-to-brain transfer constants from multiple-time uptake data. *J Cereb Blood Flow Metab.* Mar 1983;3(1):1-7.

7. Logan J. Graphical analysis of PET data applied to reversible and irreversible tracers. *Nucl Med Biol.* Oct 2000;27(7):661-670.

8. Logan J, Fowler JS, Volkow ND, Wang GJ, Ding YS, Alexoff DL. Distribution volume ratios without blood sampling from graphical analysis of PET data. *J Cerebr Blood F Met.* Sep 1996;16(5):834-840.

9. Prinzen FW, Bassingthwaighte JB. Blood flow distributions by microsphere deposition methods. *Cardiovasc Res.* Jan 1 2000;45(1):13-21.

10. Zuckier LS. *Principles of Nuclear Medicine Imaging Modalities*: World Scientific Publishing Co. Pte. Lt; 2009.

11. Marcus RP, Nikolaou K, Theisen D, Reiser MF, Bamberg F. Myocardial perfusion imaging by computed tomography: today and tomorrow. *Int J Clin Pract.* Oct 2011;65:14-22.

12. Iida H, Hayashi T, Eberl S, Saji H. Quantification in SPECT cardiac imaging. *J Nucl Med.* Jan 2003;44(1):40-42.

13. Kapur A, Latus KA, Davies G, et al. A comparison of three radionuclide myocardial perfusion tracers in clinical practice: the ROBUST study. *Eur J Nucl Med Mol I.* Dec 2002;29(12):1608-1616.

14. Taillefer R, DePuey EG, Udelson JE, Beller GA, Latour Y, Reeves F. Comparative diagnostic accuracy of Tl-201 and Tc-99m sestamibi SPECT imaging (perfusion and ECG-gated SPECT) in detecting coronary artery disease in women. *J Am Coll Cardiol.* Jan 1997;29(1):69-77.

15. Jakoby BW, Bercier Y, Conti M, Casey ME, Bendriem B, Townsend DW. Physical and clinical performance of the mCT time-of-flight PET/CT scanner. *Phys Med Biol.* Apr 21 2011;56(8):2375-2389.

16. Phelps ME. *PET physics, instrumentation, and scanners*: New York ; Berlin : Springer; 2006.

17. Schindler TH, Schelbert HR, Quercioli A, Dilsizian V. Cardiac PET imaging for the detection and monitoring of coronary artery disease and microvascular health. *Jacc-Cardiovasc Imag.* Jun 2010;3(6):623-640.

18. Schelbert HR, Phelps ME, Huang SC, Macdonald NS, Hansen H, Kuhl DE. N-13 ammonia as an indicator of myocardial blood-flow. *Circulation.* 1981;63(6):1259-1272.

19. Mullani NA, Goldstein RA, Gould KL, et al. Myocardial perfusion with rubidium-82 .1. measurement of extraction fraction and flow with external detectors. *J Nucl Med.* 1983;24(10):898-906.

20. Di Carli MF. Advances in positron emission tomography. *J Nucl Cardiol.* Nov-Dec 2004;11(6):719-732.

21. Di Carli MF, Hachamovitch R. New technology for noninvasive evaluation of coronary artery disease. *Circulation.* Mar 20 2007;115(11):1464-1480.

22. Webb AR. *Introduction to biomedical imaging*. Hoboken, N.J.: Wiley; 2003.

23. Hendrix A, ed. *Magnets, Spins, and Resonances: An introduction to the basics of Magnetic Resonance*: Siemens AG Medical Solutions; 2003.

24. Adrian P. Crawley JP, Paul Ferrari, and Timothy P.L. Roberts. Basics of diffusion and perfusion MRI. *Applied Radiology.* April 2003;32.

25. Thomas SJ. Relative electron density calibration of CT scanners for radiotherapy treatment planning. *Brit J Radiol.* Aug 1999;72(860):781-786.

26. Abudurexiti A, Kameda M, Sato E, et al. Demonstration of iodine K-edge imaging by use of an energy-discrimination X-ray computed tomography system with a cadmium telluride detector. *Radiol Phys Technol.* Jul 2010;3(2):127-135.

27. Coursey CA, Nelson RC, Boll DT, et al. Dual-energy multidetector CT: How does it work, what can it tell us, and when can we use it in abdominopelvic imaging? *Radiographics.* Jul-Aug 2010;30(4):1037-1055.

28. Riederer SJ, Mistretta CA. Selective iodine imaging using K-edge energies in computerized x-ray tomography. *Med Phys.* Nov-Dec 1977;4(6):474-481.

29. Konstas AA, Goldmakher GV, Lee TY, Lev MH. Theoretic basis and technical implementations of CT perfusion in acute ischemic stroke, part 2: technical implementations. *AJNR Am J Neuroradiol.* May 2009;30(5):885-892.

30. Miles KA, Griffiths MR. Perfusion CT: a worthwhile enhancement? *Brit J Radiol.* Apr 2003;76(904):220-231.

31. Konstas AA, Goldmakher GV, Lee TY, Lev MH. Theoretic basis and technical implementations of CT perfusion in acute ischemic stroke, part 1: theoretic basis. *Am J Neuroradiol.* Apr 2009;30(4):662-668.

32. Nakauchi Y, Iwanaga Y, Ikuta S, et al. Quantitative myocardial perfusion analysis using multi-row detector CT in acute myocardial infarction. *Heart.* Apr 2012;98(7):566-572.

33. Hamberg LM, Hunter GJ, Kierstead D, Lo EH, Gonzalez RG, Wolf GL. Measurement of cerebral blood volume with subtraction three-dimensional functional CT. *Am J Neuroradiol.* Nov-Dec 1996;17(10):1861-1869.

34. Lin ZMS, Pohlman S, Cook AJ, Cook AJ, Chandra S. CT perfusion, comparison of gamma-variate fit and deconvolution. *P Soc Photo-Opt Ins.* 2002;4683:102-109.

35. Fieselmann A, Kowarschik M, Ganguly A, Hornegger J, Fahrig R. Deconvolution-based CT and MR brain perfusion measurement: theoretical model revisited and practical implementation details. *Int J Biomed Imaging.* 2011;2011:467563.

36. Mischi M, den Boer JA, Korsten HHM. On the physical and stochastic representation of an indicator dilution curve as a gamma variate. *Physiol Meas.* Mar 2008;29(3):281-294.

37. James Sorenson SRCaMP. *Physics in Nuclear Medicine*. 3RD Edition ed: W.B. Saunders Co. ; 2003.

38. Morris ED. Automated determination of the arterial input function for MR perfusion analysis. *8th ISMRM*. Denver, CO; 2000.

39. Mouridsen K, Christensen S, Gydensted L, Ostergaard L. Automatic selection of arterial input function using cluster analysis. *Magn Reson Med.* Mar 2006;55(3):524-531.

40. Chen S, Liu HL, Yang YH, Hsu YY, Chuang KS. Determination of arterial input function in dynamic susceptibility contrast MRI using group independent component analysis technique. *Nucl Instrum Meth A.* Dec 20 2006;569(2):617-621.

41. G. J. Parker AJ, J. C. Waterton, D. L. Buckley. Automated arterial input function extraction for T1-weighted DCE-MRI. Paper presented at: ISMRM; Nov, 2003.

42. Buckley DL, Roberts C, Parker GJM, Logue JP, Hutchinson CE. Prostate cancer: Evaluation of vascular characteristics with dynamic contrast-enhanced T1-weighted MR imaging - Initial experience. *Radiology.* Dec 2004;233(3):709-715.

43. Chen J, Yao JH, Thornasson D. Automatic determination of arterial input function for dynamic contrast enhanced MRI in tumor assessment. *Lect Notes Comput Sc.* 2008;5241:594-601.

44. Shriki JE, Shinbane J, Lee C, et al. Incidental myocardial infarct on conventional nongated CT: a review of the spectrum of findings with gated CT and cardiac MRI correlation. *Am J Roentgenol.* Mar 2012;198(3):496-504.

45. Mehra VC, Ambrose M, Valdiviezo-Schlomp C, et al. CT-based myocardial perfusion imaging-practical considerations: acquisition, image analysis, interpretation, and challenges. *J Cardiovasc Transl.* Aug 2011;4(4):437-448.

46. So A, Lee TY. Quantitative myocardial CT perfusion: a pictorial review and the current state of technology development. *J Cardiovasc Comput Tomogr.* Nov-Dec 2011;5(6):467-481.

47. Herrero P, Markham J, Weinheimer CJ, et al. Quantification of regional myocardial perfusion with generator-produced Cu-62-PTSM and positron emission tomography. *Circulation.* Jan 1993;87(1):173-183.

48. Gould KL, Goldstein RA, Mullani NA, et al. Noninvasive assessment of coronary stenoses by myocardial perfusion imaging during pharmacological coronary vasodilation .8. clinical feasibility of positron cardiac imaging without a cyclotron using

generator-produced Rb-82. *Journal of the American College of Cardiology.* Apr 1986;7(4):775-789.

49. Beanlands RSB, Muzik O, Mintun M, et al. The kinetics of copper-62-PTSM in the normal human heart. *J Nucl Med.* May 1992;33(5):684-690.

50. Herrero P, Hartman JJ, Green MA, et al. Regional myocardial perfusion assessed with generator-produced copper-62-PTSM and PET. *J Nucl Med.* Aug 1996;37(8):1294-1300.

51. Nichols TE, Qi JY, Leahy RM. Continuous time dynamic PET imaging using list mode data. *Information Processing in Medical Imaging, Proceedings.* 1999;1613:98-111.